9-3-2010

Control of neutral atoms in optical lattices

Brian Mischuck

Follow this and additional works at: https://digitalrepository.unm.edu/ose_etds
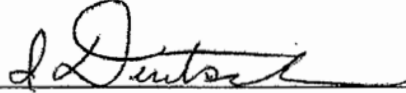
Brian Mischuck

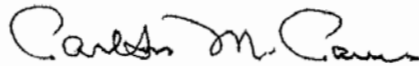*Candidate*

Optical Science and Engineering

Department
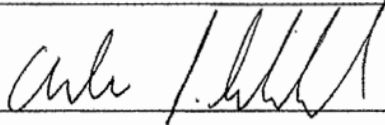
This dissertation is approved, and it is acceptable in quality
and form for publication on microfilm:
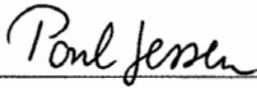
Approved by the Thesis Committee:

_____ , Chairperson

Accepted:

_____

Dean, Graduate School

_____

Date

Control of Neutral Atoms in Optical Lattices

by

Brian Mischuck

B.S., Wake Forest University, 2002

M.S., Optical Science, University of Arizona, 2005

DISSERTATION

Submitted in Partial Fulfillment of the

Requirements for the Degree of

Doctor of Philosophy

Optical Science and Engineering

The University of New Mexico

Albuquerque, New Mexico

July, 2010

Dedication

To my parents, for all their support through the years.

Acknowledgments

I would chiefly like to thank my advisor, Ivan Deutsch, for all the support and encouragement over the years, as well as giving me the opportunity to work on theoretical problems in the first place. I also I owe a great deal of gratitude to Poul Jessen. First for his patience when I was a student at the University of Arizona, and his support later when I moved to the University of New Mexico.

I am also indebted to the many people within the Center for Quantum Information and Control with whom I have had the opportunity to work. These include those with whom I have directly collaborated, including Seth Merkel, Satyan Bhongale, Rene Stock, Worawarong Rakreungdet, Kim Fook Lee, Jae Hoon Lee, Enrique Montaño, Aaron Smith and Brian Anderson. Some of the others within CQuIC with whom I have mulled over various physics problems are Sergio Boxio, Animesh Datta, Bryan Eastin, Matt Elliott, Steve Flammia, Iris Reichenbach, Anil Shaji, Alexendre Tacla, Carl Caves, Andrew Landahl, Greg Smith, and Souma Chadhury. I am also grateful for the opportunity to have discussed physics with many of the folks in the broader quantum optics community at Arizona, including Dr. Brian Anderson, Dave Scherer, Chad Weiler, Alex Cronin, John D. Perreault and Vincent Lonij.

I would also like to thank the two undergraduate professors who gave me a start in research at Wake Forest, Paul Anderson and Richard Williams.

Control of Neutral Atoms in Optical Lattices

by

Brian Mischuck

ABSTRACT OF DISSERTATION

Submitted in Partial Fulfillment of the
Requirements for the Degree of

Doctor of Philosophy
Optical Science and Engineering

The University of New Mexico

Albuquerque, New Mexico

July, 2010

Control of Neutral Atoms in Optical Lattices

by

Brian Mischuck

B.S., Wake Forest University, 2002

M.S., Optical Science, University of Arizona, 2005

PhD, Optical Science and Engineering, University of New Mexico, 2010

Abstract

Neutral atoms are promising candidates to store and manipulate quantum information. In this thesis we examine several problems related to the control of neutral atoms for quantum computation and simulation.

In the first problem we show how the transport of atoms in an optical lattice can be controlled through variation of the polarization of the optical lattice and the application of global microwave pulses. This type of control control is a first step in many of the schemes for quantum computation and quantum simulation. We show that with the available tools for global control, the synthesis of any unitary transformation, consistent with translational invariance, may be performed and provide an explicit method for carrying this out.

In the second problem, we study a spectroscopic method for probing atomic interactions that may form the basis for two-qubit quantum logic gates. The confinement of atoms required to perform quantum computation can strongly affect how they interact. Probing the nature of those confinement-induced effects is a first step towards quantum computing with neutral atoms. Transport of the atoms to overlapping wells is achieved through microwave pulses that drive population between hyperfine levels in a lin-perp-lin polarization-gradient lattice. By measuring the amount of population transferred into certain excited states, we can detect changes in the spectrum of the two-atom system induced by the interaction.

In the third problem, we consider a cloud of cold atoms driven by both microwave and radio-frequency magnetic fields. The large number of spin sublevels available in individual atoms makes them candidates for a qudit-based quantum computer. Because the applied fields that drive the system may be inhomogeneous, the collection of atoms forms an ensemble of different qudits. Borrowing ideas developed for NMR control, we show how to drive the ensemble through a given evolution. We show that even in the presence of large experimental errors, state preparation may be achieved with high fidelities. We also show that intentionally applied variations in spatial magnetic fields can be used to synthesize different states in different regions of space.

Contents

Contents

Contents

Contents

List of Figures

List of Figures

List of Tables

Chapter 1

Introduction

Coherent control over quantum systems is increasingly important in a variety of fields, including computation [1], metrology [2], chemical dynamics [3, 4] and others [5]. Such control open the doors to a variety of applications and allow us to perform some tasks that would otherwise be intractable. For instance, computers which can make use of quantum coherence have the capability to factor numbers exponentially faster than classical computers, as well perform certain tasks like unstructured searches with a polynomial speedup over their classical counterpart. Metrology is another area in which coherent control offers advantages. It has been shown that full quantum control allows greater sensitivity in parameter estimation than the "standard quantum limit" as the number of particles is increased [2]. Control over chemical dynamics has greatly improved as a result of applying ideas from coherent control [3, 4]. In many cases, a particular reaction is desired, but there exist many other pathways that a chemical reaction could follow, other than the desired route. Coherent control provides a variety of techniques which can be used to find experimental parameters that drive only the desired reaction.

Generically, the problem of quantum control can be stated as follows. We have

a desired transformation that we want to apply to our system, given by a unitary evolution U_{target}. To perform the transformation, we have access to a time dependent Hamiltonian,

$$H(t) = H_0 + \sum_j b_j(t) H_j. \tag{1.1}$$

The Hamiltonian has two basic parts, a time independent part H_0 over which we have no control, and a set of time dependent control fields $b_j(t)$ that "drive" Hamiltonians H_j. The goal is then to choose the time evolution of $b_j(t)$ so that the system implements the target unitary,

$$U_{target} = \mathcal{T} e^{-i \int_0^T H(t)\, dt}, \tag{1.2}$$

where $\mathcal{T}$ is the time ordering operator and the evolution occurs over a time T. Given a particular set of available controls, characterized by the Hamiltonians H_j, the first task is to determine whether those controls allow the desired transformation to be performed. With the "controllability" of the system defined, one needs to choose the $b_j(t)$ so that the desired evolution actually occurs.

There are several approaches one might take to showing that the available controls can generate the desired evolution. In the first method, one examines the Lie algebra generated by the available controls. This approach makes use of the fact that from a given set of controls we can expand the set of available Hamiltonians through the use of a commutator via backwards and forwards evolution,

$$e^{-iH_j dt} e^{-iH_k dt} e^{iH_j dt} e^{iH_k dt} \approx e^{-dt^2 [H_j, H_k]}. \tag{1.3}$$

If $[H_j, H_k]$ is linearly independent of H_j, then we have effectively added a new Hamiltonian to the set of available controls. Iterating this procedure we can generate $[H_l, [H_j, H_k]]$, $[H_m[H_l, [H_j, H_k]]]$ and so on. If the number of linearly independent Hamiltonians available in this way is $d^2 - 1$ where d is the dimension of the system, then we can generate any desired SU(d) and hence, any desired evolution [6] . While

this procedure provides a method for implementing arbitrary unitaries if a system is controllable, it isn't necessarily optimal in the amount of time required to synthesize the desired evolution. Once the system is shown to be controllable, other techniques like numerical optimization [7, 5] are often utilized to find $b_j(t)$.

An alternate approach, often taken when one is considering quantum computation, is useful when the system under study can be broken up into subsystems [1]. The most common approach is to consider the subsystems to be two level systems known as qubits, though it is also possible to generalize this to d-dimensional subsystems known as qudits. The key idea to generating arbitrary evolutions is to show that they can be broken up into a series of unitaries applied either to individual subsystems or pairs of subsystems. These unitaries are generally referred to as 1 or 2 qubit (or qudit) gates. Furthermore, an appropriately chosen but finite number of such gates is sufficient to generate any evolution. For instance, in the qubit case, the single qubit Hadamard, phase, $\pi/8$ gates and the two qubit CNOT gate are sufficient. Other choices are also possible [1]. As a result, to show that a set of controls is sufficient to generate any evolution, one merely has to show that appropriate single subsystem gates and gates between paris of subsystems may be performed.

A third approach is useful when the goal is to simulate quantum evolution [8]. In this case full control is not necessary. Instead one usually shows that by appropriately choosing constant values of b_j, the Hamiltonian one creates in the lab approximates some desired Hamiltonian. If the b_j are allowed to change slowly, one can begin with a relatively well understood Hamiltonian and adiabatically transform the system into a new Hamiltonian with less well understood properties. For at least some systems of interest, if one begins in the ground state of the initial Hamiltonian, the system will finish in the ground state of the final Hamiltonian [9, 10]. If appropriate measurements can be performed on the system, then the ground state properties of the final Hamiltonian may be determined.

1.1 Quantum Control of Neutral Atoms

1.1.1 Overview

A variety of physical systems have been considered as platforms for coherent control, such as trapped ions, NMR, and chemical dynamics, with goals ranging from controlled chemistry to quantum computing [1, 3, 4, 5]. In this thesis, we will focus on control of trapped neutral atoms. Because of their weak interaction with the environment, neutral atoms provide a promising candidate for quantum computing and simulation. In addition, there is also a long history of single particle coherent control that can be used as a foundation for more complex goals. Some of the outstanding accomplishments in the field are the observation of a quantum phase transition in the Bose-Hubbard Hamiltonian [9] and the demonstration of two qubit gates between isolated pairs of atoms [11]. Relatively less attention has been played to the possibility of applying the more general ideas of coherent control. The primary goal of this thesis is to explore the ideas of coherent control to manipulate the spin and/or spatial degrees of freedom of trapped ultracold atoms.

A variety of tools are available to control atoms' dynamics. Far off resonance laser beams can shift an atom's energy level without driving any transitions between states. If either the intensity or polarization varies spatially, this leads to a spatial variation in the shift of the atom's energy level which in turn can act as a potential to trap the atoms [12]. Time-dependent variations in the polarization and/or intensity can be used as a means for controlling the atom's motion. Atoms' rich internal structure may be manipulated with a combination of radio-frequency(rf) and microwave fields [13, 14]. An appropriate choice of the power and phase of those fields can allow any state to be synthesized. Because of the tight confinement induced by the lattice, the interactions between pairs of atoms can be strongly modified leading to novel effects [15]. Studying those effects is an important first step in realizing controlled

interactions between pairs of atoms, and the combination of well chosen lattice and microwave controls can provide a method for achieving this. All these controls have in common the feature of low decoherence rates, which is essential for high-fidelity quantum control.

1.1.2   Background

Quantum Simulations

The first effort to simulate condensed matter systems with atoms in optical lattices was the observation of the superfluid to Mott insulator transition [9, 10]. The experiment began with a BEC of cold atoms which was adiabatically loaded into a 3D optical lattice. Because of the cold temperatures involved, the atoms were loaded into the lowest energy eigenstate of the system. The Hamiltonian which describes the system is

$$H = -J \sum_{<i,j>} a_j^\dagger a_i + \frac{1}{2} U \sum_i n_i(n_i - 1). \tag{1.4}$$

The first term describes tunneling of the atoms between nearest neighbor sites in the lattice, while the second term describes on-site interactions. The nature of the ground state is determined by the ratio of the tunneling rate of the atoms to the interaction strength, U/J. For weak interactions, tunneling dominates and the ground state corresponds to each atom in the zero quasi momentum state. For strong interactions, there is an energy cost associated with adding an extra atom to a site, so the ground state corresponds to one atom per site. Tuning the ratio U/J drives a phase transition between the two ground states. In real experiments there is also a parabolic confining potential, so at higher densities "wedding cake" like structures form in which regions with differing numbers of atoms per site can form in the Mott insulating regime [16].

More recent interest has focused on spin-1/2 fermions in optical lattices, moti-

vated primarily by the ability to simulate Hamiltonians thought to be involved in high temperature superconductivity [17]. The Hamiltonian for that system is similar to the Bose Hubbard Hamiltonian,

$$H = -J \sum_{<i,j>,s} a_{j,s}^\dagger a_{i,s} + U \sum_i n_{i,\downarrow} n_{i,\uparrow} + V_t \sum_i (i_x^2 + i_y^2 + \gamma i_z^2)(n_{i\downarrow} + n_{i\uparrow}). \quad (1.5)$$

In this case the creation and annihilation operators obey anti-commutation relations appropriate for fermions and s represents the two possible spin states. The last term is due to an overall trapping potential with γ determining the ratio between the trapping potential in the xy plane and the trap in the z direction. Again, several different phases have been observed experimentally [17]. When tunneling dominates, the atoms minimize their kinetic energy by delocalizing across the lattice. When the interactions dominate, a Mott-insulating phase can form with one atom per site. When the confining potential is the dominant term, the ground state is a band insulator in which the Pauli exclusion principle limits individual lattice sites to contain a single spin up and a single spin down atom. Direct imaging of the atomic cloud's density profile allows the different phases to be detected.

Disorder plays an important role in condensed matter systems, and it can be controllably introduced into cold atom systems. If a second lattice beam with a much smaller intensity and incommensurate period is added to another optical lattice potential, the incommensurate nature of the two potentials leads to a nearly random variation in on site energy levels. If a Feshbach resonance is used to reduce the interactions between the atoms, the problem becomes a single particle problem and the Hamiltonian is

$$H = J \sum_m (w_m \ w_{m+1} + w_{m+1} \ w_m) + \Delta \sum_m \cos(2\beta m + \phi) \, w_m \ w_m . \quad (1.6)$$

The first term results in tunneling throughout the lattice. The second term represents an additional, incommensurate lattice with a strength Δ, where β is the ratio of the wavelengths of the two lattices. The nature of the ground state can undergo a phase

transition as the strength of the disorder relative to the tunneling, Δ/J, is changed. For low disorder, the eigenstates are delocalized across the lattice, while for high disorder, the eigenstates are localized with exponentially decreasing tails in the wave function. Such a transition was observed in [18]. By examining the spatial profile of the atoms in the lattice, the transition from a delocalized state to a localized state could be observed.

Quantum Computation

Because neutral atoms interact relatively weakly, demonstrating two qubit gates is one of the primary challenges in neutral atom quantum computing. The first demonstration of controlled interactions between neutral atoms [19] occurred in the same system used to study quantum phase transitions of bosons described above. Beginning from a Mott insulating state, a microwave pulse places atoms into an equal superposition of the $F = 1, m = -1$ and $F = 2, m = -2$. Rotation of the relative angle of two of the lattice beams splits the atoms' wave packets and leads to collisions. Atoms will pick up an interaction-induced phase shift depending upon whether or not they collide with other atoms. This leads to the controlled creation of entanglement between pairs of atoms, which can be observed via a collapse and revival in the visibility of subsequent Rabi oscillations.

Though the above experiment represented an important first step, since each atom interacted with both of its neighbors simultaneously, it was an intrinsically many-body effect. The next experimental step was to demonstrate controlled interactions between pairs of atoms in a large ensemble containing many such pairs [20]. In this case, beginning from a Mott insulating state, the potential is transformed into a lattice of double wells which serves to isolate pairs of atoms. The qubit states were chosen to be $1 = F = 1, m_F = -1$ and $0 = F = 1, m_F = 0$. The barrier between the double wells can be reduced until they are transformed into single wells.

Since both atoms now occupy the same well, they can undergo a collision. At ultra-cold temperatures, atoms can collide if their relative-coordinate spatial wave function is in the symmetric state, while no collision occurs if the spatial wave function is antisymmetric. Because the atoms are bosons, a spatially symmetric wave function requires a symmetric spin state lying in the triplet subspace, while an antisymmetric wave function implies that the spin is in the singlet state. If the atoms are either both spin-up or both spin-down initially, then when they are combined in the same well, they are in an eigenstate of the interaction and so they only pick up an overall phase. If one of the atoms is initially spin up and the other spin down, when they are combined in the same well, the state of the two atom system is a superposition of singlet and triplet states. Since only the triplet states collide, careful control of the double-well potential can lead to an exchange interaction, which in turn can be used as an entangling gate. The fidelity of the gate was found to be 0.64.

Most recently, two qubit gates have been demonstrated between isolated pairs of Rydberg atoms [11, 21]. Two optical dipole traps separated by $10\mu m$ each hold one atom apiece. The basic idea behind the gate is that when the control atom is excited into a Rydberg level, the interaction between the atoms shifts the energy of the target atom's Rydberg level. The qubit states were chosen to be $|1\rangle = |F = 2, m_F = 0\rangle$ and $|0\rangle = |F = 1, m_F = 0\rangle$. If a rotation between the the target atom's $|0\rangle$ state and the unshifted Rydberg level is attempted, it will only occur if the control atom is not in its Rydberg state. The CPHASE gate can be implemented by a π rotation between $|0\rangle$ and the Rydberg level of the control atom, followed by a 2π rotation between $|0\rangle$ and the Rydberg level of the target atom, and then a π rotation between $|0\rangle$ and the Rydberg level of the control atom. The target atom then picks up a π phase shift conditioned on whether the control atom is in the Rydberg state. This conditional phase shift is the two qubit gate from which a CNOT gate is built. A fidelity of 0.72 was accomplished experimentally.

Qudit Control and Inhomogeneous Control

While much of the original work on both quantum computation and quantum simulation has involved the study of collections of interacting two level systems, it is possible to generalize such systems to qudits, in which the information is stored in higher dimensional systems. In fact, such qudit quantum computation schemes may have advantages [22]. Since many qubits actually lie within higher dimensional system, there may be advantages to making use of the extra dimensions. However, controlling larger dimensional quantum systems can be more challenging than simply controlling qubits.

A natural candidate for a qudit is the spin states of an alkali atom. The state space is given by the tensor product of the nuclear spin with the outermost electron's spin and the dimension can be rather large. For instance, Cs has a ground electronic hyperfine manifold which is 16-dimensional. The earliest proposals for qudit control in alkalis involved the use of Raman laser to drive transitions between magnetic sublevels [23]. More recently, time-dependent magnetic fields and a static tensor light shift have been used for arbitrary state preparation in the lower hyperfine manifold [24], which was subsequently used to study quantum chaos [25]. Alternative schemes which employ radio-frequency and microwave magnetic fields have also been studied for quantum control [13, 14].

The studies just discussed made the assumption that the experimental parameters which parameterize the system's evolution were perfectly known. Often, this is not the case, and the sensitivity of quantum systems to experimental imperfections has been an issue since the earliest days of quantum computation. A wide variety of techniques have been developed to deal with such errors in qubit systems, from fault tolerance and dynamical decoupling [26, 1], to composite pulse sequences that are more robust to such errors [27, 28]. For instance, the CORPSE and SCROFULOUS

sequences were designed to perform single qubit gates in a manner that is robust to detuning and power errors, respectively. Much less is known about how to deal with such errors in systems of qudits, though there has been some work extending techniques of error correction to higher dimensional systems [29].

In addition to inhomogeneities that arise from experimental errors, inhomogeneities may be intentionally introduced in order to improve control over the system. In traditional NMR, nearly arbitrary control as a function of detuning or Rabi frequency has been demonstrated [30, 7, 31]. Some of these techniques have also begun to be studied in AMO settings. For instance, the use of robust pulses has been explored with atoms in optical lattices [32]. Theoretical proposals exist which describe how one might use the fictitious magnetic field induced by a laser beam to address individual sites in an optical lattice [33]. Real magnetic fields have been used to achieve some spatial selectivity in systems of atoms in optical lattices. For instance, the shells of a Mott insulator have been probed [16].

1.2 Thesis Overview

The primary contribution of this thesis is developing a theoretical understanding of several problems related to the control of ultracold neutral atoms, motivated by applications to quantum information processing. The goal is to expand the range of unitaries which may be synthesized with realistic experimental controls. We will use a combination of rf, microwave, and optical fields to understand how to control individual atoms and pairs of atoms.

Much of the work presented here has been published, or is preparation to be published, as listed in Table 1.1. The majority of Ch. 3 was published in *Coherent control of atomic transport in spinor optical lattices* [34]. For this work, I studied transport of atoms through an optical lattice. I described the limitations imposed by

the translational invariance of the controls, and developed a protocol to perform state preparation and unitary design with such controls. Ch. 5 is based on *Inhomogeneous Neutral Atom Qudit State Preparation*, which is in preparation. In collaboration with Seth Merkel, I described how a series of rotations could perform state preparation, even in the presence of experimental inhomogeneities, and developed numerical optimization routines to find pulse sequences which can perform such state preparation. In addition to the published work, in Ch. 4 I describe an approach to detecting the trap induced resonances first discovered by Stock, *et al.* [15]. For this project, I used the method originally devised by Stock *et al.* to study the spectrum of strongly interacting atoms in separated traps and found a regime where a spectroscopic approach to detecting such effects would be useful. I have also had the opportunity to work directly on an optical lattice experiment in the lab of Poul Jessen. This work led to [32], the first paper listed in Table 1.1, in which my collaborators and I demonstrated high fidelity manipulation of an ensemble of single neutral atom qubits. The thesis is organized as follows.

In Ch. 2 we review previous results on the controllability of two-level systems in the presence of experimental inhomogeneities. First, the Lie algebra associated with inhomogeneities in the Rabi frequency is studied, followed by inhomogeneity in the detuning. These results are combined to show how to attain arbitrary control with respect to inhomogeneous parameters.

In Ch. 3 we study the control of transport of atoms through optical lattices. A combination of microwaves and time dependent optical lattices are used as the control fields. It is shown that all states and all unitaries with a finite width consistent with translational invariance may be synthesized. We also discuss the impact of inhomogeneities. We show that the controllability of the system is not dramatically improved by the application of a time-dependent linear gradient, the simplest method for breaking the translational symmetry.

Journal Reference	Coauthors	Chapter
PRA **79**, 022316 (2009)	W. Rakreungdet, J. H. Lee, K. F.Lee, E. Montano, P. S. Jessen	
PRA **81**, 023403 (2010)	I. H. Deutsch and P. S. Jessen	Ch. 3
In Preparation	S. Merkel, I. H. Deutsch	Ch. 5

Table 1.1: Table of published work with location in text.

In Ch. 4 we study a method for probing trap-induced resonances in optical lattices. Microwave induced transport in a lin⊥lin lattice allows us to selectively drive pairs of atoms together. By measuring the appropriate atomic populations, resonances in the spectrum associated with the interaction can be detected. Changing the lattice parameters changes the energy of the interaction-induced resonances relative to other vibrational levels, allowing the two types of resonances to be distinguished experimentally.

In Ch. 5 we study inhomogeneous control of neutral atom qudits with microwave and rf control fields. We first show that a sequence of alternating rf and microwave rotations can synthesize any state in an appropriately chosen 8-dimensional subspace. Since the state preparation routine relies on $SU(2)$ rotations, we make use of the inhomogeneous control ideas described in Ch. 2 to extend the construction to inhomogeneous control of qudits. Numerical methods are employed to find pulse sequences which implement the desired unitaries more rapidly.

Chapter 2

Ensemble Control

2.1 Introduction

In the typical approach to quantum control described in Ch. 1, the parameters that drove the system were assumed to be known exactly, but this is often not the case. Inhomogeneities can arise from a variety of sources, such as experimental imperfections or spatial variations in the drive parameters, and it is important to understand how those inhomogeneities impact the controllability of the system. In addition, inhomogeneities may also be intentionally introduced in order to gain further control over a system, such as addressing different regions of an ensemble via spatial inhomogeneities. In later chapters, we will explore the inhomogeneous control of several neutral atomic systems, while in the present chapter, we review the known general results.

By far, the system in which inhomogeneous control has been most thoroughly explored is NMR, where the emphasis is on individual or coupled two-level systems. Inhomogeneities which are the result of experimental imperfections include variation in the rf power or transition frequency of single spins [30], while imprecise knowledge

of the couplings between spins gives rise to an effective inhomogeneity in the coupling strength [35]. The types of errors that affect NMR are common to other systems, such as electron paramagnetic resonance, where spatial variation in the rf field leads to inhomogeneity in the rotation angle of the electron's spin [36]. Nitrogen vacancy centers in diamond are driven by a combination of microwave and rf fields, both of which suffer from amplitude and frequency inhomogeneities [37]. Imperfections in rf fields also play a role in superconducting circuits [38]. Although they arise from different physical mechanisms, variations in laser amplitude and frequency affect the fidelity of single qubit gates in trapped ions in a manner analogous to the rf and microwave fields just described [39]. Spatial variations in the intensity of optical lattice light also leads to variation in the transition frequencies of trapped neutral atomic qubits [32].

The use of inhomogeneities to tomographically address different members of an ensemble has been studied in a variety of systems. In NMR, spatial variations in a magnetic field can be used to selectively excite the spins in chosen spatial regions [40, 41]. Natural variations in the transition frequencies of rare-earth-metal-ions doped into inorganic crystals makes frequency selection of qubits possible [42]. In atomic physics experiments, spatially varying magnetic fields have been used to study the shells of a Mott insulating system [16], and achieve site selective excitation within optical lattices [43].

In the presence of inhomogeneities like those described above or those considered in later chapters, the controls take the form

$$H(t, \ \nu_j \ ) = \nu_0 H_0 + \sum_j \nu_j b_j(t) H_j. \tag{2.1}$$

As in Ch. 1, $b_j(t)$ are time dependent controls that "drive" the Hamiltonians H_j. The inhomogeneities are described by the classical parameters ν_j, which do not change with time and are individually assumed to fall within a known range, ν_j

$[n_{j,min}, n_{j,max}]$. We model the inhomogeneities as an ensemble of different particles, each of which takes on different of values of the inhomogeneous parameters ν_j. For instance, if the inhomogeneities are the result of miscalibration in the power of some driving field, then the imagined ensemble consists of different particles, each of which experiences a different drive power. If the inhomogeneities are the result of spatial variation of some parameter, such as a magnetic field, then the physical ensemble consists of a collection of particles which are spread out in space so that each experiences a different magnetic field.

The time evolution and the unitary transformation that is generated by the control Hamiltonian become functions of the inhomogeneities,

$$U_{actual}(\nu_j) = \mathcal{T}e^{-i\int_0^T H(t,\{\nu_j\})\,dt}. \tag{2.2}$$

The target transformations can also vary with the inhomogeneous parameters, and the nature of that variation typically depends on the source of the inhomogeneity. If the inhomogeneities are the result of experimental errors, then we choose the target transformation to be identical for all members of the ensemble. In this case, referred to as *robust control*, we seek control waveforms $b_j(t)$ such that the actual transformation, Eq. (2.2), is the same for all members of the ensemble,

$$U_{actual}(\nu_j) \approx U_{target}. \tag{2.3}$$

Although each member of the ensemble will undergo a different evolution, at the end of that evolution the synthesized transformation will be the same for each member of the ensemble, up to some desired accuracy. If some of the inhomogeneities are intentionally introduced, while others are the result of errors, we choose the target transformation to vary only with the intentionally introduced inhomogeneity. In this case we seek controls $b_j(t)$ such that the actual transformation, Eq. (2.2), is independent of some of the inhomogeneous parameters, ν_i, but dependent on others, ν_i^*, so that $U_{actual}(\nu_j) \approx U_{target}(\nu_i^*)$. For instance, a spatial gradient in

the magnetic field may be used to excite certain portions of an ensemble, while the Rabi frequency which drives the system's evolution may be miscalibrated.

The most general type of transformation is one which is an arbitrary function of the inhomogeneity, $U(\nu_j)$. It may be a constant function, which covers the case of robust control, it may vary only with some of the parameters, or it may vary with all of the parameters. Once we have shown that arbitrary control with respect to the inhomogeneity is possible, robust control and variation with only some of the parameters follows immediately. Demonstrating this type of arbitrary control in large dimensional systems will be the goal of several later chapters. For the remainder of this chapter, however, we will focus on control of "geometric" $SU(2)$ rotations.

2.2 Inhomogeneous Control of $SU(2)$ Rotations

Our primary motivation for studying inhomogeneous rotations is that they provide a foundation upon which we may build control of more complicated systems, as we will see in Ch. 5. Additionally, $SU(2)$ rotations are one of the simplest systems for which inhomogeneous control is important, so they provide a natural starting point for the study of such control. Inhomogeneous control over $SU(2)$ rotations is also an important goal in itself, since such rotations are the basic method for controlling the evolution of individual qubits. In this section, we will study representations of $SU(2)$ rotations in two dimensions (the defining representation). However, everything we describe here applies equally well to higher dimensional irreducible representations, which will become important in Ch. 5.

The controls we consider consist of the slowly varying amplitude, Ω, and phase, ϕ, of a drive field and our goal is to find the time dependence of the controls that generates the desired unitary transformation. We model variations in the Rabi frequency and detuning as an ensemble of particles, each of which experiences a different

Hamiltonian. The evolution of each member of the ensemble is then described by the Hamiltonian,

$$H = \frac{1}{2}\eta\Omega(\cos(\phi)\sigma_x + \sin(\phi)\sigma_y) + \frac{1}{2}\Delta\sigma_z. \tag{2.4}$$

The Rabi frequency inhomogeneity is given by $\eta \quad [1-e, 1+e]$ and the detuning inhomogeneity is given by $\Delta \quad [-D, +D]$. The inhomogeneity in Rabi frequency is assumed to be positive, which is typical for most experimental situations. The phase of the drive field is assumed to be known precisely.

A wide variety of techniques already exist to control rotations in the presence of inhomogeneities [30, 28, 27]. For instance, Cummins *et. al.* developed the CORPSE pulse sequence to allow unitary rotations to be performed in a manner robust to detuning variations, while the SCROFULOUS sequence was developed to allow for robustness to Rabi frequency inhomogeneities. Both pulse sequences were developed by assuming that only one source of inhomogeneity was present, either detuning inhomogeneity in the case of CORPSE or Rabi frequency inhomogeneity in the case of SCROFULOUS. To find the appropriate pulse sequence, Cummins *et. al.* expanded the fidelity of the transformation which was actually synthesized as a Taylor series in the relevant inhomogeneity. They found a pulse sequence with no second order variation in the inhomogeneity, leaving only higher order variations. Thus, composite pulses out perform plain pulses for small to medium errors.

On the other hand, inhomogeneities may be introduced intentionally, as is done in MRI, where a spatial gradient in detuning is used to selectively excite certain portions of a sample. In this case, the goal is to perform different unitary maps for different Rabi frequencies or detunings. A typical goal is to synthesize a passband, in which a π rotation is performed within a given range of detunings, while outside

that range, the system is left unchanged. Shaped pulses of the form

$$\Omega(t) = \Omega_0 \text{sech}(\beta t),$$
$$\phi(t) = \mu \ln\left[\text{sech}(\beta t)\right], \tag{2.5}$$

with appropriate choices of β, μ, Ω_0 are known provide such a passband [40]. Much more arbitrary functions of the detuning are also possible. The Shinnar-Roux algorithm, described below, is one approach to designing such excitations [41].

In the following sections, we review the results of [30], where it was shown that arbitrary rotations, $U(\eta, \Delta)$, as a function of the inhomogeneous parameters η and Δ may be performed. The nature of the two inhomogeneities is very different, so we will use two different approaches to proving that the system may be controlled in the presence of one or the other inhomogeneity. We then combine the approaches developed for Rabi frequency and detuning inhomogeneity to show that we can perform arbitrary transformations in the presence of both inhomogeneities. The reasons why two different approaches to the Rabi frequency and detuning inhomogeneity are appropriate will be clearer after we have described them, so we postpone a comparison until after then. We conclude the section with a discussion of numerical methods for finding pulse sequences which synthesize the desired unitary.

2.2.1   Inhomogeneous Rabi Frequency

We begin with the case of Rabi frequency inhomogeneity alone, and use the Lie algebra to prove controllability. The desired transformation is first decomposed into η dependent Euler angles,

$$U(\eta) = e^{-i\alpha(\eta)\sigma_x} e^{-i\beta(\eta)\sigma_y} e^{-i\gamma(\eta)\sigma_x}. \tag{2.6}$$

The problem is thus reduced to producing sufficiently general rotations around either the x or y axis, which we will show is indeed possible. We begin by noting that merely

by changing the phase of the drive by π we can perform rotations according to the Hamiltonians $\pm\eta\sigma_x, \pm\eta\sigma_y$. Next, we make use of the Lie algebra to generate higher order powers of η through the sequence of rotations,

$$\begin{aligned}
U_{1,z}(dt) &= e^{-i\eta\sigma_y \overline{dt/2}} e^{-i\eta\sigma_x \overline{dt/2}} e^{i\eta\sigma_y \overline{dt/2}} e^{i\eta\sigma_x \overline{dt/2}} \\
&\approx e^{-\eta^2 dt[\sigma_y,\sigma_x]/2} \\
&= e^{i\eta^2\sigma_z dt}.
\end{aligned} \tag{2.7}$$

While this constitutes a higher power in η, it is not sufficient by itself to prove arbitrary controllability. Such a proof requires arbitrary rotations around *two* axes, in order to make use of the Euler angle decomposition. Thus, we need to generate

$$\begin{aligned}
U_{2,x}(dt) &= e^{i\eta\sigma_y \overline{dt/2}} U_1^\dagger\left(\sqrt{dt/2}\right) e^{-i\eta\sigma_y \overline{dt/2}} U_1\left(\sqrt{dt/2}\right) = e^{i\eta^3\sigma_x dt}, \\
U_{2,x}(dt) &= e^{-i\eta\sigma_x \overline{dt/2}} U_1^\dagger\left(\sqrt{dt/2}\right) e^{i\eta\sigma_x \overline{dt/2}} U_1\left(\sqrt{dt/2}\right) = e^{i\eta^3\sigma_y dt}.
\end{aligned} \tag{2.8}$$

Repeating this procedure shows that we can generate rotations around x or y which vary as odd powers of η. Since we are only concerned with $\eta > 0$, we can always expand the Euler angles as odd polynomials in η, and so we can generate arbitrary rotations as a function of η.

Consideration of the time required to synthesize such rotations shows that it may scale exponentially with the highest order term in the polynomial, which implies that the time required to synthesize a desired rotation with this approach may be impractically large. Thus, the preceding construction provides a proof of principle that arbitrary rotations may be synthesized, but it leaves open the question whether they may be synthesized more efficiently. In fact, it is often the case that numerical optimizations can find pulse sequences which perform the desired rotations much more rapidly, an approach we will exploit in Ch. 5

2.2.2 Detuning inhomogeneity

In the case of detuning inhomogeneity alone, we will use the Shinnar-Roux algorithm
[41]. We assume that $\Omega \gg \Delta$, which allows us to apply control pulses which are
independent of Δ. Our goal is to synthesize Δ-dependent unitary transformations,
which we can write as

$$
U(\Delta) = \begin{bmatrix} \alpha(\Delta) & -\beta^*(\Delta) \\ \beta(\Delta) & \alpha^*(\Delta) \end{bmatrix}. \tag{2.9}
$$

Rather than breaking the transformation up into its Euler angles, it is more conve-
nient in this case to work directly with $U(\Delta)$. Our goal is to synthesize a unitary
transformation U_n which approximates the desired transformation U, so we want to
show we can generate the corresponding $\alpha_n(\Delta)$ and $\beta_n(\Delta)$. We begin by breaking
the evolution up into a sequence of pulses,

$$
U(\Delta) \approx U_n = W(\theta_n, \phi_n)W(\theta_{n-1}, \phi_{n-1}) \dots W(\theta_1, \phi_1), \tag{2.10}
$$

where θ_j is the angle by which an on-resonance system is rotated and ϕ_j is the angle
of the torque vector in the xy plane of the Bloch sphere. The individual steps in
the sequence are composed of two substeps. The first substep is a microwave pulse
that is independent of Δ because we have assumed $\Omega \gg \Delta$. The second substep is
a period of time t when the microwaves are off and the system evolves under the
effects of the detuning alone. Taken together, these two substeps are

$$
W(\theta_j, \phi_j) = e^{\frac{i}{2}\theta_j(\cos(\phi_j)\sigma_x + \sin(\phi_j)\sigma_y)} e^{\frac{i}{2}\Delta\sigma_z t}, \tag{2.11}
$$

Multiplying out a sequence of such pulses, one can verify that after $2m$ pulses the
parameters which define the resulting total transformation, $\alpha_n(\Delta)$ and $\beta_n(\Delta)$, can
form a Fourier series of order $m - 1$. It may be shown that appropriate choices of
the parameters Ω_j and ϕ_j allow any such Fourier series to be generated, which is
sufficient to show that arbitrary unitary transformations may be synthesized [41].

Since the total time grows linearly with the number of pulses, the time required to synthesize a given dependence on Δ will simply grow linearly with the desired order of the Fourier series.

2.2.3 Rabi Frequency and Detuning Inhomogeneity

We have just seen how to construct a unitary that is different for different detunings by concatenating a series of unitaries with different on-resonance Rabi frequencies and phases, Eq. (2.10). So to make this also a function of Rabi frequency inhomogeneity, we need to make those rotation angles and phases a function of Rabi frequency inhomogeneity,

$$U(\delta, \eta) \approx W\left(\theta_n(\eta), \phi_n(\eta)\right) W\left(\theta_{n-1}(\eta), \phi_{n-1}(\eta)\right) \ldots W\left(\theta_1(\eta), \phi_1(\eta)\right). \qquad (2.12)$$

As before, we can break up the individual steps in the above sequence into two substeps,

$$W(\theta_l(\eta), \phi_l(\eta)) = e^{i\left(\frac{1}{2}\theta_l(\eta)(\cos(\phi_l(\eta))\sigma_x + \sin(\phi_l(\eta))\sigma_y)\right)} e^{\frac{i}{2}\Delta\sigma_z dt}. \qquad (2.13)$$

We can then decompose the first step into its Euler angles,

$$e^{i\left(\frac{1}{2}\theta_l(\eta)(\cos(\phi_l(\eta))\sigma_x + \sin(\phi_l(\eta))\sigma_y)\right)} = e^{-i\alpha_l(\eta)\sigma_x} e^{-i\beta_l(\eta)\sigma_y} e^{-i\gamma_l(\eta)\sigma_x}. \qquad (2.14)$$

We know how to generate rotations of the form $e^{-i\alpha_l(\eta)\sigma_x}$ from infinitesimal rotations of the form $e^{-i\eta\Omega\sigma_x dt/2}$. As long as we can assume $\eta\Omega \gg \Delta$ for all η, we can generate such infinitesimal rotations.

Putting it all together, if $\eta\Omega \gg \Delta$, then we can generate rotations of the form $e^{-i\eta\Omega\sigma_x dt/2}$ even in the presence of detuning inhomogeneities. These infinitesimal rotations are then used to build up the η-dependent Euler angles of Eq. (2.14). The η-dependent Euler angles then are used to synthesize the first substep of Eq. (2.13). The combined effect of both substeps of Eq. (2.13) allows us to synthesize the individual steps, which then can be used to generate the desired unitary, Eq. (2.12).

2.2.4   Comparison of the Lie algebraic and Shinnar-Roux Approach to Ensemble Control

We have used two different approaches to proving controllability in the presence of either detuning or Rabi frequency inhomogeneity because the nature of these two inhomogeneities is very different. The Shinnar-Roux approach to proving controllability in the presence of detuning inhomogeneities has the advantage that it can be used to show that the system can be efficiently controlled, in the sense that generating the mth order Fourier coefficients requires a time that only scales linearly with m. This linear scaling is to be contrasted with the exponential scaling with the order of the polynomial used to synthesize arbitrary transformations with respect to η. It would be preferable to use a Shinnar-Roux-like approach to synthesizing arbitrary transformations with respect to η. To do so, we would begin with η dependent unitaries,

$$U(\eta) = \begin{bmatrix} \alpha(\eta) & -\beta^*(\eta) \\ \beta(\eta) & \alpha^*(\eta) \end{bmatrix}. \tag{2.15}$$

Just as in the case of detuning inhomogeneities, we would need to develop a simple relationship between the $\alpha_n(\eta)$ generated by n pulses and an approximation to the desired $\alpha(\eta)$. However, it is not known whether such a simple relationship exists and so the Shinnar-Roux approach cannot be used with inhomogeneities in the Rabi frequency at present.

2.2.5   Numerical Optimization

While the preceding construction provided a proof of principle that arbitrary control with respect to the inhomogeneity was possible, it didn't necessarily provide a pulse sequence that synthesized the desired transformation in as short a time as possible. In practice, it is often the case that numerical optimization can find pulse sequences

that perform the desired unitary more rapidly than the analytic constructions just described, an approach which we will find useful in Ch. 5. In such a procedure one defines an objective function and performs a numerical search to find a pulse sequence that maximizes the objective. A common objective function is simply the fidelity, or overlap between the state which is actually synthesized and the target state, both of which may vary with η and Δ,

$$\mathcal{F} = \sum_{\eta, \Delta} \left| \psi_T(\eta, \Delta) \, \psi_A(\eta, \Delta) \right|^2, \tag{2.16}$$

where $\psi_A(\eta, \Delta)$ is the state which was actually synthesized and $\psi_T(\eta, \Delta)$ is the target state. The Rabi frequency, Ω, and phase, ϕ, of the drive are used as the controls, and are assumed to be piecewise constant. We can then consider the controls to form a vector,

$$\overline{\theta} = (\Omega_1, \phi_1, \Omega_2, \phi_2, ..., \Omega_n, \phi_n). \tag{2.17}$$

The goal is to find the vector that optimizes the objective function. While a variety of optimization routines exist [5, 7], we use either MATLAB's constrained optimization routine, $fmincon$, or its unconstrained optimization routine $fminunc$. We seed the algorithm with a random guess for the controls, and the algorithm iterates until a sufficiently high fidelity is reached. The average in Eq. (2.16) is performed on a grid in parameter space defined by choosing discrete values of η $[1-e, 1+e]$ and Δ $[D, D]$. Because the time required to calculate the average fidelity increases as we calculate the fidelity over a denser and denser grid in parameter space, we perform the optimizations over a sparse grid in parameter space. To ensure the pulses perform as desired, we then calculate the fidelity over a much denser grid in parameter space.

2.3   Conclusion

In this chapter we have described a variety of issues relating to inhomogeneous quantum control, a problem which arises in numerous settings, from NMR to atomic physics. The inhomogeneities can arise from experimental errors or may be intentionally introduced, and the goals range from robust to completely arbitrary control with respect to the inhomogeneity. Since they will form the building blocks for more complicated controls in later chapters, we have focused on $SU(2)$ unitary transformations, showing that arbitrary rotations with respect to the Rabi frequency and detuning are possible. In the presence of detuning inhomogeneity alone, we have shown that rotations may be synthesized efficiently, while the efficiency with which they may be synthesized in the presence of Rabi frequency inhomogeneity remains an open question. We have also described a numerical technique that may be used to find pulses sequences that will perform the desired unitary transformation more rapidly than the analytic constructions provided.

Chapter 3

Microwave Driven Transport

3.1 Introduction

Neutral atoms trapped in optical lattices have emerged as a rich platform for exploring a wide variety of phenomena and devices based on coherent quantum dynamics. Examples include quantum computers [44, 45, 19, 46], quantum simulators of condensed matter [47, 48], topological quantum field theory [49, 50], and quantum chaotic dynamics [51, 52, 53]. An essential ingredient in these systems is the coherent control of atomic transport in the lattice. Such transport is driven by time-dependent variations in the lattice potential and the application of external fields. In its most basic form, the atoms' ballistic tunneling between sites in a sinusoidal potential can be controlled through time-dependent modulations of the lattice depth and phase. The latter can be used to impart a time-dependent acceleration to the lattice, thereby simulating the effects of an applied electric field for electrons in a crystal that give rise to the fundamental paradigms of coherent transport in solid-state physics. Bloch oscillations [54], Wannier-Stark ladders [55], Landau-Zener tunneling [56], and dynamical localization [57] have all been demonstrated in optical lattices and explored

as mechanisms for coherent control.

More complex lattice geometries introduce additional features. For example, in a lattice of double-wells, one can drive transport between sites in a pairwise manner, assuming a sufficient barrier to ignore tunneling between different double-wells [58, 59, 60, 61]. In this case, the control problem is substantially simplified, as the relevant Hilbert space in a given time interval is restricted to a small discrete set of energy levels, as opposed to the infinite chain of levels in a sinusoidal lattice. Control across the entire lattice can be implemented by modifying the geometry so that the wells are alternatively coupled to all nearest neighbors (left or right in 1D). Double-well lattices have been explored as a platform for quantum information processing tasks such as quantum computing [20] and simulations of condensed-matter phenomena [62].

Still richer control is possible for spinor lattices where the optical potential depends on the atom's internal spin state [63]. The lattice's morphology can now be modified through variation of the laser polarization as well as intensity, lattice phase, etc. The earliest proposals for quantum logic in optical lattices via controlled collisions involved transport of the atoms via time-dependent rotation of the direction of a laser beam's polarization [44, 45, 64]. Discrete time quantum walks have also been studied with atoms in spinor lattices [65] and observed in the laboratory [66]. An alternative and perhaps more robust route to coherent control of atomic transport is to use external fields to drive spin-changing transitions that are correlated with atomic motion, similar to the scheme proposed by Foot *et al.* [67]. Such protocols can make use of the tools for robust control of spins [28, 30, 32], as developed in NMR, to the control of atomic motion in the lattice.

In this chapter we explore methods for coherent control of atomic transport with microwave-induced spin rotations between hyperfine levels and polarization-gradient lattices. Our main focus is on controllability – how the Hamiltonian that governs

the dynamics restricts the possible unitary maps that one can implement, and how to design specific waveforms to carry out a given task. We will consider here the simplest problem of noninteracting atoms in one dimension. While extensions to the interacting case are nontrivial, the current work is an important stepping-stone in that direction.

The remainder of the chapter is organized as follows. In Sec. 3.2 we establish the formalism necessary to describe spinor lattices and their interaction with external fields. We apply this to study the conditions for wave function control (the preparation of a desired spinor wave function starting from a known localized Wannier state) and prescribe a constructive algorithm for carrying out this task in Sec. 3.3 when the target wave function has finite extent. We then generalize this in Sec. 3.4 to the case of more general unitary maps for unknown initial states. We remove the constraint of finite extent and describe a numerical method which can perform state synthesis in Sec. 3.5. Finally, we summarize and give an outlook towards future research in this area in Sec. 3.6.

3.2 Microwave-Driven Spinor Lattices

An optical lattice is formed when two counter propagating beams of light are incident on a cloud of cold atoms. We will focus specifically on the alkalis. The resulting spatial variation in the light shift acts as a potential on the atoms and because of the tensor nature of atom-photon interaction, different atomic internal states will experience a different potential. In a monochromatic laser field $\mathrm{Re}\left(\mathbf{E}(\mathbf{x})e^{-i\omega_L t}\right)$, the light-shift potential takes the form,

$$V(\mathbf{x}) = -\frac{1}{4}\alpha_{ij}E_i^*(\mathbf{x})E_j(\mathbf{x}), \tag{3.1}$$

where α_{ij} is the atomic dynamic polarizability at frequency ω_L, for atoms in a particular ground-state manifold. In a one-dimensional optical lattice with polarization gradients, the electric field can be written as, $\mathbf{E}(z) = \boldsymbol{\epsilon}(z)E_0 e^{-i\omega_L t}$, where $\boldsymbol{\epsilon}(z)$ is the local polarization vector (not normalized) and E_0 is a chosen characteristic electric field. The polarizability can be conveniently decomposed in terms of a scalar, vector, and tensor component. Then the light shift for an atom in a particular ground state manifold with total angular momentum F coupled to an excited state with electronic angular momentum J' and total angular momentum F' is

$$
V_{J',F',F} = - \alpha^{(0)}_{J',F',F} E_0^2 \left[C^{(0)}_{J',F',F} \, \boldsymbol{\epsilon}(z)^{\,2} + C^{(1)}_{J',F',F} \left(\frac{\boldsymbol{\epsilon}^*(z) \times \boldsymbol{\epsilon}(z)}{i} \right) \cdot \mathbf{F} \right.
$$
$$
\left. + C^{(2)}_{J',F',F} \epsilon_i(z)\epsilon_j(z) \left(\frac{1}{2}(F_i F_j + F_j F_i) - \frac{1}{3}\mathbf{F}^2 \delta ij \right) \right], \tag{3.2}
$$

where $C^{(k)}_{J',F',F}$ are tensor coefficients derived via the Wigner-Eckart theorem and $\alpha^{(0)}_{J,F',F}$ is the characteristic polarizability given by

$$
\alpha^{(0)}_{J',F',F} = -\frac{3\lambda^3\Gamma}{32\pi^3\Delta_{J',F',F}}. \tag{3.3}
$$

The total light shift for an atom in a ground state manifold with total angular momentum F is the sum of the light shifts from all the excited states,

$$
V_F = \sum_{J',F'} V_{J',F',F}. \tag{3.4}
$$

The ground state manifold is given by the coupling of a single valence electron to a nuclear spin I, leading to two possible values of F, $F_\uparrow = I + 1/2$ and $F_\downarrow = I - 1/2$ and the two ground state manifolds are split by the hyperfine interaction. When the detuning is large compared to the hyperfine splitting, the light shift is effectively independent of the state of the nucleus, and the system evolves as if the light only coupled to the electron. Because the ground state manifold corresponds to a spin-1/2 system, it can support at most rank 1 components, and the tensor portion of the Hamiltonian must vanish [68]. The scalar and vector coefficients for the D1 transition

then become

$$C_{1/2,F}^{(0)} = \sum_{F'} C_{1/2,F',F}^{(0)} = \frac{1}{3}, \tag{3.5a}$$

$$C_{1/2,F}^{(1)} = \sum_{F'} C_{1/2,F',F}^{(1)} = \frac{g_F}{3}, \tag{3.5b}$$

$$C_{1/2,F}^{(2)} = \sum_{F'} C_{1/2,F',F}^{(2)} = 0, \tag{3.5c}$$

while for the D2 transition they are

$$C_{1/2,F}^{(0)} = \sum_{F'} C_{1/2,F',F}^{(0)} = \frac{2}{3}, \tag{3.6a}$$

$$C_{1/2,F}^{(1)} = \sum_{F'} C_{1/2,F',F}^{(1)} = -\frac{g_F}{3}, \tag{3.6b}$$

$$C_{1/2,F}^{(2)} = \sum_{F'} C_{1/2,F',F}^{(2)} = 0. \tag{3.6c}$$

If we note that

$$-\frac{1}{4}\alpha_{J',F',F}^{(0)} E_0{}^2 = \frac{\hbar\Gamma}{8} \frac{I}{I_{sat}} \frac{\Gamma}{\Delta_{J',F',F}}, \tag{3.7}$$

the resulting light shift operator for the hyperfine manifold F is,

$$V_F(z) = V_F^{(0)} \, \boldsymbol{\epsilon}(z)^2 + V_F^{(1)} \left(\frac{\boldsymbol{\epsilon}^*(z) \times \boldsymbol{\epsilon}(z)}{i} \right) \cdot \mathbf{F}, \tag{3.8a}$$

$$V_F^{(0)} = \frac{I_0}{I_{sat}} \frac{\hbar\Gamma^2}{8} \left(\frac{1}{3}\frac{1}{\Delta_{F1}} + \frac{2}{3}\frac{1}{\Delta_{F2}} \right), \tag{3.8b}$$

$$V_F^{(1)} = \frac{g_F}{3} \frac{I_0}{I_{sat}} \frac{\hbar\Gamma^2}{8} \left(\frac{1}{\Delta_{F1}} - \frac{1}{\Delta_{F2}} \right), \tag{3.8c}$$

where $\Delta_{F1,2}$ are the detunings of the ground state hyperfine manifold F from the D1 and D2 resonances, g_F is the Landé g-factor (without nuclear magneton), $I_0 = cE_0^2/8\pi$ is the characteristic intensity of the field, and I_{sat} and Γ are respectively the saturation intensity and linewidth for either the D1 or the D2 transition. Note that the ratio Γ^2/I_{sat} depends only on the dipole matrix element, and is thus the same for both D1 and D2, so we can factor it out in this way. The ellipticity in the

laser field leads to a fictitious magnetic field that varies in space, and results in a spin-dependent light shift due to the rank-1 contribution [12]. A critical aspect of optical lattices is that the trap depth scales with intensity and detuning as I_0/Δ, whereas the photon scattering rate scales as I_0/Δ^2. As a result, for a given trap depth, the photon scattering can can be minimized and the atom's evolution will be fully coherent [69].

We consider a 1D geometry consisting of counter propagating laser beams with linear polarizations, forming a relative angle θ (the "lin-θ-lin" geometry). The local polarization vector can be written, $\boldsymbol{\epsilon}(z) = \mathbf{e}_1 e^{ik_L z} + \mathbf{e}_2 e^{-ik_L z}$ where $\mathbf{e}_1 \cdot \mathbf{e}_2 = \cos\theta$, and $\mathbf{e}_1 \times \mathbf{e}_2 = \sin\theta$, with I_0 chosen to be the intensity of one of the beams. Taking the atom's quantization axis along z, substituting in Eq. (2), the optical lattice for magnetic sublevel F, m is

$$V_{F,m} = 2V_F^{(0)} + A_{F,m}(\theta)\cos\left(2k_L z - \delta_{F,m}(\theta)\right), \tag{3.9a}$$

$$A_{F,m}(\theta) = 2\sqrt{\left(V_F^{(0)}\right)^2 \cos^2\theta + m^2 \left(V_F^{(1)}\right)^2 \sin^2\theta}, \tag{3.9b}$$

$$\delta_{F,m}(\theta) = \tan^{-1}\left[\left(mV_F^{(1)}/V_F^{(0)}\right)\tan\theta\right]. \tag{3.9c}$$

Typical potentials for three different lattice angles are shown in Fig. (3.1). The potential takes the form of a sinusoidally varying potential whose depth and phase depend on the atom's magnetic sublevel. If an atom in a particular magnetic sublevel is sufficiently cold, it can sit at the minimum of its respective potential. We can change the relative position of the minima that different magnetic sublevels experience by changing the polarization between the two lattice beams, thus changing the position of an atom. In particular, if the atom begins in a superposition of different magnetic sublevels, then when the polarization is rotated, the atom's wave function will be coherently split among multiple potential wells.

The addition of a static bias magnetic field breaks the degeneracy between Zeeman sublevels within a manifold and allows us to spectrally isolate different mi-
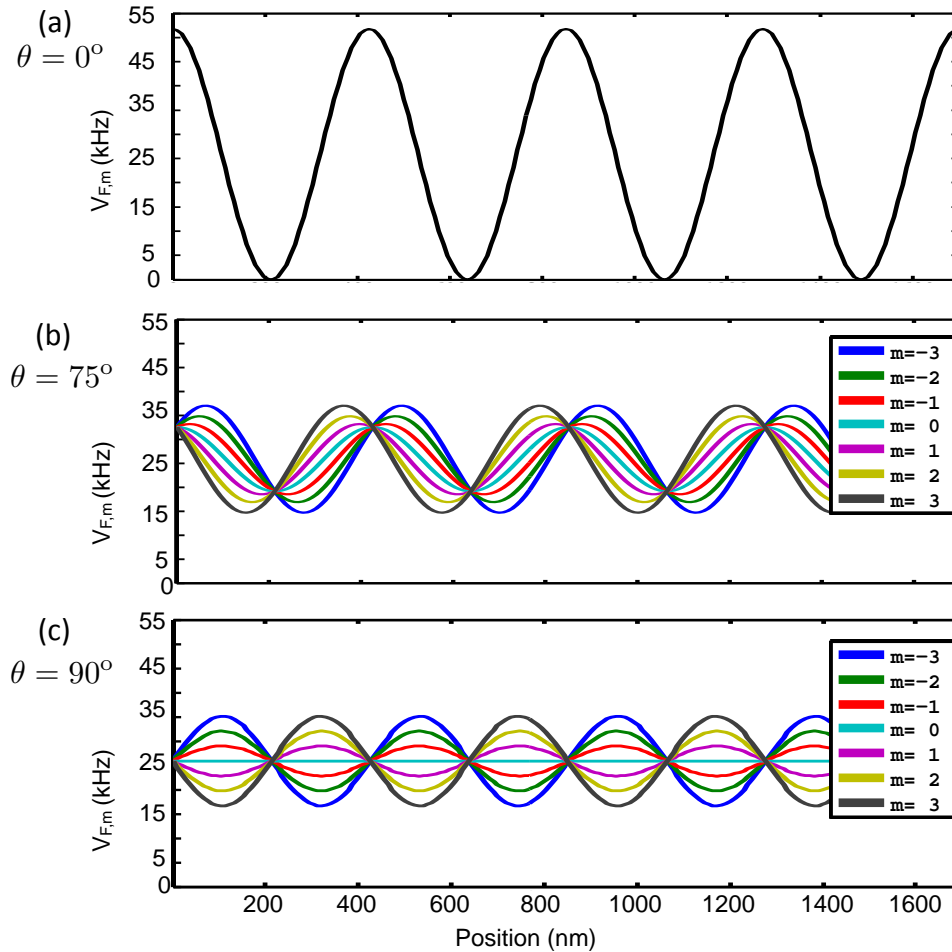
Figure 3.1: Optical lattices for a relative angle between the polarization of the lattice of (a.) 0º, (b.) 75º and (c.) 90º for the $F=3$ manifold. The $F=4$ manifold is similar, except that for $\theta = 0$ the potential for a given m moves in the opposite direction for $F=4$ than it does for $F=3$. There is no legend in (a.) the lattice is identical for all magnetic sublevels.

crowave transitions between the manifolds. For concreteness, we consider ^{133}Cs, and choose a two-state subspace $F = 4, m = 3 \equiv$, $F = 3, m = 3 \equiv$ to define a pseudo-spin-1/2 particle. Restricting to this subspace, and adding a near-resonant microwave field with magnetic field $B_{\mu w} \cos (\omega_{\mu w} t + \phi)$ that couples these spin states,

the Hamiltonian in the rotating frame takes the form $H = H_{latt} + H_{\mu w}$, where

$$H_{latt} = \frac{p^2}{2m} - V_0 \cos(2k_L z + \delta_0) \qquad - V_0 \cos(2k_L z - \delta_0) \qquad , \qquad (3.10a)$$

$$H_{\mu w} = -\frac{\Delta_{\mu w}}{2}\sigma_z - \frac{\Omega_{\mu w}}{2}(\cos\phi_{\mu w}\,\sigma_x + \sin\phi_{\mu w}\,\sigma_y). \qquad (3.10b)$$

Here $V_0 = A_{4,3} \approx A_{3,3}$, $\delta_0 = \delta_{4,3} \approx -\delta_{3,3}$, $\Omega_{\mu w} = \quad \hat{\mu} \quad B_{\mu w}/\hbar$ is the microwave resonant Rabi frequency, $\hat{\mu}$ is the atom's magnetic moment, $\Delta_{\mu w}$ is the microwave detuning from a hyperfine resonance defined by the untrapped atoms, $\phi_{\mu w}$ is the phase of the microwave oscillator, and the Pauli-σ operators are defined relative to the pseudo-spin. Note, in general $A_{F,m}$ will vary with θ. We ignore this for now and return to it later when we consider the performance of our protocol under realistic experimental conditions.

Neglecting the kinetic energy and diagonalizing the Hamiltonian leads to adiabatic or microwave-dressed potentials ,

$$V_{\pm}(z) = -V_0 \cos\delta_0 \cos(2kz) \pm \frac{1}{2}\sqrt{(2V_0 \sin\delta_0 \sin(2kz) - \Delta_{\mu w})^2 + \Omega_{\mu w}^2}. \qquad (3.11)$$

At $\Delta_{\mu w} = 0$, in the lin $\,$ lin ($\theta = \pi/2$) geometry, the adiabatic potentials yield a period $\lambda/4$ "subwavelength" lattice [70, 71, 72, 73]. In the context of a Hubbard Hamiltonian describing interacting particles moving on a lattice [10], this configuration gives us greater freedom to independently control the site-to-site tunneling rate J and the onsite interaction strength U [74]. By employing both optical and microwave fields, the lattice depth dominates the control of U while the the applied microwave dominates control of J. Moreover, the tunneling matrix element is complex, set by the microwave phase, allowing for time-reversible tunneling and further control [75, 76].

For $\theta = n\pi/2$, the adiabatic potentials take the form of a lattice of double-well potentials arising from the asymmetry for transport to the left vs. the right. The parameters characterizing the double well, including barrier height, tunneling matrix element, and energy asymmetry ("tilt"), can be controlled through variations

of lattice intensity/polarization, microwave power, and detuning. The richness of this system should enable us to control wave function coherence for spinors over multiple sites. Our early work on this subject demonstrated spinor double-well coherence driven by Larmor precession in a quasistatic magnetic field [63]. The current approach, based on applied microwave fields, should be much more robust and controllable.

While the dressed-lattice adiabatic potentials guide intuition about the transport, quantitative predictions are more accurately made by considering the band structure of the Hamiltonian, H_{latt}, in Eq. (3.10). Associated with the spin $s = \uparrow$ and $s = \downarrow$ lattices are Bloch states for band-n and quasimomentum-q, $\psi_{n,q}^{(s)}$, and Wannier states for that band and lattice site-l, $\phi_{n,l}^{(s)}$, related by the usual Fourier transform over the first Brillouin zone,

$$\phi_{n,l}^{(s)} = \int_{-1/2}^{1/2} e^{i2\pi lq} \, \psi_{n,q}^{(s)} \, dq. \tag{3.12}$$

Here and throughout, lengths are measured in units of the lattice period $L = \lambda_L/2$ and wave numbers in units of the reciprocal lattice vector $K = 4\pi/\lambda_L$. For sufficiently deep lattices and atoms in the lowest lying bands, tunneling between sites is completely negligible over the timescales of interest. In that case, the lattice Hamiltonian is diagonal both in the Bloch and Wannier bases, with no energy variation over the q or l index.

Transport dynamics are driven by the microwaves tuned to cause transitions between the ground bands associated with the spin-up and spin-down lattices. We assume that the detuning and Rabi frequency are sufficiently small so that single-band/lattice tight-binding (TB) model is a good approximation. Henceforth we drop the band index and set $n = 0$. To simplify notation, we set $\phi_{n=0,l}^{(s)} = |l,s\rangle$ and $\psi_{n=0,q}^{(s)} = |q,s\rangle$ In the Wannier basis, the total Hamiltonian in the TB approximation

is

$$H_{TB} = \sum_{l=-\infty}^{\infty} -\frac{\Delta_{\mu w}}{2}\sigma_z^l - \frac{1}{2}\left[e^{-i\phi_{\mu w}}\left(\Omega_R \sigma_+^{l,R} + \Omega_L \sigma_+^{l,L}\right) + h.c.\right], \qquad (3.13)$$

where,

$$\sigma_z^l \equiv |l,\uparrow\rangle\langle l,\uparrow| - |l,\downarrow\rangle\langle l,\downarrow|, \qquad (3.14a)$$

$$\sigma_+^{l,R} \equiv |l,\uparrow\rangle\langle l,\downarrow|, \qquad (3.14b)$$

$$\sigma_+^{l,L} \equiv |l-1,\uparrow\rangle\langle l,\downarrow|, \qquad (3.14c)$$

are the Pauli operators for two-level transitions that pairwise couple spin-down Wannier states to their neighbors on the right, $|l,\uparrow\rangle\langle l,\downarrow|$, and on the left $|l,\uparrow\rangle\langle l-1,\uparrow|$. Note, we have chosen an arbitrary labeling of the Wannier state indices by convention so that a spin-down state and spin-up state to its right are both associated with the same lattice period label, l. Because the microwaves transfer negligible momentum to the atoms, translation of the atomic wave packet is possible only when the probability amplitude of an atom overlaps between neighboring sites. The Rabi frequencies for transitions to the left or right are thus weighted by Franck-Condon factors, $\Omega_R = \langle\phi_l^\uparrow|\phi_l^\downarrow\rangle\Omega_{\mu w}$, $\Omega_L = \langle\phi_{l-1}^\uparrow|\phi_l^\downarrow\rangle\Omega_{\mu w}$. For the ground bands in the TB approximation, a large asymmetry in right-left transport and isolation of double wells arises from small asymmetry in right-left displacement of the lattice due to the Gaussian overlap of the wave packets (see Fig. (3.2)).

The combination of spinor optical lattices and microwave-driven spin dynamics provides a wide variety of parameters that can be modulated in real time during an experiment to coherently control atomic transport. In the next section we study the formal controllability of this system and develop constructive protocols to implement desired unitary maps.
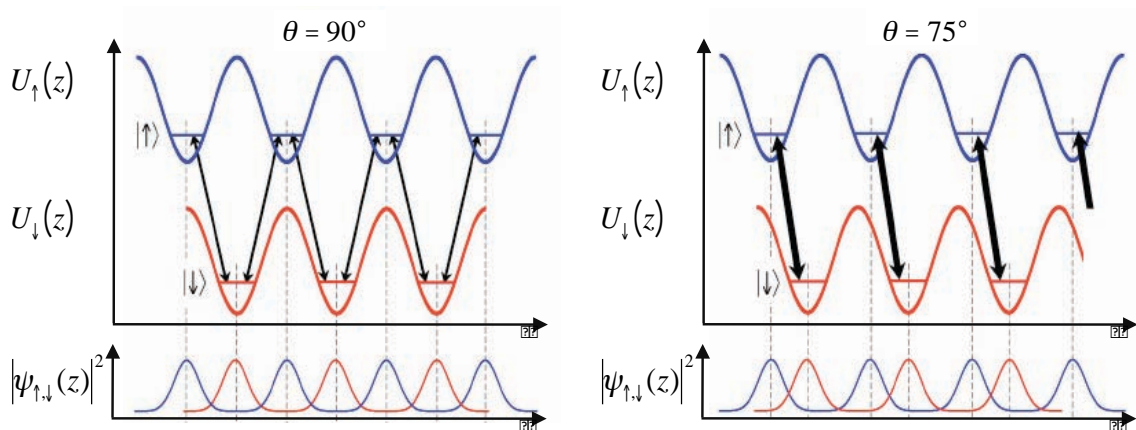
Figure 3.2: Controlled transport in lin-θ-lin. Spin-dependent lattices have a relative phase shift due to polarization gradient. In the lin ⊥ lin configuration, $\theta = 90°$, there is no asymmetry in right-left transport, and atoms can ballistically tunnel in the dressed potential. For a change of just 15° degrees away from lin ∥ lin, in a lattice with an oscillation frequency of 35kHz, the ratio of the effective tunneling rates is $\Omega_L/\Omega_R \approx 780$. The result is lattice of double wells with pair-wise tunneling couplings.

3.3 Wave packet Control

Given the time-dependent Hamiltonian at hand, a first question to address is "controllability", i.e., which class of unitary transformations can be generated by the arbitrary design of the waveforms that parameterize that Hamiltonian. We consider first the problem of preparing an arbitrary wave packet that is coherently distributed over multiple sites of the lattice, starting from an initially localized Wannier state. Unless specially designed to allow for individual site addressability [46, 33], control in a typical lattice is limited by translational invariance of the operations. Although a linear gradient breaks the translational symmetry, the controllability of the system is still limited, as we show below. We thus restrict our attention to strictly periodic lattices and allow for an additional constant force F on the atoms, as in the case of lattices held vertically in gravity, or when the overall lattice is accelerated through

time-dependent changes of the standing wave pattern.

We consider Hamiltonians which are composed of a translationally invariant part, H_0, with period L, and an applied force, F,

$$H(t) = H_0(t) + F(t)x. \tag{3.15}$$

A particular example is $H_0(t) = H_{TB}(t)$, as given in Eq. (3.13), with time-dependent variations in microwave power and/or phase. The time evolution of such a system may be written in the form of the time-ordered exponential

$$U(t) = T \exp \left\{ -i \int_0^t \left(H_0(t') + F(t')x \right) dt' \right\}. \tag{3.16}$$

Such a map has the property that if we translate the entire system by j times the period of H_0, then $U \quad e^{-i \int_0^t F(t') \, dt' \, jL} U$. If the initial state ϕ is a localized Wannier state, it satisfies

$$\phi \, T_j \, \phi \ = \delta_{j,0}, \tag{3.17}$$

where T_j translates the system by jL. If state ϕ maps to ϕ' under a unitary evolution of this form, then the evolved state satisfies this same condition, as follows from the identity

$$\phi' \, T_j \, \phi' \ = \ \phi \, U^\dagger T_j U \, \phi \ = e^{i \int_0^t F(t') \, dt' \, jL} \ \phi \, T_j \, \phi \ = \delta_{j,0}. \tag{3.18}$$

Thus any wave packet prepared by these controls must be orthogonal to itself after a translation by an arbitrary number of periods. Furthermore, since the force F has dropped out, the linear gradient does not impact the range of states that may be reached.

Are all states that satisfy this constraint reachable through some choice of the control waveforms that parameterize H_{TB} in Eq. (3.13)? To show that this is the case, we employ a protocol for constructing a desired state-to-state mapping as defined by

Eberly and Law in the context of Jaynes-Cummings ladder [77]. First note that if we can map the state ϕ to another state ϕ', and the control Hamiltonian allows the unitary map to be time-reversible, then we can map ϕ' to ϕ. Thus, in order to show that we can get from a localized state to any state satisfying Eq. (3.18), we consider the time-reversed problem of mapping such a state to the initial Wannier state.

To construct the desired map, we employ a series of $SU(2)$ rotations on resolvable subspaces of the total Hilbert space. Such a collection of disjoint two-level systems can be addressed in a lin-θ-lin spinor lattice in either an asymmetric configuration ($\theta = \pi/2$), or in a lin lin configuration in the presence a sufficiently strong uniform force so that isolated pairs of states are spectroscopically addressable (see Fig. (3.3)). Note that in the latter case, because of the presence of an external force, if we translate the system by an integer multiple of $\lambda/2$, the state picks up an extra phase due to the linear gradient. As we will see below, our construction does not require these phases, and since the construction is capable of synthesizing all reachable states, the phases are redundant. We can ignore the phases if we choose the time over which the two level unitaries operate to be an integer multiple of $2\pi/FL$, and we will assume this to be the case for the rest of this section.

We will restrict our attention to states with support strictly on a finite set of lattice sites and zero probability amplitude outside some range. Such spinors can be represented as

$$\psi = \sum_{l=l_{min}}^{l_{max}} (c_{l\downarrow} l \; + c_{l\uparrow} l \;). \tag{3.19}$$

The finite extent of the wave function, together with the condition expressed in Eq. (3.18), places a constraint on the two-level subspaces. If we translate the entire state by $l_{max} - l_{min}$ then,

$$\psi T_{l_{min}-l_{max}} \psi = c^*_{l_{min}\uparrow} c_{l_{max}\uparrow} + c^*_{l_{min}\downarrow} c_{l_{max}\downarrow} = 0. \tag{3.20}$$
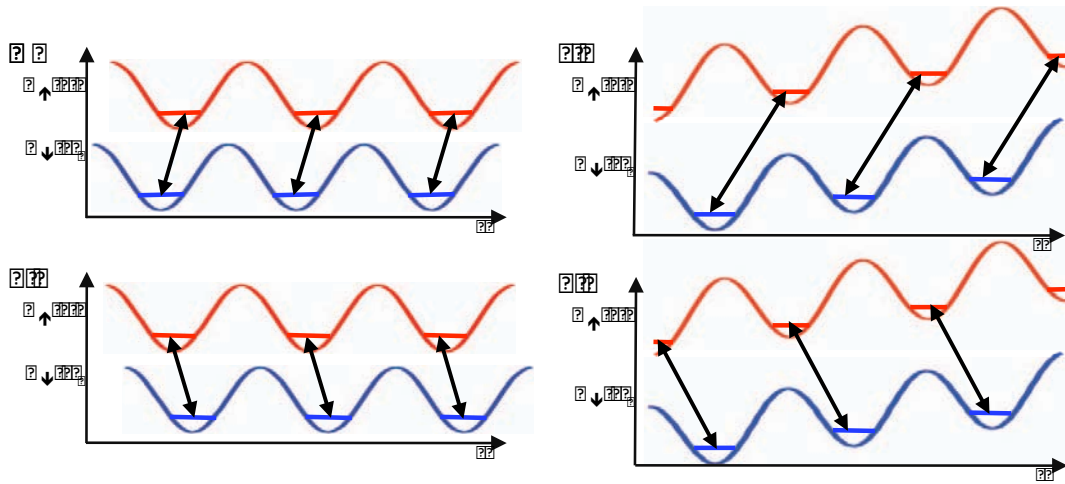
Figure 3.3: Two different methods for isolating unitary maps on two-level subspaces. In (a) and (b), the choice of polarization angles in a lin-θ-lin lattice isolate different sets of two-level systems with transport either to the right or to the left. In (c) and (d), two-level systems in a lattice with a linear gradient are spectrally addressed through their distinct microwave transition frequencies, which differ by $\pm FL/2\hbar$

Thus, in order to satisfy Eq. (3.18), the two outermost two-level subspaces must be orthogonal. Moreover, because of translational invariance, the unitary transformations that we apply are equivalent at each period of the lattice. In particular, by unitarity, if we apply a rotation operator that maps the subspace on the left end of the atomic distribution to pure spin up, the subspace at the right end of the distribution must be rotated to pure spin down.

These observations are the core of our construction (see Fig. (3.4)). A sequence of two-level rotations can be used to map a coherent superposition delocalized across the lattice to one localized at a single site in a single spin state. In the first step, a rotation is applied to map all population at the left-most two-level system ($l = l_{min}$) to spin-up according to the microwave-driven $SU(2)$ transformation,

$$S = \frac{1}{\overline{N}} \begin{bmatrix} c^*_{l_{min},\uparrow} & c^*_{l_{min},\downarrow} \\ -c_{l_{min},\downarrow} & c_{l_{min},\uparrow} \end{bmatrix}, \tag{3.21}$$
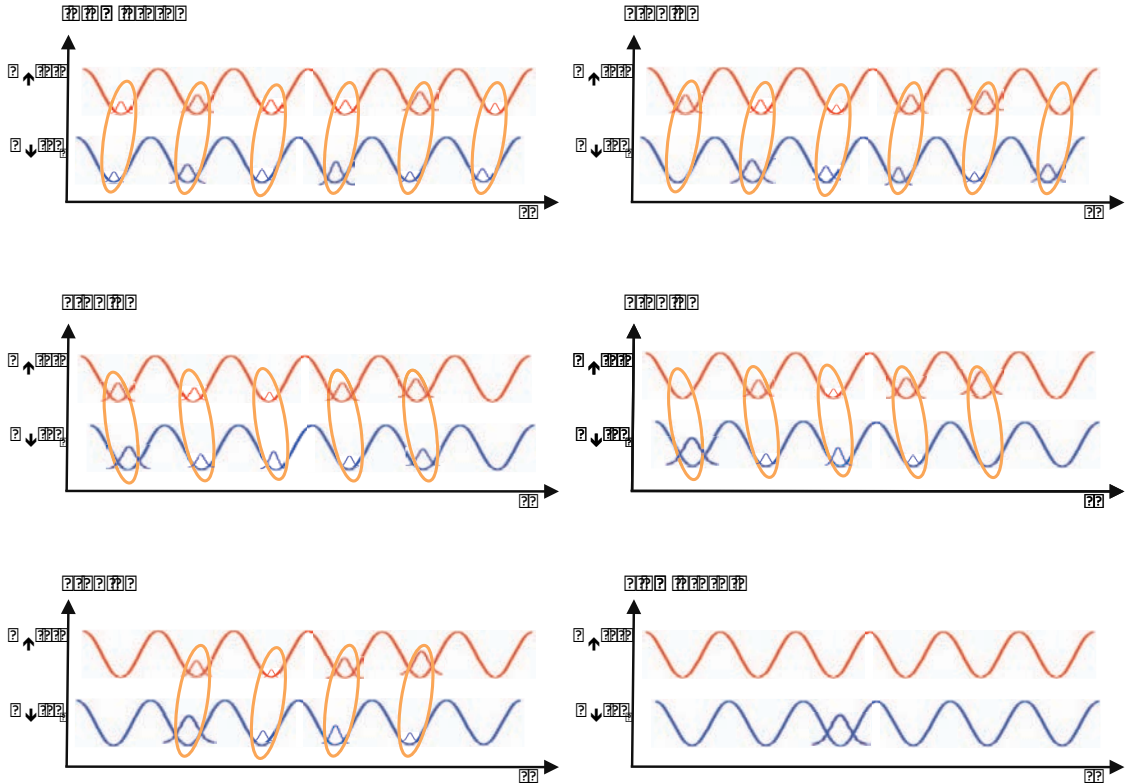
Figure 3.4: An example of state preparation through sequential $SU(2)$ rotations. The polarization of the two counter propagating beams is chosen to isolate sets of two-level systems. In step 1, population in the leftmost two-level system is mapped to entirely spin up, forcing population in the right most two level system to be entirely spin down by Eq. (3.20). In step 2, the polarization is rotated so that a different set of two level systems are coupled. In step 3, the population in the leftmost level is then mapped to entirely spin down. In step 4 the polarization is set to its original configuration and steps 1-4 are repeated until the state is localized. For this particular case, we have chosen to end the sequence spin down. A different choice for the final pulse would have ended with the state spin up.

where $N = c_{l_{min},\uparrow}{}^2 + c_{l_{min},\downarrow}{}^2$. By the translation symmetry this simultaneously maps all population at the right-most two-level system ($l = l_{max}$) to spin-down,

resulting in the spinor state

$$\psi' = c'_{l_{min}\uparrow}\,|l_{min}\uparrow\rangle + \sum_{l=l_{min}+1}^{l_{max}-1}\left(c'_{l\downarrow}\,|l\downarrow\rangle + c'_{l\downarrow}\,|l\uparrow\rangle\right) + c'_{l_{max}\downarrow}\,|l_{max}\downarrow\rangle \quad , \tag{3.22}$$

thereby shrinking the extent of the wave function by $\lambda/2$. The lattice is then reconfigured (either through polarization rotation, a change of microwave frequency, or a change in acceleration) so that the opposite neighbors are coupled (spin-down now coupled to spin-up neighbor on left). An appropriate $SU(2)$ rotation is then applied to map all population on the left most edge to spin down (simultaneously moving all population on right-most edge to spin-up). Repeating, we form a sequence of rotations that take the outer edges of the distribution and map them inwards in steps of $\lambda/4$ until all the population is localized at one Wannier state. Reversing the order of the sequence provides the desired protocol for constructing any single particle wave function in the given band and with support on a finite number of lattice sites, subject to the constraint Eq. (3.18).

To understand how such a protocol would perform in the laboratory, it is important to consider a variety of possible imperfections. Microwave pulse control can be achieved with extreme precision and will contribute negligibly to any infidelity in the state preparation. The residual errors thus arise from the effects of the optical lattice itself. Firstly, to achieve sufficient localization that a single band TBA is appropriate, and also to ensure a good double-well configuration for small rotations of the polarization away from $\theta = 90°$, an intense optical lattice is required, and this will inevitably lead to photon scattering, optical pumping, and decoherence. Secondly, because of inhomogeneity in the laser intensity, there will generally be variations in the optical potentials as function of position. This leads to microwave detuning variations across the lattice, as the spin-up and spin-down states see differential light shifts that vary from site to site. Moreover, the atomic localization will vary over the lattice, and thus so will the Frank-Condon overlap, leading to errors in the effective microwave Rabi frequencies $\Omega_{L,R}$. Finally, as the lattice polarization is rotated

and the spin-up and spin down optical potentials translated relative to each other, the spin-up and spin-down states will accumulate differential phase shifts that vary from site to site. This is equivalent to inhomogeneous microwave phase errors during subsequent pulses.

In principle, tools such as composite pulses and spin echoes can be employed to mitigate some of these errors. The NMR community has developed a variety of pulse families that are designed to be robust under different circumstances. We consider three examples: CORPSE, SCROFULOUS and BB1 [30, 27, 28]. CORPSE is robust to detuning errors to 4th order, while SCROFULOUS and BB1 are robust to errors in the Rabi frequency to 4th and 6th order, respectively. At the same time, CORPSE will perform roughly as well as uncompensated (plain) pulses with respect to errors in the Rabi frequency, while BB1 will perform roughly as well as plain pulses and SCROFULOUS worse than plain pulses with respect to errors in the detuning. One drawback to all composite pulses is that they require more time to implement than plain pulses. In the presence of photon scattering, this can degrade the performance of composite pulses and ultimately make them perform worse than the shorter plain pulses [32].

To illustrate the various tradeoffs, we consider a quantum walk implemented by alternating microwave pulse sequences with rotations of the lattice polarization to the left- and right- coupling configurations, Fig. (3.3). The microwave pulses are chosen to generate a $\pi/2$ rotation of the pseudo-spin on the Bloch sphere about the x-axis, using either a single plain pulse, or one of the three composite sequences discussed above. We choose the optical lattice to have a wavelength of 865 nm and a mean intensity of 250 W/cm^2, similar to the parameters used in a recent transport experiment by Widera *et al.* [66]. Atoms are transported to the left and right by toggling the polarization angle between $\theta_L = 75°$ and $\theta_R = 105°$. For these parameters, and working with a pseudo-spin composed of the states $F = 4, m_F = 3$

and $F = 3, m_F = 3$, the atomic oscillation frequency in the lattice potential wells is 35 kHz and the photon scattering time is $t_s = 1.3$ s. Also, the ratio of Ω_L to Ω_R or vice versa is equal to 780 when the lattice angle is in left- or right-coupling configuration, ensuring a lattice of highly isolated double wells. For the microwave drive we choose the free-space pseudo-spin Rabi frequency to be $\Omega_{\mu w} = 5.9$ kHz; this leads to an effective Rabi frequency in the lattice of $\Omega_{L,R} = 1.0$ kHz due to the Franck-Condon factor. To confirm that the single-band approximation is valid for these parameters, we studied a simple four-level model that included the two lowest Wannier states for each spin. In that case, starting from the spin-down ground Wannier state and driving microwave transitions to the spin-up ground Wannier states for a time much longer than the effective Rabi periods, the populations in the first excited Wannier states never exceed 0.95%.

To model the lattice inhomogeneity, we assume a Gaussian spread in laser intensities with a standard deviation of 2.5% about the mean. This leads to a spread in the effective microwave Rabi frequencies due to Franck-Condon inhomogeneity, $\delta\Omega_{R,L} = 24$ Hz, and a spread of microwave detunings due to the spread of differential light shifts, $\delta\Delta_{\mu w} = 8.8$ Hz. In addition, the relative phase accumulated between spin-up and spin-down states due to the variation of potential depths during transport averages $8 \times 10^{-4\circ}$, with a spread of $\delta\phi_{\mu w} = 0.002°$ due to lattice inhomogeneity. To determine the effect of these errors, we evolve a pseudo-spin through a series of lattice polarization rotations and microwave pulses for a given lattice intensity, and calculate the fidelity of the resulting state relative to the target state after each rotation-and-pulse step in the quantum walk. The overall fidelity is then obtained by averaging a number of such calculations over the distribution of lattice intensities. To account for the effects of light scattering, we multiply the fidelity by a factor of e^{-nT/t_s} where T is the time required for a single step in the quantum walk and n is the number of such steps. For the different pulse types we have $T_{plain} = 4 \times 10^{-4}t_s$, $T_{CORPSE} = 2.9 \times 10^{-3}t_s$, $T_{SCROFULOUS} = 1.7 \times 10^{-3}t_s$ and $T_{BB1} = 3.3 \times 10^{-3}t_s$,

where t_s is the photon scattering time.

The results are shown in Fig. (3.5). We find that SCROFULOUS and BB1 outperform CORPSE and plain pulses, which suggests that the dominant error is the spread in Rabi frequencies, even though $\delta\Omega_{R,L}$ is only about 2.7 times greater than $\delta\Delta_{\mu w}$. To see why this is the case, consider the effect of a spread in Rabi frequencies and a spread in detunings on the generalized Rabi frequency, $\tilde{\Omega}_{L,R} = \sqrt{(\Omega_{L,R} + \delta\Omega_{L,R})^2 + \delta\Delta_{\mu w}^2}$, where $\Omega_{L,R}$ is the mean Rabi frequency. If the generalized Rabi frequency is expanded to lowest non-vanishing order, it is first order in $\delta\Omega_{L,R}$ and second order in $\delta\Delta_{\mu w}$. As a result, the spread in effective Rabi frequencies will have greater impact than the spread in detunings. We also see that SCROFULOUS outperforms BB1 because decoherence by photon scattering is not negligible. After 25 steps left-right steps, the fidelity for SCROFULOUS is 95%, nearly 10% greater than the fidelity of plain pulses. In general, different lattice configurations – lattice intensity, detuning, rotation angle, etc. – will have different tradeoffs. Nevertheless, the example considered here demonstrates that high fidelity coherent transport can be achieved within the accessible range of experimental parameters.

3.4 Implementing General Unitary Transformations

In the previous section we studied the construction of a particular unitary transformation — mapping an initially localized Wannier state to a spinor wave function delocalized over a finite number of lattice sites, under the constraint of Eq. (3.18). In this section we consider the most general unitary map that we can implement under these constraints. We begin with the case of perfect translational invariance of the lattice. In addition, since the microwave photons possess negligible momen-
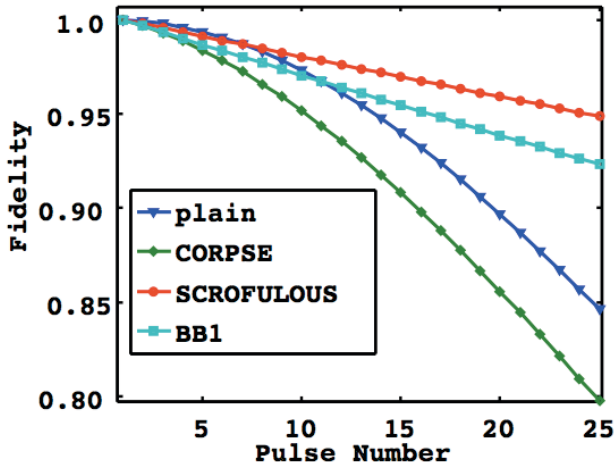
Figure 3.5:   Fidelity of a quantum walk as function of number of steps for four different pulse sequences. CORPSE corrects detuning errors up to 4th order, SCROFULOUS corrects errors in the generalized Rabi frequency up to 4th order and BB1corrects errors in the generalized Rabi frequency up to 6th order, but takes longer to perform than SCROFULOUS. Because errors in the generalized Rabi frequency and decoherence by photon scattering are the dominate errors, SCROFULOUS performs the best.

tum, only Bloch states with the same quasimomentum are coupled. Because of these symmetries, any unitarity transformation that we can synthesize will be block diagonal in the Bloch basis, where each block is a $U(2)$ matrix that connects spin-up and spin-down states with the same quasimomentum q. In the basis $\{|q, \uparrow\rangle, |q, \downarrow\rangle\}$, these blocks take the form

$$U_q = e^{i\gamma(q)} \begin{bmatrix} \alpha(q) & -\beta^*(q) \\ \beta(q) & \alpha^*(q) \end{bmatrix}, \tag{3.23}$$

where $|\alpha(q)|^2 + |\beta(q)|^2 = 1$. If the two lattices are sufficiently deep, tunneling is suppressed so γ is independent of q and can be factored out of the problem, leading to $SU(2)$ rotations in each block.

The decomposition of a translationally invariant unitary transformation into blocks of $SU(2)$ matrices has important implications for the design of arbitrary maps.

Generally the design of a time-dependent waveform that generates an arbitrary unitary map is substantially more complex than a protocol for state-to-state mapping on an initially known state [78]. Intuitively, this is because state-to-state maps only constrain one column of a unitary matrix, whereas the evolution of the orthogonal complement is not fully specified. An exception to this is the case of a spin-1/2 system. By unitarity, specifying one column of an $SU(2)$ matrix necessarily constrains the other. Since our spinor lattice is described by a collection of noninteracting spin-1/2 subspaces labeled by quasimomentum q, if we specify a state-to-state mapping of a spinor Bloch state, we specify the $SU(2)$ matrix on this block. We can achieve this using the state-mapping protocol defined in Sec. 3.3 that takes an initially localized Wannier state to a state distributed over a finite number of lattice sites. Such a map specifies a transformation on each Bloch state according to the Fourier relationship between the probability amplitudes in the Wannier and Bloch bases. Based on this relationship, we can use our state-to-state map to design a more general class of unitary maps on the wave function.

To see this explicitly, consider the unitary evolution of an initial spin-up Wannier state (take $l = 0$ without loss of generality),

$$
\begin{aligned}
U\,|0,\uparrow\rangle &= \int_{-1/2}^{1/2} dq\,(\alpha(q)\,|q,\uparrow\rangle + \beta(q)\,|q,\downarrow\rangle) \\
&= \sum_{l=-\infty}^{\infty} (c_{l,\uparrow}\,|l,\uparrow\rangle + c_{l,\downarrow}\,|l,\downarrow\rangle).
\end{aligned}
\tag{3.24}
$$

The quasimomentum functions $\alpha(q)$ and $\beta(q)$ in Eq. (3.23) are the Fourier sums of probability amplitudes in Wannier space,

$$
\alpha(q) = \sum_{l=-\infty}^{\infty} c_{l,\uparrow} e^{-i2\pi l q}, \quad \beta(q) = \sum_{l=-\infty}^{\infty} c_{l,\downarrow} e^{-i2\pi l q}.
\tag{3.25}
$$

As long as the Fourier transform of $\alpha(q)$ and $\beta(q)$ have support only over a finite extent in l, we can generate these functions by applying the state-mapping protocol

of the previous section to synthesize the probability amplitudes c_l in Eq. (3.25). For unitary maps defined by $\alpha(q)$ and $\beta(q)$ whose Fourier expansion in Wannier states does not have a strictly finite support, more general control methods are required.

We can easily generalize our result to include control through applied spatially uniform (possibly time-dependent) forces. In the TB approximation, expressed in the Wannier basis, the Hamiltonian for a linear gradient potential in dimensionless units takes the form

$$H_{grad}(t) = \sum_{l=-\infty}^{\infty} -F(t)L\left[l\,|l\rangle\langle l| + (l+\delta l(t))\,|l\rangle\langle l|\right],\qquad(3.26)$$

where $\delta l(t)$ arises due to the off-set between spin-up and down lattices. We allow for modulations of the overall force as studied in "shaken lattices" [79, 80, 81, 82, 83], and the possibility of time-dependent variations in the relative positions of the two spin states, as could be implemented through modulations in the laser beams' polarization direction. The combination of this Hamiltonian, together with microwave-driven control described by H_{TB} in Eq. (3.13), gives rise to a general unitary transformation that can be written using the interaction picture in the form,

$$U(t) = D(t)U_I(t),\qquad(3.27)$$

where,

$$D(t) = e^{-i\int_0^t H_{grad}(t')dt'} = e^{i\chi/2}\int_{-1/2}^{1/2} dq\,|q+\eta\rangle\langle q|\otimes e^{i\chi\sigma_z/2},\qquad(3.28)$$

where $\chi = \int_0^t \delta l(t')F(t')L\,dt'$, $\eta = \int_0^t F(t')dt'$, with $q+\eta$ is taken in the first Brillouin zone and

$$i\frac{d}{dt}U_I(t) = H_I(t)U_I(t),\qquad(3.29)$$

where $H_I(t) = D^\dagger(t)H_{TB}(t)D(t)$. The exact form of H_I is rather complicated, but all that really matters for our argument is that it is translationally invariant with

the period of the lattice, $T_j^\dagger H_I(t) T_j = H_I(t)$. As a result, the solution, $U_I(t)$, will be block diagonal in quasimomentum space, with the blocks consisting of $SU(2)$ rotations. Thus by Eq. (3.27), the general unitary evolution will have the form,

$$U(t) = e^{i\chi/2} \int_{-1/2}^{1/2} dq \, |q + \eta\rangle \langle q| \otimes U_q. \tag{3.30}$$

A control sequence of microwave driven rotations in a uniform lattice followed by a time dependent linear gradient can reach any unitary map of this form.

We contrast this control with that achievable in a one dimensional sinusoidal optical lattice with time-dependent uniform forces and modulation of the lattice depth in the TB approximation, without symmetry breaking for right vs. left transport. Haroutyunyan and Nienhuis derived a general expression for the propagator in such a situation.[84]. In the quasimomentum basis, the map is

$$U(t) |q\rangle = e^{-ia(t)\cos(2\pi q - b(t))} |q - \eta\rangle, \tag{3.31}$$

where

$$a(t)e^{ib(t)} = \int_0^t dt' \, \Omega(t') e^{i\eta(t')}, \tag{3.32}$$

and $\Omega(t)$ is the hopping rate between sites (symmetric to the left or to the right), and $\eta(t)$ is the same as above. The effect of the propagator is solely to induce a phase that varies as the first order Fourier coefficient, in addition to shifting all of the quasimomentum by an amount η. In contrast, Eq. (3.30) allows a broader class of unitaries to be synthesized.

3.5 Control Beyond Finite Extent

We have just seen that is possible to perform exact state synthesis and unitary design when the states and unitaries we seek to define have a finite extent. However,

suppose we had sought to synthesize states that did not have a finite extent, but rather had the property that asymptotically $c_l{}^2 \to 0$ for large l? This is equivalent to synthesizing unitaries for which the parameters that define the unitary, α and β, do not have a strictly finite Fourier transform, but rather have a Fourier transform which goes to zero for large values of l in Eq. (3.25).

At first glance, it might seem simplest to take the state we desire to synthesize, project it onto some finite width, and then use the procedures described above to synthesize it. However, this will not work because the resulting projected state will not satisfy condition 3.18. As a result, we cannot use the previous results to synthesize the projected state. Instead we must take a different approach.

Our goal is to synthesize arbitrary $SU(2)$ transformations as a function of the quasi-momentum

$$U = \int_{-1/2}^{1/2} dq \; q \quad q \; e^{-i\theta(q)\mathbf{n}(q)\cdot\boldsymbol{\sigma}/2}. \tag{3.33}$$

We can think of this system as an ensemble of different two-level systems with different control parameters for each quasimomentum, allowing us to draw on known results for ensemble control [85], as described in Ch. 2. To demonstrate that we can synthesize such unitaries, we first break them up into their Euler angles,

$$U = \int_{-1/2}^{1/2} dq \; q \quad q \; e^{-i\gamma(q)\sigma_x} e^{-i\beta(q)\sigma_y} e^{-i\alpha(q)\sigma_x}. \tag{3.34}$$

Thus, we need to show that we can generate arbitrary rotations around the x and y axis of the Bloch sphere. We consider unitary transformations of the form

$$M_1(\theta,\phi) \;=\; e^{-i\theta(\cos(\phi+2\pi q)\sigma_x-\sin(\phi+2\pi q)\sigma_y)/2}, \tag{3.35}$$

$$M_2(\theta,\phi) \;=\; e^{-i\theta(\cos(\phi)\sigma_x-\sin(\phi)\sigma_y)/2}, \tag{3.36}$$

The first unitary connects states with position indices which vary by -1, while the second connects states with position indices which are equal. In these expressions, the integral $\int_{-1/2}^{1/2} dq \; q \quad q$ is implied.

It turns out these unitaries are nearly identical to those that occur in a certain context in NMR, and so we can simply draw on the results of [85], which we restate here. Consider the pulse sequence which corresponds to translating a spin-down atom by $\lambda/2$,

$$V_1 = M_1(\pi, 0)M_2(\pi, \pi) = e^{i2\pi q\sigma_z}. \tag{3.37a}$$

If we reverse the order of the pulses we have

$$V_2 = M_2(\pi, \pi)M_1(\pi, 0) = e^{-i2\pi q\sigma_z}. \tag{3.38}$$

Then we can generate the following sequences:

$$U_{1n} = V_2^n M_2(\beta_n/2, -\pi/2)V_1^n = e^{-\frac{i}{4}\beta_n(\cos(2\pi 2nq)\sigma_y - \sin(2\pi 2nq)\sigma_x)}, \tag{3.39a}$$

$$U_{2n} = V_1^n M_2(\beta_n/2, -\pi/2)V_2^n = e^{-\frac{i}{4}\beta_n(\cos(2\pi 2nq)\sigma_y + \sin(2\pi 2nq)\sigma_x)}, \tag{3.39b}$$

$$U_{3n} = V_2^n M_2(\beta_n/2, \pi/2)V_1^n = e^{-\frac{i}{4}\beta_n(-\cos(2\pi 2nq)\sigma_y + \sin(2\pi 2nq)\sigma_x)}, \tag{3.39c}$$

$$U_{4n} = V_1^n M_2(\beta_n/2, 0)V_2^n = e^{-\frac{i}{4}\beta_n(\cos(2\pi 2nq)\sigma_x - \sin(2\pi 2nq)\sigma_y)}, \tag{3.39d}$$

$$U_{5n} = V_1^n M_2(\beta_n/2, 0)V_2^n = e^{-\frac{i}{4}\beta_n(\cos(2\pi 2nq)\sigma_x + \sin(2\pi 2nq)\sigma_y)}, \tag{3.39e}$$

$$U_{6n} = V_1^n M_2(\beta_n/2, \pi)V_2^n = e^{-\frac{i}{4}\beta_n(-\cos(2\pi 2nq)\sigma_x + \sin(2\pi 2nq)\sigma_y)}. \tag{3.39f}$$

Furthermore, we can generate approximate combinations of the sin and cos terms by combining the above unitaries as,

$$U_{1n}U_{2n} \approx e^{-\frac{i}{2}\beta_n \cos(2\pi 2nq)\sigma_y}, \tag{3.40}$$

$$U_{5n}U_{6n} \approx e^{-\frac{i}{2}\beta_n \sin(2\pi 2nq)\sigma_y}, \tag{3.41}$$

$$U_{4n}U_{5n} \approx e^{-\frac{i}{2}\beta_n \cos(2\pi 2nq)\sigma_x}, \tag{3.42}$$

$$U_{2n}U_{3n} \approx e^{-\frac{i}{2}\beta_n \sin(2\pi 2nq)\sigma_x}. \tag{3.43}$$

Thus, we see that we can synthesize arbitrary even orders of the Fourier series of the Euler angles as a function of q.

While the even terms were sufficient for NMR applications, we also need to show we can generate odd terms like $e^{-\frac{i}{2}\beta_n \sin(2\pi(2n+1)q)\sigma_y}$. To show that we can generate such terms we can make use of the sin and cos identities,

$$e^{-\frac{i}{2}\beta_n \sin(2\pi(2n+1)q)\sigma_y} = e^{\frac{i}{2}\beta_n(\sin(2\pi 2nq)\cos(2\pi q)\sigma_y + \cos(2\pi 2n)\sin(2\pi q)\sigma_y)}, \tag{3.44}$$

$$= e^{\frac{i}{2}\beta_n \sin(2\pi 2nq)\cos(2\pi q)\sigma_y} e^{\frac{i}{2}\beta_n \cos(2\pi 2q)\sin(2\pi q)\sigma_y}. \tag{3.45}$$

Thus, to generate a $\sin(2\pi(2n+1)q)\sigma_y$ term, we have to generate a term like $\sin(2\pi 2nq)\cos(2\pi q)\sigma_y$. We can do this with the following commutator,

$$[\sin(2\pi 2nq)\sigma_z, \cos(2\pi q)\sigma_x] = 2i\sin(2\pi 2nq)\cos(2\pi q)\sigma_y. \tag{3.46}$$

We've already shown that terms like $\sin(2\pi 2nq)\sigma_z$ can be generated, so all that is left to show is that $\cos(2\pi q)\sigma_x$ can be generated, which follows from

$$e^{-id\theta \cos(2\pi q)\sigma_x/2} \approx M_1(d\theta, 0)M_2(\pi, 0)M_1(d\theta, 0)M_2(\pi, \pi). \tag{3.47}$$

Since we can generate all terms of the form

$$\cos(2\pi nq)\sigma_x, \sin(2\pi nq)\sigma_x, \cos(2\pi nq)\sigma_y, \sin(2\pi nq)\sigma_y \ , \tag{3.48}$$

we can synthesize all unitaries of the form Eq. (3.33). A detailed consideration of the time required to synthesize the various Fourier coefficients is left to future work.

Similar to the case of inhomogeneous controls, while the above proof yields an understanding of what sorts of unitaries may be synthesized, it does not necessarily provide constructions which are optimal in the amount of time required to synthesize the unitaries. Once again, we can turn to numerical optimization. In this case we consider unitary transformations of the form

$$U = M_1(\theta_N, \phi_N)M_2(\theta_{N-1}, \phi_{N-1})\ldots M_1(\theta_2, \phi_2)M_2(\theta_1, \phi_1). \tag{3.49}$$

We can numerically optimize the sequence of rotation angles and phases to synthesize a desired unitary.

(a.)   Spin up population vs. q   (b.)   Spin down population vs. q
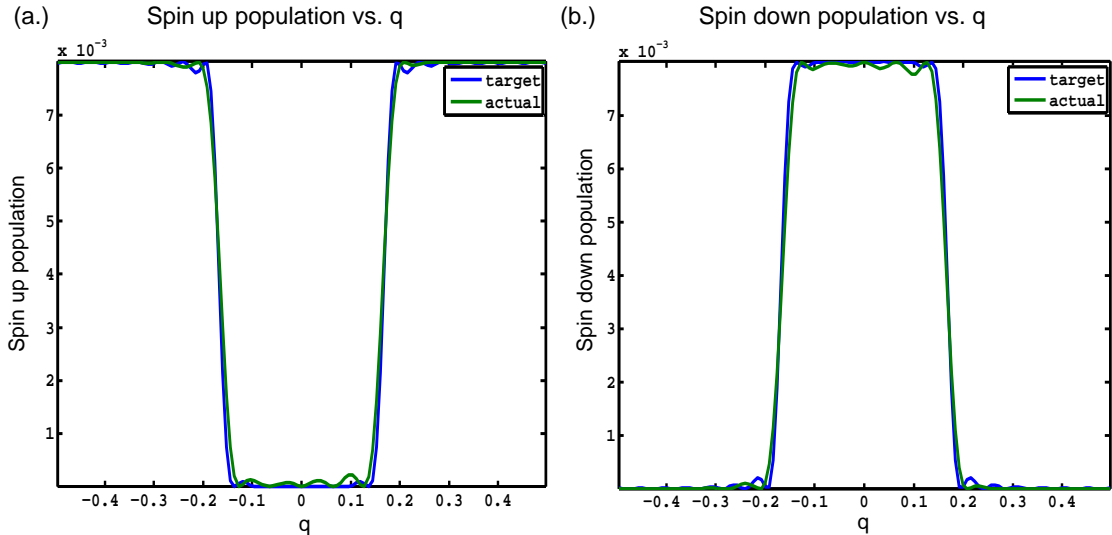
Figure 3.6:   Numerical optimization of a pulse sequence designed to invert the spin in a region $q \quad [-\frac{1}{6}, \frac{1}{6}]$. Blue is the target state, and green is the actual state after a 15 step sequence.

We see the results of such a optimization in Fig. (3.6). The initial state is $l = 0, \quad = \int_{-1/2}^{1/2} dq \, q \quad$ and the goal is to perform a unitary transformation defined by $n_x = 1$, $n_y = n_z = 0$ and

$$\theta(q) = \begin{cases} \pi & q \leq \frac{1}{6} \\ 0 & q > \frac{1}{6} \end{cases} . \tag{3.50}$$

Because $\theta(q)$ is discontinuous and we can only synthesize transformations with a finite number of terms in the Fourier series expansion, we keep only the first 20 terms in the Fourier expansion. The unitary is synthesized with 15 steps, with each step given by an application of M_1 followed by an application of M_2. As can be seen from the figure, the actual state is quite close to the desired state and a fidelity of 0.991 is achieved.

3.6   Summary and Outlook

We have described the control of transport of atoms through a microwave-dressed spinor optical lattice. Asymmetric lattices and spectral isolation provides a means to break the system up into a series of two-level systems, which aided the design of control routines. We restricted our attention to translationally invariant systems, with no local addressing, but the possibility of a uniformly applied time-dependent force. Under these conditions, we can determine the constraints of reachable states and more general reachable unitary maps that take a localized atom at one site to a state coherently extended over n sites. Based on these constraints, we propose a constructive protocol for carrying out these control tasks through a sequence of $SU(2)$ rotations acting in the two-level subspaces when the target state has a finite width. When the target state does not have a finite width, but instead goes to zero for large l, we showed it is still reachable with the available controls, and we provided a numerical approach capable of finding a sequence of pulses which performs the transformation.

An important consideration for practical implementation of our protocol is robustness of the control sequences to imperfections in the system. Because single particle transport is driven by a series of $SU(2)$ maps, certain errors may be fixed by borrowing techniques from robust control of NMR systems. We have shown how errors in the lattice intensity can be corrected with such techniques. Additional errors from spatial variations or miscalibrations in the microwave field strength and real magnetic fields can also be corrected. On the other hand, the inevitable spatial inhomogeneities in the lattice potential can lead to spatial variations in the energy common to both of the levels, which causes an overall phase on the two-level systems that varies in space. Because this phase error is not an $SU(2)$ map, it cannot be removed with the standard NMR composite pulse protocols nor their generalizations, and we must develop new methods to correct this in order to make our protocol

robust to lattice inhomogeneity. This will be a topic of future investigation.

In the current work we restricted our attention to the single band, tight-binding approximation, in uniform lattices with two spin levels. More general protocols that do not restrict the bands can be used to study the control of coupled spin and spatial degrees of freedom in a broader context. Moreover, it has recently been shown [13] that the entire hyperfine manifold of magnetic sublevels is controllable with applied rf and microwave waveforms, leaving open the possibility of combining the control of high dimensional spin and spatial degrees of freedom. In addition, breaking the translational invariance with quadratic or higher order potentials should allow the controllability of the system to be significantly enhanced. Other modifications of the spin-dependent potentials, such as the spatial variation in microwave transition frequency that arises in a strong magnetic field gradient, can in principle allow spectral addressing of individual two-level systems and extend the controllability of the system.

Finally, the techniques proposed here may also be extended to control the dynamics of many-body systems. For instance, it might be possible to use the microwave drive to synthesize more arbitrary interactions between atoms than are dictated by the static Hamiltonian. Once interactions are included in the model, many-body unitary maps can by built from maps acting on restricted subspaces, as we have done here for single particles. Such tools can play an essential role for quantum simulations of many-body Hamiltonians, both for studies of equilibrium properties such as the many-body phase diagram and non-equilibrium phenomena such as Lodschmidt echos [75] and the dynamics of phase transitions.

Chapter 4

Microwave Induced Collisions

4.1 Introduction

All quantum computation can be broken down into a series of single qubit and two qubit gates, which greatly simplifies the design of such a computer [1]. This makes possible a "ground up" design philosophy in which one first learns to perform single qubit gates, then moves on to two qubit gates between a pair of qubits, and finally learns to wire large numbers of qubits together. In atomic systems, there already exists a long history of single particle coherent control, so much work has focused on taking the next step and designing two qubit gates. The neutrality of neutral atoms causes them to interact weakly with their environment, which makes them strong candidates for a quantum computer, but also results in a relatively weak interaction between atoms. Several proposals exist which attempt to overcome that weak interaction. By placing atoms into the same potential well, it is possible to force them to interact strongly [19, 45]. Experiments implementing this idea have already been performed, with reported gate fidelities of 0.64 [20]. The long range nature of the dipole-dipole interaction reduces the need to bring atoms close together [44].

When excited to Rydberg states with large dipole moments, gate fidelities between atoms separated by $10\mu m$ of 0.72 have been reported [11, 21] .

In many of the proposals for quantum computing and quantum simulation, it is typically assumed that the effects of the interaction are sufficiently weak that they may be treated perturbatively, but this is not always this case. When the perturbative shifts become comparable to the bandgap of the lattice, perturbation theory breaks down and other methods are necessary to study the interaction. The impact of such strong interactions was first examined by Busch *et al.* [86], who found that the spectrum of two particles was substantially altered by sufficiently strong interactions between pairs of atoms by exactly solving the case of two atoms in a harmonic trap. Busch found that when there is a bound molecular state close to dissociation, the trap can alter the energy of bound state, to the point where the energy actually becomes positive. Such a trap induced effect was observed by by rf spectroscopy [87, 88].

Several studies have explored the effects of strong interactions in a many-body context. The authors of [89] used a band mapping technique and a Feshbach resonance to observe interaction induced population of higher lying bands. Theoretically, the effects of strong interactions can lead to a rich array of phases [90]. Even in relatively weakly interacting systems, recent work has shown that higher order effects may be important [91, 92]

When the interactions between atoms become strong enough, they can have an effect even when the atoms are not in the same well. This effect was first explored by Stock *et al.*, who found that under the right circumstances, the trap can lead to resonances between atomic states and bound molecular states [93, 15]. The existence of resonances between separated atoms may relax the requirement that atoms be brought directly into contact in order to interact, which could ease the design of two qubit gates. The first step towards such a gate is to design experiments which can

show the existence of such trap resonances. In this chapter we propose a spectroscopic method for probing the interactions between such atoms.

In order to study the interactions between the atoms, we place them into a lin   lin lattice in which a spin-down atom experiences a sinusoidal potential that is 90° out of phase with the spin-up potential. Once again, as described in Ch. 3, when we flip the spin of an atom, we must also change its position. In the same way, microwave driven spin flips can bring a pair of atoms in adjacent spin down wells together. Because of the interactions between the atoms, the energy levels of pairs of atoms are shifted, and these shifts may be detected by scanning the microwave frequency. For the case of weakly interacting atoms, similar ideas have been suggested as a basis for two qubit gates [67].

4.2 Trap Induced Resonance

4.2.1 Two Interacting Atoms in Harmonic Traps

Before describing the microwave spectrum, we first briefly review the trap induced-resonances first discovered by Stock *et al.* [93, 15]. The Hamiltonian for two trapped atoms can be written in terms of the individual atomic trapping potential and the molecular binding potential. For simplicity, we will for the time being assume that the two atoms can be distinguished. The Hamiltonian is,

$$H = \frac{\hat{\mathbf{p}}_1^2}{2m} + \hat{V}_a\left(\mathbf{r}_1\right) + \frac{\hat{\mathbf{p}}_2^2}{2m} + \hat{V}_b\left(\mathbf{r}_2\right) + \hat{V}_{int}\left(\mathbf{r}_1 - \mathbf{r}_2\right), \tag{4.1}$$

where V_a and V_b refer to the two traps , and V_{int} is the interaction.

If the atoms are trapped near the minima of their respective lattice potentials, then we can approximate the potential as harmonic. For two such atoms, the Hamiltonian can be separated into the center of mass (cm) Hamiltonian and the relative

coordinate (rel) Hamiltonian, which contains the binding potential.

$$H_{cm} = \frac{\hat{\mathbf{p}}_R^2}{2m} + \frac{1}{2}M\omega_{osc}^2\left(\mathbf{R} + \frac{\delta\mathbf{z_a} - \delta\mathbf{z_b}}{2}\right)^2, \tag{4.2a}$$

$$H_{rel} = \frac{\hat{\mathbf{p}}_r^2}{2m} + \frac{1}{2}\mu\omega_{osc}^2(\mathbf{r} - (\delta\mathbf{z_a} + \delta\mathbf{z_b}))^2 + \hat{V}_{int}(\mathbf{r}), \tag{4.2b}$$

where R is the center-of-mass, r is the relative coordinate, M is the total mass, μ is the reduced mass, ω_{osc} is the trap frequency and $\delta\mathbf{z_{a(b)}}$ is the location of the minimum of trap a (b) in which particle one (two) is trapped. The center of mass Hamiltonian is just a harmonic oscillator. The relative coordinate Hamiltonian contains a potential term

$$V_{total}(\mathbf{r}) = +\frac{1}{2}\mu\omega_{osc}^2(\mathbf{r} - (\delta\mathbf{z_a} + \delta\mathbf{z_b}))^2 + \hat{V}_{int}(\mathbf{r}), \tag{4.3}$$

which has a contribution from the harmonic trap as well as the molecular interaction, depicted schematically in 4.1.

Because the range over which the interactions are strong is typically a few nm, while the typical scales involved in the atoms' trap is hundreds of nm, we can approximate the interaction as a delta potential. Furthermore, because of the low energies involved in the collisions between ultracold atoms, we can limit our consideration to s-waves, for which the total angular momentum $l = 0$. In this case the interaction potential is

$$V_{int} = \frac{2\pi\hbar^2}{\mu}a\delta(\mathbf{r})\frac{\partial}{\partial r}r. \tag{4.4}$$

The scattering length, a, is a single parameter which takes into account the details of the interaction. For weak interactions the scattering length is negative for attractive potentials and positive for repulsive potentials. However, if an attractive potential is sufficiently deep that it supports bound states, then the scattering length can take on all values from positive to negative infinity. In particular, if the potential has a state close to dissociation, then the scattering length is related to the binding energy,

(a.)
$V_{total}(r)$

(b.)
$V_{total}(r)$

0          $\delta z_a + \delta z_b$ r   0 $\delta z_a + \delta z_b$ r
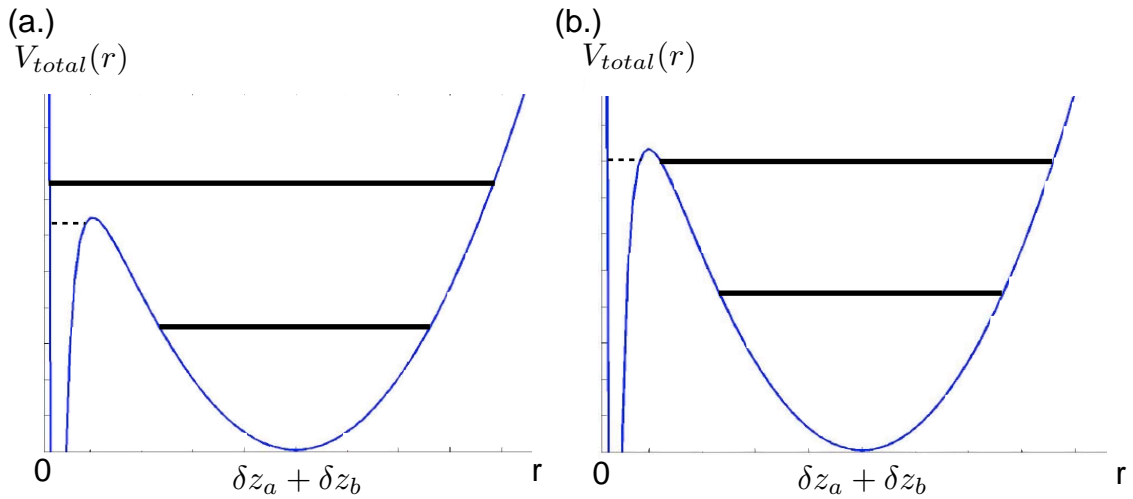
Figure 4.1: Schematic depiction of trap induced resonance. The thick line are harmonic oscillator levels. The dashed line is the molecular level. For the trap frequency in (a.) the molecular level lies in between the harmonic oscillator levels. For the trap frequency in (b.) there is a resonance between the molecular level and the trapping potential.

E_b, by

$$a^2 = \frac{\hbar^2}{2\mu E_b}. \tag{4.5}$$

The key idea behind the trap induced resonance is that the interaction potential contains a bound state near dissociation which is shifted by the harmonic potential. We can estimate the position of the bound state to be

$$U_{mol} = E_b + \frac{1}{2}\mu\omega_{osc}^2\Delta z^2, \tag{4.6}$$

where E_b is the binding energy. The position of the molecular level can be shifted by changing either ω or Δz. If the binding energy is sufficiently small, the molecular level can be brought into or out of resonance with harmonic oscillator levels, as shown in Fig. (4.1). As a particular example, the binding energy of the dimer Cs_2 is

only 6.7kHz, making it a strong candidate for observing the resonances. To perform a detailed calculation of the spectrum and to find the eigenfunctions, we follow a method originally devised by Stock et. al. [93, 15].

Busch Solutions

For the rest of the chapter, we will work in units with $\hbar$ equal to one. The first step in calculating the spectrum is to find the solution for the case in which both atoms are in the same trap, so that $\Delta z = 0$, as originally considered by Busch [86]. The basic idea is to use the spherical symmetry of the problem to write the eigenfunctions as spherical harmonics and a radial wave function,

$$\psi(\mathbf{r}) = \sum_n c_{nl} \phi_{nl}(r) Y_l^m, \tag{4.7}$$

where c_{nl} is an expansion coefficient, ϕ is the radial wave function and Y_l^m is the spherical harmonic. Only the $l = 0$ solutions are nonzero at the origin, so only these states will be effected by the presence of the interaction potential. Busch then derived a transcendental equation for the eigen-energies,

$$2\frac{\Gamma(-E/2 + 3/4)}{\Gamma(-E/2 + 1/4)} = \frac{1}{a}, \tag{4.8}$$

which can then be related to the wave functions,

$$\psi(\mathbf{r}) = \frac{1}{2}\pi^{-3/2} A e^{-r^2/2} \Gamma(-\nu) U\left(-\nu, \frac{3}{2}, r^2\right), \tag{4.9}$$

where U is the confluent hypergeometric function, ν is related to the energy by $E = 2\nu + \frac{3}{2}$, and A is a normalization factor.

Stock Solutions

Stock *et al.* [93, 15] used the Busch wave functions as a basis for the problem of two displaced traps. We can rewrite the Hamiltonian in Eq. (4.2b) as

$$H = H_{Busch} + \frac{1}{2}\mu\omega_{osc}^2\Delta z^2 - \mu\omega_{osc}^2\Delta z r \cos(\theta). \tag{4.10}$$

Next we express this Hamiltonian in the Busch basis. The first two terms are trivial in this basis. The last term, proportional to $\cos(\theta)$, couples partial waves with total angular momentum l to partial waves with total angular momentum $l \pm 1$ while leaving the projection of the angular momentum along the interatomic axis unchanged. The radial portion can be calculated using ladder operators [94]. The resulting Hamiltonian can be diagonalized numerically, giving the spectrum and the wave functions.

A plot of the energy levels of the relative coordinate Hamiltonian vs. oscillation frequency for a trap separation of $\lambda/4$ and scattering length of $2000a_B$ is shown in Fig. (4.2.a), where λ is the lattice wavelength. This separation corresponds to one atom in the spin-up potential and the other at a neighboring site in the spin-down potential. The flat lines are the expected spectra of a harmonic oscillator. In addition, one can see the molecular level shifting into and out of resonance with different harmonic oscillator levels, showing the avoided crossings of a trap induced resonance. Similarly, a plot of the energy levels taking into account the center of mass harmonic oscillator levels is shown in Fig. (4.2.b). Careful inspection shows that the spectrum consists of repetition of the relative coordinate spectrum with additional energies of $\omega_{osc}(n+3/2)$. Of particular importance, we see that at certain lattice oscillation frequencies, such as 17 kHz, the molecular level is well resolved from the harmonic oscillator levels.
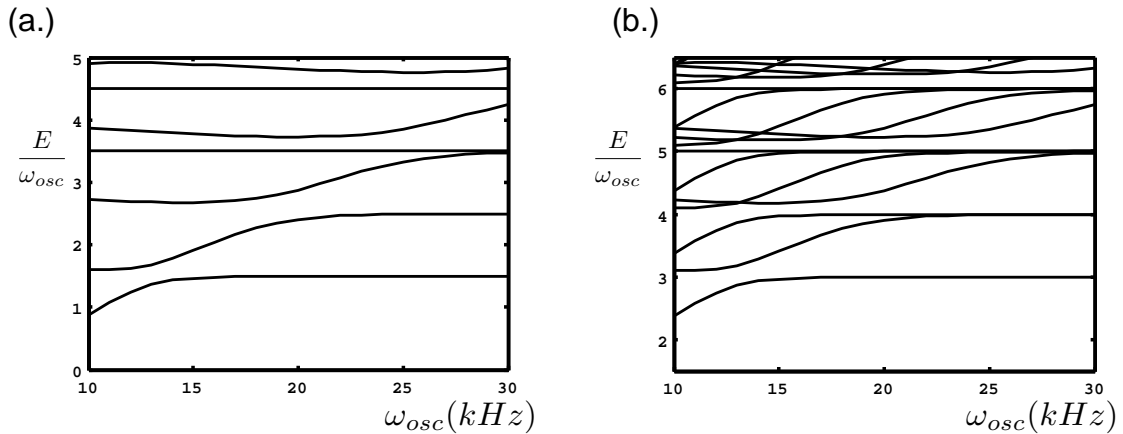
Figure 4.2: (a.) Spectrum of the relative coordinate Hamiltonian when the two atoms' traps are separated by $\lambda/4$. (b.) Full spectrum, including both the relative and center of mass coordinate Hamiltonians, when the two atoms' traps are separated by $\lambda/4$.

4.2.2 Approximating an Optical Lattice with Three Harmonic Traps

The basic experimental configuration we analyze is depicted in Fig. (4.3). We consider Cs atoms and define the spin-up and spin-down states as $\uparrow \; = \vert F = 3, m = 3 \rangle$, $\downarrow \; = \vert F = 4, m = 4 \rangle$. Two atoms are initially in neighboring wells in the spin-down optical lattice, labeled L and R. If the atoms are sufficiently cold that they lie near the minima of the lattice potentials, we can treat them as lying within harmonic oscillators. The oscillation frequency is related to the trap depth defined in Eq. (3.10b) by $\omega_{osc} = 2\sqrt{2V_0 E_R}$, where the recoil energy, E_R, is the energy imparted to an atom when the atom scatters a photon. The microwave drive flips the atoms' spins, and because of the presence of the lin$\perp$lin lattice, when we flip an atom's spin, we must also change its position as described in Ch. 3. If the microwave frequency corresponds
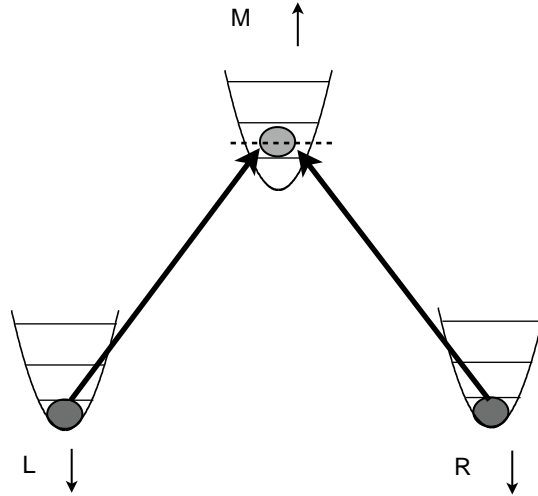
Figure 4.3: Schematic depiction of spectroscopic method for probing trap induced resonances. Solid lines are harmonic oscillator energy levels. The dashed line represents a molecular resonance.

to an interaction-induced resonance lying between any free atomic resonances, then one or the other atom will be driven into the intermediate spin up well, which is also approximated as a harmonic oscillator.

In order to detect the interaction-induced resonances, several criteria need to be fulfilled. First of all, the microwave response will contain resonances associated with single-atom transitions. For instance, atoms in a given band will be driven into the same or different bands, depending on which transition is on resonance. The two-atom resonances need to be well separated from such single-atom resonances in order to be unambiguously detected. This implies that the energy level associated with the two-atom interaction needs to lie in between the single atoms' energy levels. As can be seen from Fig. (4.2), if we choose the lattice frequency to be 17kHz, the molecular level will lie in between two levels associated with the harmonic oscillator. Thus, we can resolve a resonance here that is associated with the molecular level alone.

Secondly, we need to ensure that atoms that are initially located in neighboring wells will be driven together, rather than apart. This has two implications. We again need to make sure that the resonances we seek lie in between the single atom resonances. Then to first order, the atoms cannot tunnel throughout the lattice. The second implication is that we cannot use resonances associated with driving two atoms into the same well. While such resonances exist, the process of bringing two atoms together in the same well is a two-photon process. At the microwave powers required to drive such processes, other two photon-processes that move atoms apart are no longer negligible. Alternately, we can look for single-photon resonances associated with moving one or the other atom over a lattice site. When a single atom is moved into a neighboring well, the atoms are separated by only a quarter of the lattice wavelength, typically around 200nm. At such separations, the wave functions overlap and if the interaction is sufficiently strong, the atoms may experience a significantly shifted energy spectrum. We will concentrate on this configuration in this chapter.

Because we are only interested in situations in which single atoms will not move through the lattice, we can simplify the description of the system. In particular, we do not need to consider the entire extent of the lattice. Instead, we can focus on three lattice minima - the two spin-down minima, in which the pairs of atoms are initially located and the intermediate spin-up minima into which we seek to drive them. Approximating the potential around these minima as a harmonic trap allows us to use the spectrum calculated in the previous section to determine the response to a microwave drive. This leads to several possible configurations of the two atoms, as depicted in Fig. (4.4). The two atoms may be in separated spin down wells $\lambda/2$ apart (labeled L and R in Fig. (4.4)). Alternately, one atom may be in the middle spin up well (labeled M) while the other atom is in either the left or the right spin down well, in which case the atoms are separated by $\lambda/4$. In addition, we include the possibility for two atoms to be in the middle spin up potential. Measuring the resulting spin-up

population for different microwave frequencies then provides a probe of the molecular interactions.

The quality of the harmonic approximation can be checked by examining Fig. (4.2.b). In general, anharmonic contributions to the potential will couple the relative motion to the center of mass. Crossings and degeneracies are evident in the full spectrum. The anharmonic terms will break the degeneracies and lead to avoided crossings. As long as we choose to operate in a regime where there are no such crossings or degeneracies, we can expect the effect of such anharmonic terms to be negligible. In particular, if we set the lattice frequency to 17 kHz and tune the microwaves around the lowest molecular level, we can see there are no avoided degeneracies nearby, and so we can expect the effect of the anharmonic terms to be minimal.

In the absence of microwaves, the Hamiltonian is block diagonal with the blocks consisting of the different configurations of the atoms just described. Each of these blocks will contain a Hamiltonian corresponding to the trap induced resonances described above, with values of $\mathbf{\Delta z}$ chosen to be $\lambda/2$, $\lambda/4$ and zero. The total TIR for all four configurations is

$$H_{TIR} = H_{LR} + H_{MR} + H_{LM} + H_{MM}, \tag{4.11}$$

where H_{AB} refers to one atom in either left (L), middle (M), or right (R).

To include the effects of particle statistics and the spin degree for freedom, we take the eigenstates of the spatial Hamiltonian for distinguishable atoms, symmetrize them, and add the spin degree or freedom, yielding

$$E_{AB}; s\, s' \; = N(\; E_{1:A,2:B}; 1:s, 2:s' \; + \; E_{1:B,2:A}; 1:s', 2:s\;), \tag{4.12}$$

where N is a normalization factor. The spatial wave function, including the relative and center of mass coordinate, for a state with atom 1 at site A and atom 2 at site B and with total energy E is $E_{1:A,2:B}$. The two possible spin states are accounted for by s and s'. The corresponding symmetrized state is $E_{AB}; s\, s'$
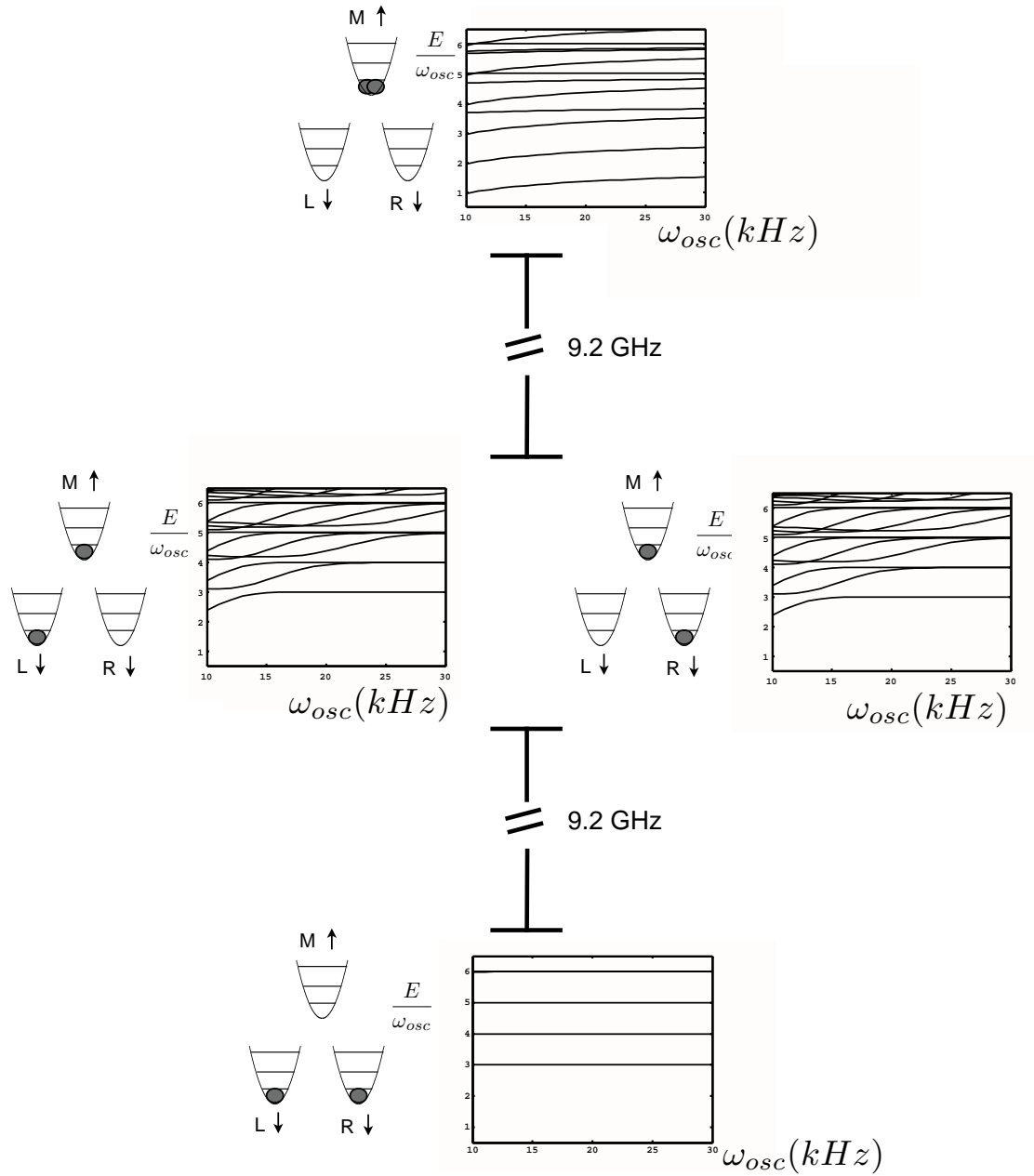
Figure 4.4: Two atom spectrum, including the spin, relative coordinate, and center of mass. The corresponding configurations of atoms in the left (L), right (R) or middle (M) are shown, along with the spin state of an atom in that trap. The graphs show the total external energy of the two atom pair.

4.3 Calculation of Microwave Spectrum

4.3.1 Microwave Hamiltonian

In order to perform a spectroscopic probe of the atomic interaction, we drive the spins with microwaves, described by a Hamiltonian

$$H_{\mu w} = \frac{1}{2}\Omega(t)\left(\sigma_x^{(1)} + \sigma_x^{(2)}\right).$$

(4.13)

Then the total Hamiltonian is

$$H = H_{TIR} + H_{\mu w}.$$

(4.14)

We work in the basis given by Eq. (4.12). In this basis, H_{TIR} is diagonal, but $H_{\mu w}$ isn't, since it will couple different spin states. We can simplify the calculation of the matrix elements in this basis somewhat by noting,

$$\langle E_{MR} | H_{\mu w} | E_{LR} \rangle = \frac{1}{2}\Omega(\langle E_{1:M,2:R} | E_{1:L,2:R} \rangle + \langle E_{1:R,2:M} | E_{1:R,2:L} \rangle),$$

(4.15)

where we have used the fact that the microwaves carry negligible momentum, and thus cannot directly move an atom from one spin-down well to another. Under this approximation,

$$\langle E_{1:M,2:R}\{1:\downarrow,2:\uparrow\} | H_{\mu w} | E_{1:R,2:L}\{1:\uparrow,2:\downarrow\}\rangle = 0,$$

(4.16a)

$$\langle E_{1:R,2:M}\{1:\uparrow,2:\downarrow\} | H_{\mu w} | E_{1:L,2:R}\{1:\downarrow,2:\uparrow\}\rangle = 0.$$

(4.16b)

We can further simplify Eq. (4.15) by noting $\langle E_{1:M,2:R} | E_{1:L,2:R} \rangle = \langle E_{1:R,2:M} | E_{1:R,2:L} \rangle$, so that

$$\langle E_{MR} | H_{\mu w} | E_{LR} \rangle = \Omega \langle E_{1:M,2:R} | E_{1:L,2:R} \rangle.$$

(4.17)

Thus, to calculate the matrix elements involved in moving an atom from either the left or right well into the center well, we need only calculate the overlap of the unsymmetrized states.

Because we are interested in observing the interactions between pairs of atoms, we must avoid many-body effects associated with a fully filled lattice. We therefore consider a lattice loaded from a thermal cloud of atoms. As a result, the lattice consists of a large number of isolated atoms plus a small number of atoms which have a neighbor. We assume for the calculations presented here about 1% of the atoms have a neighbor. Since we look for molecular resonances that occur in between lattice resonances, we can use Gaussian-shaped microwave pulses, which significantly decrease the off-resonant signal from the unpaired atoms ("singles"). The microwave power has a temporal profile of

$$\Omega(t) = \Omega_{max} e^{-(t-t_{center})/\delta_t)^2)}, \tag{4.18}$$

where $\delta_t = \frac{\sqrt{\pi}}{\Omega_{max}\langle\psi|\phi\rangle}$, $t_{center} = 2.5\delta_t$, $\psi\,\phi$ is the overlap between ground state of a harmonic oscillator centered at zero and the ground state of a harmonic oscillator centered at $\lambda/4$, and the microwaves are on for a duration $t = 0$ to $t = 5\delta_t$. The form of $\Omega(t)$ is chosen so that a particle initially in ϕ would be driven into ψ.

Finally, we consider atoms that are initially in the ground state of the harmonic potential in which they are trapped, so the projection of the atoms' relative angular momentum along the z axis, m, is zero. Because the Hamiltonian in Eq. (4.14) is symmetric under rotations around the z axis, states with differing m will not couple into one another, so we only consider dynamics in the $m = 0$ subspace.

4.3.2   Results

As can be seen in Fig. (4.4), the lattice oscillation frequency and the microwave frequency provide two parameters we can change to probe the interactions in the lattice. While the single atom resonances will follow a harmonic oscillator spectrum and thus change linearly with the oscillation frequency, we expect the position of the molecular state to vary quadratically with the oscillation frequency, as described

by Eq. (4.6). The lattice is assumed to be initially filled with 99% single atoms and 1% atom pairs in the spin down lattice. The scattering length for the atoms is taken to be $2000a_0$. The microwave pulse given by Eq. (4.18) is applied to the system. By measuring the resulting spin-up population vs. microwave frequency for different lattice oscillation frequencies, we should see a resonance associated with the molecular interaction moving relative to the single particle resonances.

Figure 4.5 shows such a series of spectra associated with Fourier-transform limited line-shapes for lattice oscillation frequencies of 16, 17 and 18kHz. The arrow indicates the position of the resonance which occurs when atoms are separated by $\lambda/4$. The large resonances at the edge of the figures are single atom resonances associated with harmonic oscillator spectrum. The other resonances are a result of two atoms being in the same well. We see the expected $\lambda/4$ resonance shifting with the oscillation frequency. We also see the the resonance is well resolved from the large background of homogeneously broadened single atoms, which show only lattice resonances as well as from other resonances associated with two-photon processes. The presence of the $\lambda/4$ peaks would provide direct experimental evidence for the trap-induced resonance.

4.4 Conclusion and Future Direction

We have described a model for the interaction of tightly confined atoms and discussed the effects of that confinement, which can give rise to trap-induced resonances. A spectroscopic method to detect those resonances was described and the expected experimental spectra were calculated. It was shown that even in the presence of a large background of homogeneously broadened single atoms, interaction induced-resonances associated with atoms $\lambda/4$ apart could be detected.

It the future, the effects of lattice inhomogeneity need to be taken into account
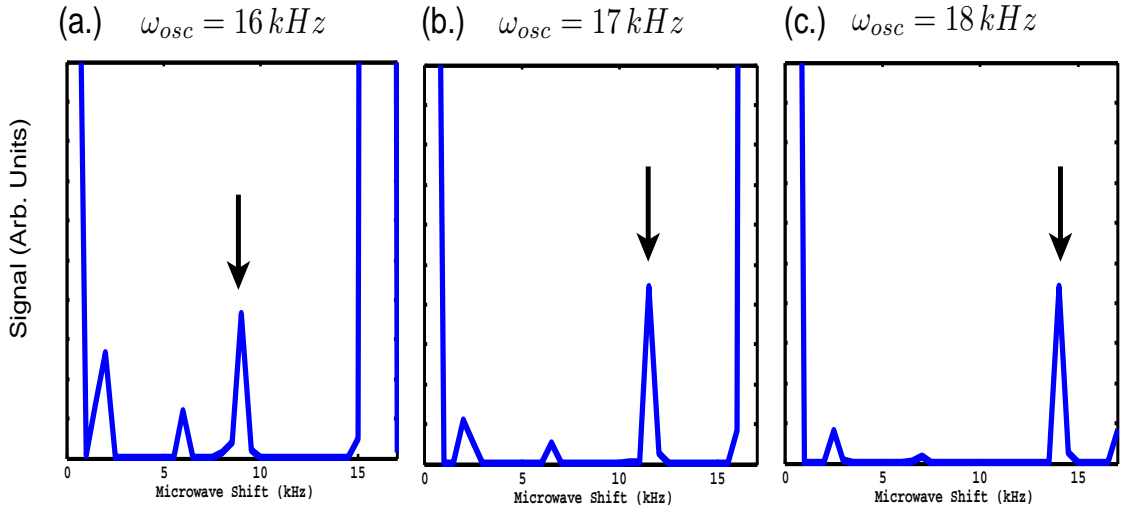
Figure 4.5: Spectrum of microwave excitations for ω_{osc} of (a.) 16kHz, (b.)17kHz and (c.) 18kHz.

since they are one of the main limitations in the current experiment. There are strong differential light shifts experienced by the spin-up, spin-down, and molecular states. In addition, the overlap integrals in Eq. 4.17 vary with the inhomogeneous lattice depth. Thus, in real experiments, the spectra will be broadened by the inhomogeneities in lattice intensity. In particular, because the molecular level has a strong quadratic dependence on the oscillation frequency, the transition frequency between the molecular state and free atomic states is significantly broadened. This broadening, in combination with low densities, makes the molecular level impossible to detect against background noise in the spectra in the current experiment. Although it is possible to choose the lattice parameters to have certain "magic" values at which the differential light shift between some of the free atomic states vanishes [95], there are no such "magic" values for the differential shifts between the free atomic and molecular levels because they experience a stronger quadratic dependence on the oscillation frequency.

There are two possible approaches to improving the current experiment. The first, is to increase the phase space density, possibly by evaporatively cooling the atoms. At higher densities there will be more pairs of atoms, making the molecular signal easier to distinguish from background noise. The second approach is to select a subensemble of atoms by using the methods of inhomogeneous control described in Ch. 2. In a lin-θ-lin lattice, for appropriate choices of θ, we can spatially isolate pairs of wells as described in Ch. 3. Because of the distance between the wells, we can neglect the interactions between pairs of atoms, leaving us with an ensemble of two-level systems. The Rabi frequency (for $\theta = 0°$) and the transition frequency will depend on the lattice intensity, and so one can selectively perform a π-rotation for chosen lattice intensities. If the atoms begin spin-up, the selected atoms will be transformed to spin-down. Strongly resonant light can blow away the remaining spin-up atoms, leaving an ensemble of spin down atoms with substantially reduced intensity inhomogeneity. After the selection process, the lattice polarization can be rotated to 90° and the spectra can be measured as described in this chapter. The best choice for the lattice polarization angle during the selection process remains an open question. While this method has the advantage that it narrows the linewidth of the spectra, it has the drawback that, by reducing the number of atoms, it also reduces the signal to noise ratio. We expect that some combination of increased density and intensity selection will yield both narrow linewidths and a high signal to noise ratio.

An additional issue is the effect of unintended microwave-induced transport of the atoms. When the microwaves are tuned near the harmonic oscillator resonances, atoms can tunnel throughout the lattice, as depicted in Fig. 3.2. Taking that movement into account will allow accurate calculation of the spectra near the harmonic oscillator resonances. Such knowledge would facilitate observation of the avoided crossings associated with the trap resonances.

There are a variety of possible applications of the trap resonances, such as the two qubit gates necessary for quantum computation. By providing tunable interactions, the trap resonances offer another possible route to study quantum phase transitions by varying the trapping parameters. Finally, the presence of trap resonances provides an additional method for quantum control of ultra-cold molecules.

Chapter 5

Qudit Control in the Presence of Inhomogeneity

5.1 Introduction

Motivated by applications ranging from chemical dynamics to computation, control over quantum systems has become an increasingly important topic [1, 2, 3, 4, 5, 14]. Computation with multilevel systems known as qudits is a natural extension of ideas involving two-level qubits, which may have some advantages [22]. In addition, most quantum systems have more than two levels, so it is reasonable to try and take advantage of the extra levels. Qudit control has already been explored in the context of alkali atoms, where Raman lasers [23]; time-dependent magnetic fields and a static quadratic light shift [24, 25]; radio-frequency (RF) and microwave controls [13, 96] have all been considered. All of these studies assumed the control parameters which drove the atoms' evolution were known precisely, but this is often not the case. Inhomogeneities can arise from experimental errors, or may be intentionally introduced to achieve further control over the system [30]. In this chapter we explore
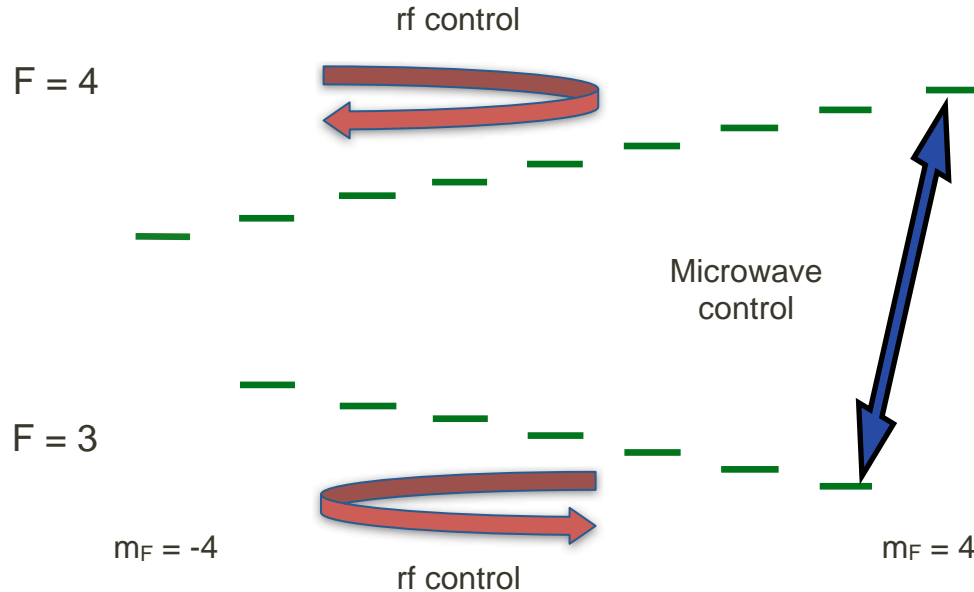
Figure 5.1: rf and Microwave control of ground state hyperfine manifold of Cs. Rotations in upper and lower manifolds are driven by rf. Because of the sign difference between the g factors in the upper and lower manifold the two rotations are in opposite directions. The microwaves are shown to be resonant with the transition between the $4,4$ and $3,3$ states.

the ability to control neutral atom qudits with rf and microwave controls in the presence of experimental inhomogeneities.

5.2   RF and Microwave control

We will focus on control of the spin state of an alkali atom in its electronic ground state. The state space is given by a tensor product between the nuclear spin I and the single valence electron spin S. The governing Hamiltonian of the system is

$$H = A\mathbf{I} \cdot \mathbf{S} + g_s \mu_B \mathbf{B}(t) \cdot \mathbf{S} - g_I \mu_N \mathbf{B}(t) \cdot \mathbf{I}. \tag{5.1}$$

The first term represents the coupling between the atom's nuclear angular momentum, $\mathbf{I}$, and the valence electron's spin, $\mathbf{S}$. The field we consider has three contributions,

$$\mathbf{B}(t) = B_0 \mathbf{e}_z + \mathbf{B}_{rf}(t) + \mathbf{B}_{\mu w}(t), \tag{5.2}$$

as depicted in Fig. (5.1). The first contribution is a static magnetic field which splits the energies of the magnetic sublevels in the linear Zeeman regime, $\mu_B B_0 \ll A$, while the next two terms are the control rf and microwave fields that drive transitions between those levels. We work in a regime in which the hyperfine coupling is significantly stronger than the interaction due to the applied magnetic fields. Then it is convenient to split the state space into a direct sum of spaces with angular total angular momentum $F_\uparrow = I + \frac{1}{2}$ and $F_\downarrow = I - \frac{1}{2}$. Since the static magnetic field does not couple the two spaces, we can use the Landé projection theorem to write it's contribution as

$$H_{B_0} = \sum_{f=\uparrow,\downarrow} g_f \mathbf{B_0} \cdot \mathbf{F}^f. \tag{5.3}$$

If we define $\Omega_0 = -g_\downarrow \mu_B B_0$ and include the hyperfine splitting, the total static Hamiltonian becomes

$$H_0 = \frac{\Delta E_{HF}}{2}(P_\uparrow - P_\downarrow) + \Omega_0(g_r F_z^\uparrow - F_z^\downarrow). \tag{5.4}$$

To take into account the small difference in magnitude and opposite signs of the g-factors in the lower and upper manifold arising from the nuclear magneton, we have defined $g_r = g_\uparrow / g_\downarrow$. The rf Hamiltonian only couples magnetic sublevels within a subspace with a given total angular momentum, so if we define $\Omega_x = -2g_\downarrow \mu_B B_x$ and $\Omega_y = -2g_\downarrow \mu_B B_y$, we can again use the Landé projection theorem to write the rf Hamiltonian as

$$H_{rf} = 2\Omega_x \cos(\omega_{rf}t - \phi_x)(g_r F_x^\uparrow - F_x^\downarrow) + 2\Omega_y \cos(\omega_{rf}t - \phi_y)(g_r F_y^\uparrow - F_y^\downarrow). \tag{5.5}$$

Transforming into a rotating frame with the transformation given by

$$U_{rf} = e^{-i\omega_{rf}t(F_z^\uparrow - F_z^\downarrow)}. \tag{5.6}$$

and making the rotating wave approximation yields

$$
\begin{aligned}
H_{rf} + H_0 =& g_r \left[\Omega_x \cos\left(\phi_x\right) - \Omega_y \sin\left(\phi_y\right)\right] F_x^\uparrow + g_r \left[\Omega_x \sin\left(\phi_x\right) + \Omega_y \cos\left(\phi_y\right)\right] F_y^\uparrow \\
& - \left[\Omega_x \cos\left(\phi_x\right) + \Omega_y \sin\left(\phi_y\right)\right] F_x^\downarrow + \left[\Omega_x \sin\left(\phi_x\right) - \Omega_y \cos\left(\phi_y\right)\right] F_y^\downarrow \\
& + \Delta(g_r F_z^\uparrow - F_z^\downarrow) + (1 - g_r)\omega_{rf} F_z^\uparrow + \frac{\Delta E_{HF}}{2}(P_\uparrow - P_\downarrow),
\end{aligned}
\tag{5.7}
$$

where $\Delta = \Omega_0 - \omega_{rf}$.

The microwave frequency and polarization are chosen so that a particular magnetic sublevel in one manifold is coupled into another magnetic sublevel in the other manifold, leaving the other states unaffected due to off-resonance effects. If the two coupled states are denoted $F^\uparrow, m_\uparrow$ and $F^\downarrow, m_\downarrow$, then we define pseudo-spin operators, $\sigma_x = F^\uparrow, m_\uparrow \ F^\downarrow, m_\downarrow + F^\downarrow, m_\downarrow \ F^\uparrow, m_\uparrow$, $\sigma_y = -i F^\uparrow, m_\uparrow \ F^\downarrow, m_\downarrow + i F^\downarrow, m_\downarrow \ F^\uparrow, m_\uparrow$ and $\sigma_z = F^\uparrow, m_\uparrow \ F^\uparrow, m_\uparrow + F^\downarrow, m_\downarrow \ F^\downarrow, m_\downarrow$, and the microwave Hamiltonian is

$$H_{\mu w} = \Omega_{\mu w} \cos(\omega_{\mu w} t - \phi_{\mu w})\sigma_x. \tag{5.8}$$

We now transform into a total rotating frame given by $U_{total} = U_{rf} e^{i\alpha t(P_\uparrow - P_\downarrow)/2}$ with $\alpha = \omega_{\mu w} - (m_\uparrow - m_\downarrow)\omega_{rf}$ and make the rotating wave approximation. Choosing the microwave frequency to be $\omega_{\mu w} = (g_\uparrow m_\uparrow - g_\downarrow m_\downarrow)\mu_B B_0 + E_{HF}$, the total Hamiltonian in the rotating frame, including the static rf and microwave contributions is

$$
\begin{aligned}
H =& g_r \left[\Omega_x \cos\left(\phi_x\right) - \Omega_y \sin\left(\phi_y\right)\right] F_x^\uparrow + g_r \left[\Omega_x \sin\left(\phi_x\right) + \Omega_y \cos\left(\phi_y\right)\right] F_y^\uparrow \\
& - \left[\Omega_x \cos\left(\phi_x\right) + \Omega_y \sin\left(\phi_y\right)\right] F_x^\downarrow + \left[\Omega_x \sin\left(\phi_x\right) - \Omega_y \cos\left(\phi_y\right)\right] F_y^\downarrow \\
& + \frac{1}{2}\Omega_{\mu w}\left(\cos\phi_{\mu w}\sigma_x - \sin\phi_{\mu w}\sigma_y\right) - \frac{1}{2}(g_r - 1)m_\uparrow \omega_{rf} F_z^\uparrow (P_\uparrow - P_\downarrow).
\end{aligned}
\tag{5.9}
$$

The controls available in this system are the powers and phases of the two rf fields, Ω_x, ϕ_x, Ω_y, ϕ_y, and the power and phase of the microwaves $\Omega_{\mu w}$, $\phi_{\mu w}$. With these controls, it can be shown that any unitary may be synthesized [13, 14].

If we choose the phases of the x and y coils to be such that $\phi_y = \phi_x + \pi/2$ and choose the powers in the two coils to be $\Omega_x = \Omega_y = \Omega$, so the the rf polarization is positive helicity circular, then the rf-field is resonant only with the lower manifold and leaves the upper manifold fixed. The Hamiltonian then reduces to

$$H = -2\Omega \cos\left(\phi_x\right) F_x^{\downarrow} + 2\Omega \sin\left(\phi_x\right) F_y^{\downarrow} + \frac{1}{2}\Omega_{\mu w}\left(\cos\phi_{\mu w}\sigma_x - \sin\phi_{\mu w}\sigma_y\right). \quad (5.10)$$

Thus we see that by the appropriate choice of powers and phases we can limit the dynamics to the lower manifold plus a single auxiliary state in the upper manifold. When we set either the microwave or the rf power to zero the control Hamiltonians are

$$H_{rf} = -2\Omega \cos\left(\phi_x\right) F_x^{\downarrow} + 2\Omega \sin\left(\phi_x\right) F_y^{\downarrow}, \quad (5.11)$$

$$H_{uw} = \frac{1}{2}\Omega_{\mu w}\left(\cos\phi_{\mu w}\sigma_x - \sin\phi_{\mu w}\sigma_y\right). \quad (5.12)$$

Each of these Hamiltonians consists of just a $SU(2)$ rotation. In the first case the rotation is in the lower hyperfine manifold, while in the second, the rotation occurs within a two-level pseudospin associated with the $F = 4, m_F = 4$ and $F = 3, m_F = 3$ levels. Thus, with the given controls, a unitary transformation on the 8-dimensional system can be constructed from a sequence of $SU(2)$ rotations. We can then leverage the methods of inhomogeneous control of rotation developed in Ch. 2 to control our qudit in the presence of inhomogeneity.

5.3   Semi-Analytic State Synthesis

5.3.1   Ideal Experimental Parameters

We study the problem of synthesizing an arbitrary state within the 8-dimensional manifold associated with the Hamiltonian of Eq. (5.10) through a series of $SU(2)$ rotations. As our fiducial initial state, we begin with all the population in the $|4,4\rangle$ state. As a proof of principle, we employ the technique originally developed by Law and Eberly [77] in which we solve the inverse problem - begin with an arbitrary state in the full 8-dimensional space, and then map it to the $|4,4\rangle$ state. Unlike the Eberly and Law approach, this method will only perform approximate state mapping, with an error that decreases exponentially with the length of the pulse.

To find a map that transfers the target state to $|4,4\rangle$, we solve a sequence of maximization problems. First we find an rf pulse that maximizes the amount of population in the state $|3,3\rangle$ and then we find a microwave rotation that maximizes the population of $|4,4\rangle$. In essence, for each rf and microwave rotation pair, we are transferring as much population as possible into the state $|4,4\rangle$. The microwave rotation can be found analytically by looking at the Bloch vector described by the subspace spanned by $\{|3,3\rangle, |4,4\rangle\}$,

$$|\phi\rangle = c_{3,3}|3,3\rangle + c_{4,4}|4,4\rangle. \tag{5.13}$$

If $\hat{n}$ is a vector that bisects the $\hat{z}$ axis of the Bloch sphere and the Bloch vector defined by $|\phi\rangle$, then a π-rotation around $\hat{n}$ will drive all the population in the $\{|3,3\rangle, |4,4\rangle\}$ subspace into $|4,4\rangle$. The rf rotation must be found numerically, though this optimization is fairly simple.

While it is not clear that this procedure results in an optimal waveform, the amount of population in the lower manifold decreases exponentially with the number of iterations. The microwave rotation can always completely transfer all population

from the $|3, 3\rangle$ state and so the only question is how much population in the lower manifold we can transfer to $|3, 3\rangle$ using rf rotations. In particular, we seek

$$\max_{\theta, \phi} \left| \langle 3, 3 | \mathcal{R}^{(3)}(\theta, \phi) | \psi \rangle \right|^2. \tag{5.14}$$

This is equivalent to the maximum value of the Husimi distribution with respect to spin-coherent states $|\theta, \phi\rangle$ in the lower hyperfine manifold. The Husimi distribution is everywhere positive, we can find a lower bound by looking at the case where the Husimi distribution is flat, i.e., the maximally mixed state. For a spin-F this value is $1/(2F + 1)$, therefore the amount of population remaining in the lower manifold, and thus our error, is bounded from below by $\epsilon = (2F/(2F + 1))^n$ where n is the number of iterations. It is important to note the we used the maximally mixed state merely to provide a lower bound to the population we can transfer into $|3, 3\rangle$ after a single rf pulse sequence. We are not bounding the performance of the microwaves, nor are we using mixed states to bound the performance over multiple steps.

5.3.2 Inhomogeneous Experimental Parameters

Inhomogeneities in the experimental parameters may occur either because these are not precisely known or because we choose to intentionally introduce some inhomogeneity in order to improve the control we have over the system. As a result of these inhomogeneities, the Hamiltonian of the actual experiment will be

$$
\begin{aligned}
H = {} & g_r \left[\Omega_x (1 + \epsilon_{rf}) \cos(\phi_x) - \Omega_y (1 + \epsilon_{rf}) \sin(\phi_y) \right] F_x^{\uparrow} \\
& + g_r \left[\Omega_x (1 + \epsilon_{rf}) \sin(\phi_x) + \Omega_y (1 + \epsilon_{rf}) \cos(\phi_y) \right] F_y^{\uparrow} \\
& - \left[\Omega_x (1 + \epsilon_{rf}) \cos(\phi_x) + \Omega_y (1 + \epsilon_{rf}) \sin(\phi_y) \right] F_x^{\downarrow} \\
& + \left[\Omega_x (1 + \epsilon_{rf}) \sin(\phi_x) - \Omega_y (1 + \epsilon_{rf}) \cos(\phi_y) \right] F_y^{\downarrow} \\
& + \frac{1}{2} \Omega_{\mu w} (1 + \epsilon_{\mu w}) \left(\cos \phi_{\mu w} \sigma_x - \sin \phi_{\mu w} \sigma_y \right) \\
& + g_r \Delta F_z^{\uparrow} - \Delta F_z^{\downarrow} + (g_r - 1) \omega_{rf} F_z^{\uparrow} - \frac{1}{2}(g_r - 1) m_{\uparrow} \omega_{rf} F_z^{\uparrow} (P_{\uparrow} - P_{\downarrow}), \tag{5.15}
\end{aligned}
$$

where ϵ_{uw} corresponds to an inhomogeneity in the microwave power, Δ corresponds to an inhomogeneity in the magnetic fields, and ϵ_{rf} corresponds to inhomogeneity in the rf coils.

We again choose the rf powers and phases so that $\phi_y - \phi_x = \pi/2$ and $\Omega_x = \Omega_y = \Omega$ then the Hamiltonian in Eq. (5.15) reduces to

$$
\begin{aligned}
H =& 2\Omega(1 + \epsilon_{rf}) \left(-\cos\left(\phi_x\right) F_x^{\downarrow} + \sin\left(\phi_x\right) F_y^{\downarrow} \right) \\
&+ \frac{1}{2}\Omega_{\mu w}(1 + \epsilon_{\mu w}) \left(\cos\phi_{\mu w}\sigma_x - \sin\phi_{\mu w}\sigma_y\right) + g_r \Delta m_\uparrow P_{m_\uparrow} - \Delta F_z^{\downarrow}.
\end{aligned} \quad (5.16)
$$

In this case, we can once again break up the evolution into a series of $SU(2)$ rotations. The individual rotations can be performed in such a way that they are completely arbitrary for different values of $\epsilon_{rf}, \epsilon_{\mu w}$ and Δ, as follows from the discussion in Ch. 2. In particular, when we set $\Omega_{\mu w} = 0$, we can synthesize unitaries which are arbitrary $SU(2)$ rotations as a function of ϵ_{rf} and Δ within the lower manifold. Likewise, if we set $\Omega_{rf} = 0$, we can synthesize arbitrary $SU(2)$ unitaries as a function of $\epsilon_{\mu w}$ and Δ within the $|3, 3\rangle$, $|4, 4\rangle$ manifold.

We now consider whether it is possible to synthesize different target states, as a function of the inhomogeneity, $\psi(\epsilon_{\mu w}, \epsilon_{rf}, \Delta)$, using the state synthesis procedure described in the previous section, beginning with the case of microwave inhomogeneities alone, $\psi(\epsilon_{\mu w})$. We will need to find an rf pulse sequence which maximizes the population in $|3, 3\rangle$, averaged over $\epsilon_{\mu w}$, so Eq. (5.14) becomes

$$
\max_{\theta,\phi} \sum_{\epsilon_{\mu w}} |\langle \theta, \phi | \psi(\epsilon_{\mu w})\rangle|^2. \quad (5.17)
$$

The rf pulses cannot distinguish between the different states $\psi(\epsilon_{\mu w})$, so this is equivalent to maximizing the population in $|3, 3\rangle$ for an initial state which is effectively an incoherent average over $\epsilon_{\mu w}$,

$$
\max_{\theta,\phi} \mathrm{Tr}\left[|\theta, \phi\rangle\langle \theta, \phi| \rho_{eff} \right], \quad (5.18)
$$

where ρ_{eff} is an effective incoherent average over $\epsilon_{\mu w}$,

$$\rho_{eff} = \sum_{\epsilon_{\mu w}} \psi(\epsilon_{\mu w}) \ \ \psi(\epsilon_{\mu w}) \ . \tag{5.19}$$

The worst case ρ_{eff} results in a completely mixed state. As described above, in the mixed state case, the rf pulses accomplish nothing, and $1/7^{th}$ of the initial population remains located in the $3,3$ state. The subsequent microwave pulse will be a π pulse which transfers all the population in $3,3$ to $4,4$. The initial state for the next rf pulse will again effectively be an incoherent mixture over $\epsilon_{\mu w}$. However, because of the preceding microwave pulse, none of the states in the sum will have any population in $3,3$, so the rf pulses can perform somewhat better than for the completely mixed state. Just as in the last section we can bound the performance by assuming a completely mixed state, so in this case at least $6/49$ of the population will be in the $3,3$ state after the rf pulses. The ensemble of initial states for the second microwave pulse sequence will in general be different for different $\epsilon_{\mu w}$ because the application of the second rf pulse will result in a complex amplitude in the $3,3$ state which varies over $\epsilon_{\mu w}$. Since the microwave pulses depend on $\epsilon_{\mu w}$, this is not equivalent to an incoherent average over $\epsilon_{\mu w}$. Furthermore, since there exist microwave pulse sequences which allow us to synthesize arbitrary unitary transformations as a function of $\epsilon_{\mu w}$, we can find a transformation which maximizes the population in $4,4$ over the range of relevant values of $\epsilon_{\mu w}$. Repeating this procedure allow us to continually increase the population in $4,4$ over the desired range of $\epsilon_{\mu w}$.

We now consider the case of rf inhomogeneities alone, $\psi(\epsilon_{rf})$. The first step is to find the rotation which maximizes the population in $3,3$ for all ϵ_{rf}. The next microwave pulse is a π-pulse which transfers all population in $3,3$ into $4,4$. In the application of the second rf pulse, we can again find a rotation which maximizes the population in $3,3$ for all ϵ_{rf}. However, the second microwave pulse will not work as needed. If ϕ is the initial state in the $3,3$, $4,4$ subspace, it will vary as a

function of ϵ_{rf},

$$\phi(\epsilon_{rf}) = c_{3,3}(\epsilon_{rf}) |3, 3\rangle + c_{4,4}(\epsilon_{rf}) |4, 4\rangle . \tag{5.20}$$

Since the microwave pulses cannot distinguish between the different states $|\phi(\epsilon_{rf})\rangle$, the initial state is effectively $\rho_{eff} = \int d\epsilon_{rf} |\phi(\epsilon_{rf})\rangle \langle\phi(\epsilon_{rf})|$. In the worst case, this could be either a state whose Bloch vector points up along the axis of the Bloch sphere or the completely mixed state. In either case, the microwaves cannot on average increase the amount of population in the $|4, 4\rangle$ state. Thus, this procedure cannot synthesis arbitrary states for different ϵ_{rf}.

However, if the target state is independent of ϵ_{rf}, the state synthesis routine can perform as required. We begin with a rf pulse sequence that is designed to be robust to ϵ_{rf}. Because the target state is independent of ϵ_{rf} and the rf pulse sequence is robust to ϵ_{rf}, the probability amplitude in $|3, 3\rangle$ after the first rf pulse sequence is independent of ϵ_{rf}. Because the probability amplitude in $|3, 3\rangle$ is independent of ϵ_{rf} and the microwave pulse sequence is independent of ϵ_{rf}, the microwaves can drive all the population in $|3, 3\rangle$ into $|4, 4\rangle$ and the resulting probability amplitude in $|4, 4\rangle$ will be independent of ϵ_{rf}. The second rf pulse sequence is again designed to be robust to ϵ_{rf} and so the resulting probability amplitudes in the $|3, 3\rangle$, $|4, 4\rangle$ subspace are independent of ϵ_{rf}. Because of this independence, the second microwave pulse sequence can move all the population into $|4, 4\rangle$. We can repeat this procedure until all the population in the $F = 3$ manifold is transferred into $|4, 4\rangle$, so we can synthesize states which are independent of ϵ_{rf}.

We now consider inhomogeneities in the detuning as might arise from an external magnetic field (either noise or intentionally applied). In this case we will need to consider the role of reversibility in the state synthesis routine with more care. We

break the Hamiltonian into two parts, $H = H_0 + H_1$, where,

$$H_0 = g_r \Delta m_\uparrow P_{m_\uparrow} - \Delta F_z^\downarrow, \tag{5.21}$$

$$H_1 = 2\Omega(1 + \epsilon_{rf}) \left(-\cos\left(\phi_x\right) F_x^\downarrow + \sin\left(\phi_x\right) F_y^\downarrow \right)$$
$$+ \frac{1}{2}\Omega_{\mu w}(1 + \epsilon_{\mu w}) \left(\cos\phi_{\mu w}\sigma_x - \sin\phi_{\mu w}\sigma_y \right). \tag{5.22}$$

For our controls, only H_1 depends on time. In the absence of a detuning inhomogeneity, the role of reversibility in the state preparation routine can be stated as follows. We seek controls such that

$$\psi_T = e^{-iH_1(t_{end})dt}...e^{-iH_1(t_1)dt} |4,4\rangle. \tag{5.23}$$

Where ψ_T is the target state. We find the appropriate controls by inverting this equation, so that

$$|4,4\rangle = e^{-iH_1'(t_1)dt}...e^{-iH_1'(t_{end})dt} |\psi_T\rangle. \tag{5.24}$$

Where $H_1'(t) = -H_1(t)$. Because we can reverse the sign of H_1 simply by changing the phase of the controls, we can reverse the state synthesis routine. The situation is more complicated in the presence of detuning inhomogeneities. We seek to perform the synthesis

$$\psi_T(\Delta) = e^{-i(H_0(\Delta)+H_1(t_{end}))dt}...e^{-i(H_0(\Delta)+H_1(t_1))dt} |4,4\rangle. \tag{5.25}$$

If we invert this equation and set $\Delta' = -\Delta$ then we find

$$e^{-i(H_0(\Delta')+H_1'(t_1))dt}...e^{-i(H_0(\Delta')+H_1'(t_{end}))dt} |\psi_T(-\Delta')\rangle = |4,4\rangle. \tag{5.26}$$

Thus we see that if we want to synthesize targets like $|\psi_T(\Delta)\rangle$ we will have to use a procedure which actually takes $|\psi_T(-\Delta)\rangle$ to $|4,4\rangle$.

There is an additional source of errors due to the fact that when we apply only the rf or the microwaves, the states that are not driven continue to evolve in the

presence of the additional magnetic field. For instance, when the rf is driving the lower manifold, the population in the $4, 4$ state will acquire a phase that depends on the detuning it experiences,

$$\phi_{44} = g_r \Delta m_\uparrow t_{rf}, \tag{5.27}$$

where ϕ_{44} is the phase acquired by $4, 4$ and t_{rf} is the total time of the rf pulse sequence. We need to include this phase when we consider the microwave pulses. However, since the microwave pulses can be arbitrary with respect to the detuning, we can compensate this effect. Similarly, during the microwave pulses, the states in the lower manifold will acquire a phase due to the inhomogeneous detuning. Once again, this phase can be compensated for in subsequent rf pulses. Therefore, we see that we can synthesize arbitrary states as a function of Δ. Similar arguments may be made when multiple inhomogeneities are present. Thus target states of the form $\psi(\epsilon_{\mu w}, \epsilon_{rf}, \Delta) = \psi(\epsilon_{\mu w}, \Delta)$ may be synthesized.

5.4 Fully Numerical State Synthesis

Although the results of the previous section indicate that it is possible to synthesize arbitrary states with a sequence of rotations, the constructions we provided there are not necessarily optimal in the amount of time required to perform a given state synthesis. Therefore, we also consider fully numerical optimization to find the desired controls. In this case, we allow the microwaves and rf to be applied simultaneously and so the evolution is no longer a simple series of rotations. Although in principle, we could we use both the power and phase of the rfs and microwaves, we have found we can attain full control of the system using only piecewise constant phases. This has the advantage that unconstrained optimizations may be performed, which often find optimum pulse sequences more rapidly than constrained optimizations.

The objective function in this case is simply the fidelity averaged over the inhomogeneous spread in $\epsilon_{rf}, \epsilon_{\mu w}$ and Δ,

$$\mathcal{F} = \sum_{\epsilon_{rf}, \epsilon_{\mu w}, \Delta} \left| \psi_T(\epsilon_{\mu w}, \Delta) \, \psi_A(\epsilon_{rf}, \epsilon_{\mu w}, \Delta) \right|^2, \tag{5.28}$$

where $\psi_T(\epsilon_{\mu w}, \Delta)$ is the target state and $\psi_A(\epsilon_{rf}, \epsilon_{\mu w}, \Delta)$ is the state which is actually synthesized from a given control sequence. For the actual optimization, we use MATLAB's unconstrained optimization routine, $fminunc$. This works similarly to the routine used to optimize geometrical rotations described in Sec. 2.2.5, though the unconstrained optimizations often find optimal sequences faster than constrained optimization.

5.5 Results

We now present results from several optimizations, beginning with targets which are meant to be independent of experimental errors. In all cases, we perform optimizations for 20 states chosen according to the Haar of measure SU(d) and then averaged the fidelity over the results for different states. The pulse sequences found either using the semi-analytic or fully numerical approaches consist of a series of steps of duration $125 \mu s$ during which the power and phase of the microwaves and rf is held constant.

The pulses sequences found according to the fully numerical approach allowed the microwaves and rf to be present simultaneously. The rf Larmor frequency on the lower hyperfine manifold from a single coil was a constant 1.5 kHz throughout the sequence, while the microwave Rabi frequency was 3.5 kHz, and was also constant. The phases of the microwave and rf were constant during each step, but changed from step to step. For the fully numerical method, a fixed end time is chosen, which sets the number of steps, and the algorithm is looped until a target fidelity of 0.99

is reached.

The pulse sequences found via the semi-analytic approach consisted of a fixed number of steps with only rf present, followed by a fixed number of steps with only microwaves present. The number of steps depended on the errors as described below. Both the power and phase of the driving field were allowed to change between steps. We allowed both the power and phase to vary to insure that the limitations of this approach, discussed below, are not the result of insufficient controls. The maximum rf power in a single pair of coils was 1.5 kHz, while the maximum microwave Rabi frequency was 3.5kHz. The semi-analytic method does not have a specified end time, so for each state we repeat the optimization 10 times and pick the optimization with the shortest time.

We begin by comparing the results for the approach based on the semi-analytic method to the fully numerical method. In the first case we optimize for errors of up to 1% in ϵ_{rf}, $\epsilon_{\mu w}$ and Δ. In both methods, the pulse sequences are found by optimizing the fidelity on a grid in parameter space defined by $\epsilon_{rf} = 0, \pm 0.01$, $\epsilon_{\mu w} = 0, \pm 0.01$ and $\Delta = 0, \pm 0.01\Omega_{rf}$, then averaged over that grid. To ensure that the pulse sequences perform as desired, we then calculate the fidelity on a grid with 15 evenly spaced points between $\pm 1\%$ in those parameters.

The results for the semi-analytic method are shown in Fig. (5.2). The total time to reach a fidelity greater than 0.99 was found to be 3.94 ms, averaged over the 20 states. The rf pulse sequences consisted of 3 steps during which the microwaves were turned off. The microwave pulse sequences likewise consisted of 3 steps during which the rf was turned off. As can be seen from the figure, a fidelity of over 0.99 is maintained over the range of parameters, and the fidelity averaged over that range is 0.997. The results of the fully numerical method are shown in Fig. (5.3). As can be seen from the figure, a fidelity of over 0.99 is maintained throughout the parameter range, and the fidelity averaged over that range is 0.994. Moreover, the fully numerical sequence

takes only 1 ms; nearly a factor of 4 speed up compared to the sequence of rotations. Thus, we see that for inhomogeneities of 1%, both approaches achieve high fidelity, but the sequence found via fully numerical optimization can do so in significantly less time.
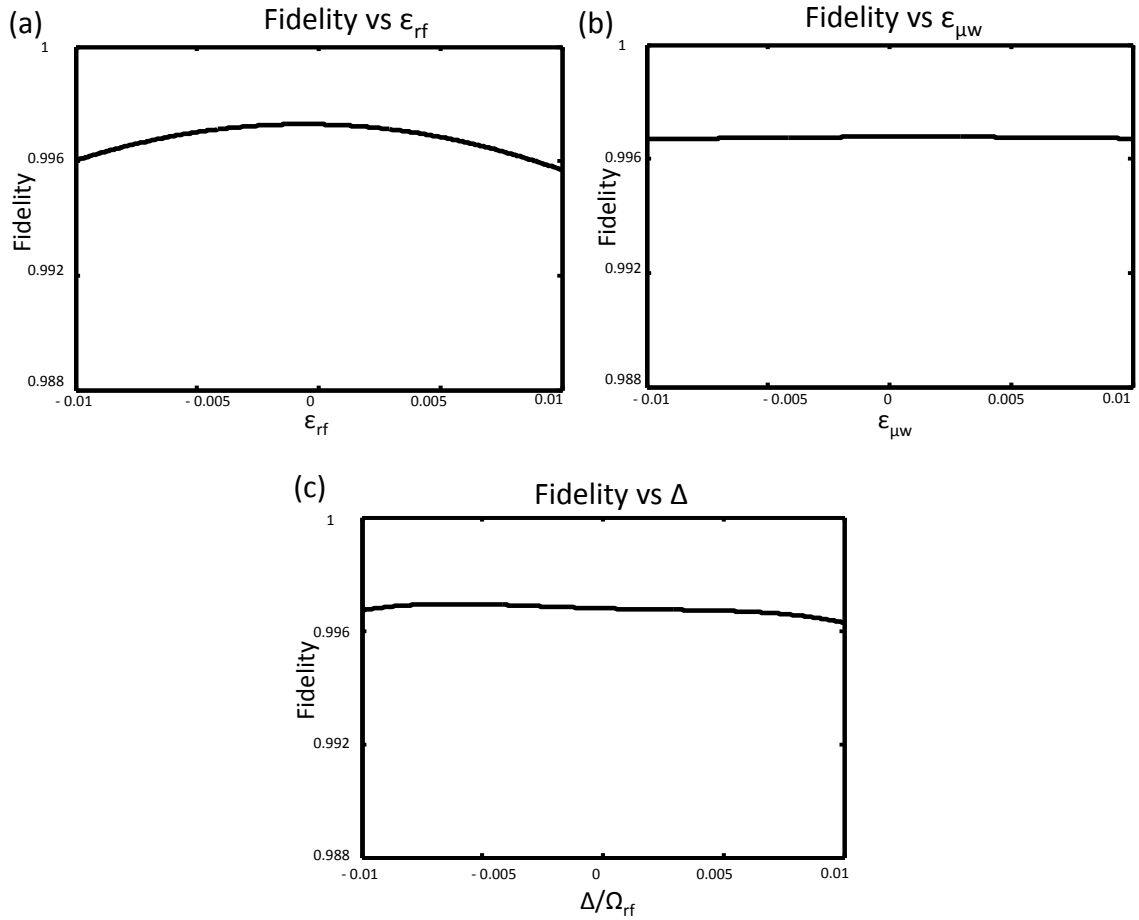

Figure 5.2: Fidelity of semi-analytic state preparation vs 1% errors in ϵ_{rf}, $\epsilon_{\mu w}$, and Δ/Ω_{rf}. In (a.) the fidelity is averaged over $\epsilon_{\mu w}$ and Δ/Ω_{rf} and plotted vs. ϵ_{rf}. Similarly in (b.) the fidelity is plotted vs. $\epsilon_{\mu w}$ and averaged over the other two variables. In (c.) the fidelity is plotted vs. Δ/Ω_{rf} and averaged over the other two variables.

Figure 5.3: Fidelity of fully numerical state preparation vs 1% errors in ϵ_{rf}, $\epsilon_{\mu w}$, and Δ/Ω_{rf}. In (a.) the fidelity is averaged over $\epsilon_{\mu w}$ and Δ/Ω_{rf} and plotted vs. ϵ_{rf}. Similarly in (b.) the fidelity is plotted vs. $\epsilon_{\mu w}$ and averaged over the other two variables. In (c.) the fidelity is plotted vs. Δ/Ω_{rf} and averaged over the other two variables.
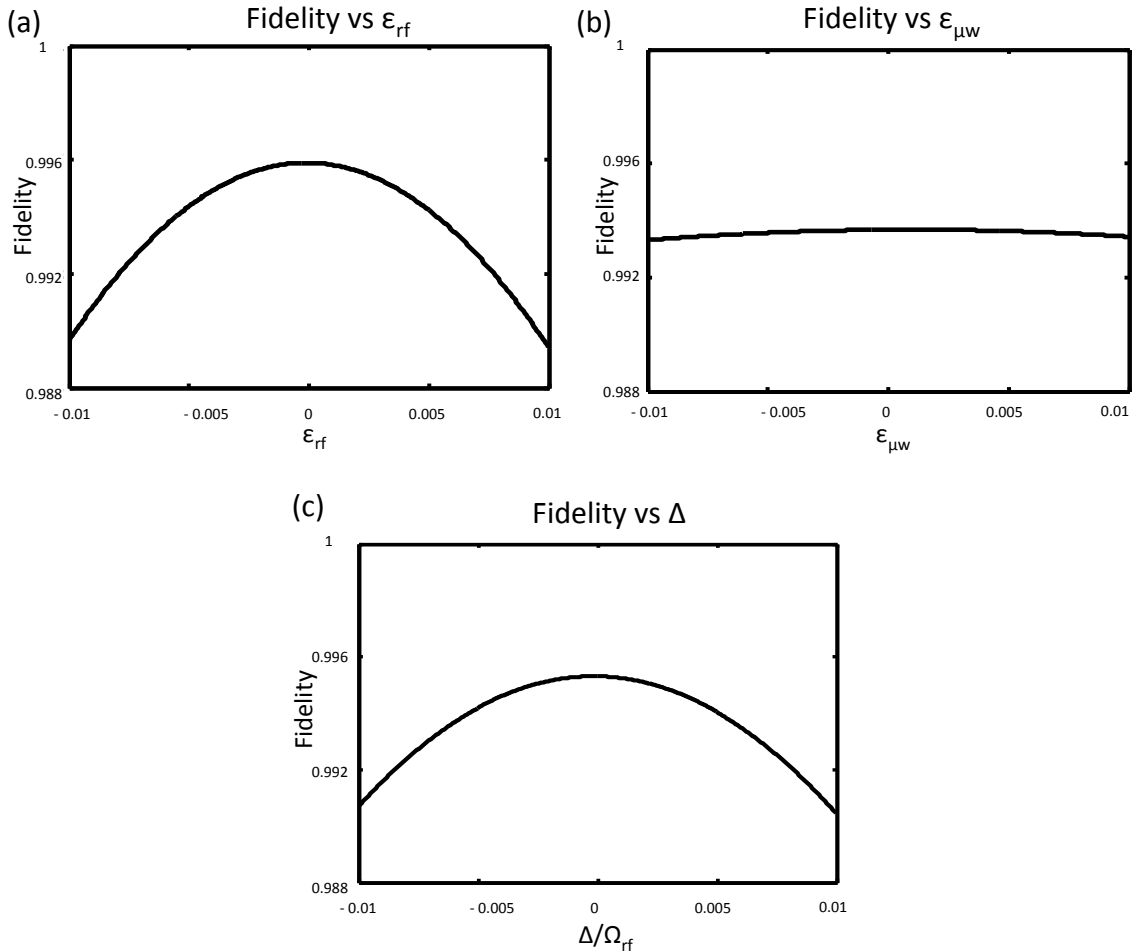
For errors beyond about 1%, the optimizations required to synthesize the state by the semi-analytic method become increasingly problematic. The main problem is an interplay between the rf power inhomogeneity and the detuning inhomogeneity. As noted in Sec. 5.3.2, problems arise if the rf pulses do not leave the probability

amplitudes in the $3, 3$ state the same for all ϵ_{rf}. In order to perform the rf rotation with sufficiently high fidelity, more time is needed as a larger spread in the rf power is considered. In addition, more optimization parameters are required to perform the rotation, which makes the optimization more complicated. In addition to correcting for errors in the rf power, rf pulse sequences which follow the microwaves will have to compensate for any errors caused by a detuning, making the optimization even more complicated. Because of these factors, we are not able to find a pulse sequence which works with the desired fidelity based on the sequence of $SU(2)$ rotations.

To show this explicitly, we have performed an optimization for errors of 2% with the semi-analytic method. For the rf rotations, 15 steps were used to ensure that a sufficiently high fidelity is reached for each rotation, while for the microwaves, 3 steps are used. This choice was found to yield the highest fidelity. We cut off the total time at 78.75 ms, since longer times did not achieve any higher fidelity. The pulses are optimized on a grid in parameter space defined by $\epsilon_{rf} = 0, \pm 0.02, \epsilon_{\mu w} = 0, \pm 0.02$ and $\Delta = 0, \pm 0.02 \Omega_{rf}$. The quality of the pulses was checked on a grid with 15 evenly spaced points between $\pm 2\%$ for ϵ_{rf} and $\epsilon_{\mu w}$ and 33 evenly spaced points between 0.02Ω for Δ. As can be seen from Fig. (5.4) the synthesis performs quite poorly, with an average fidelity of only 0.78. This fidelity, along with the time required to reach it, are typical of the problems which occur when trying to use the semi-analytic method. We believe that more sophisticated optimization approaches, such as [7], may overcome these problems.

Although the semi-analytic method is limited at present, it still serves as an adequate proof-of-principle that pulse sequences exist that can perform the desired evolution. Thus, fully numerical optimization approaches may still be used to find appropriate pulse sequences. This situation is similar to that found in two-level control, where a Lie algebraic approach provides a proof of principle that appropriate controls exist, while numerical optimization is used to find the optimum pulse
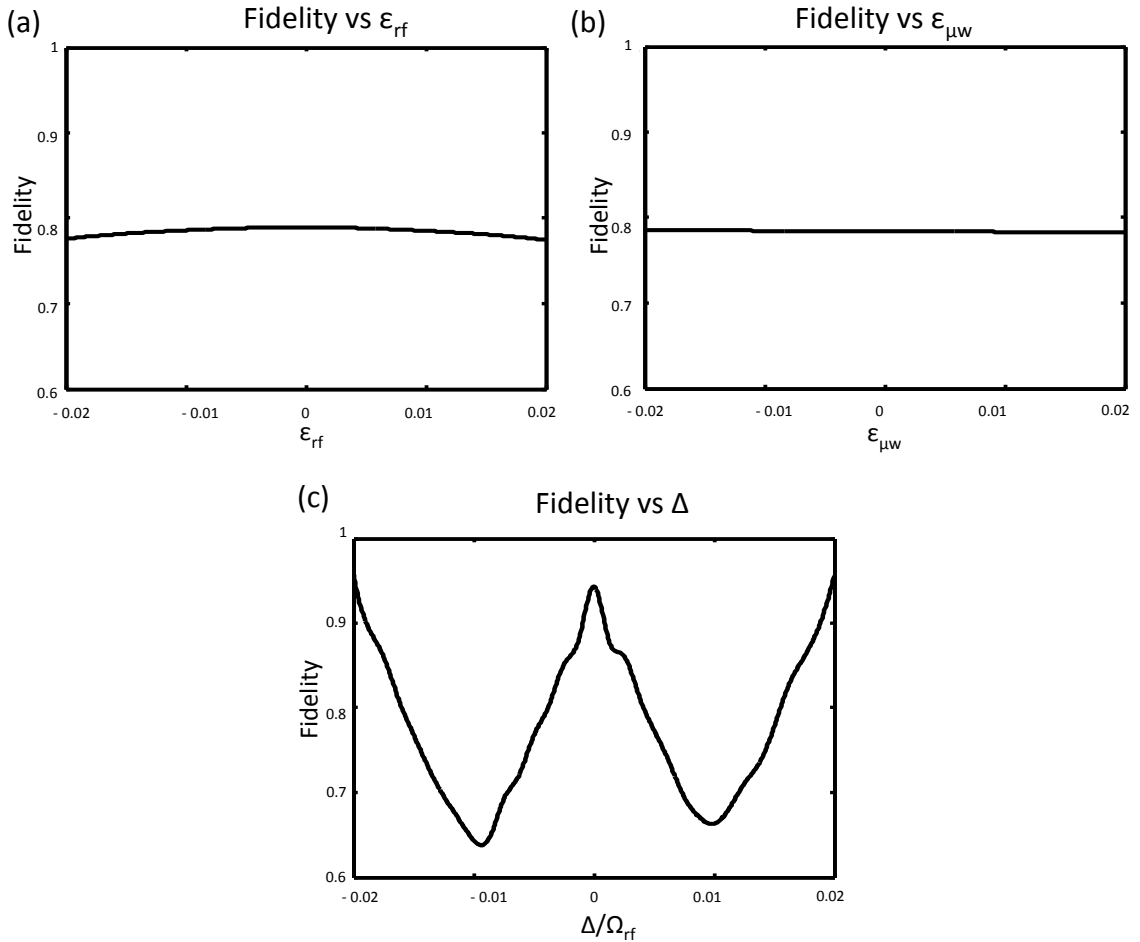
Figure 5.4: Fidelity of semi-analytic state preparation vs 2% errors in ϵ_{rf}, $\epsilon_{\mu w}$, and Δ/Ω_{rf}. In (a.) the fidelity is averaged over $\epsilon_{\mu w}$ and Δ/Ω_{rf} and plotted vs. ϵ_{rf}. Similarly, in (b.) the fidelity is plotted vs. $\epsilon_{\mu w}$ and averaged over the other two variables. In (c.) the fidelity is plotted vs. Δ/Ω_{rf} and averaged over the other two variables.

sequence [7, 30]. We focus on this approach for the rest of the chapter.

We consider fully numerical optimization with errors of 5%. In this case, the optimization was performed on a grid in parameter space defined by $\epsilon_{rf} = 0, \pm0.05$, $\epsilon_{\mu w} = 0, \pm0.05$ and $\Delta = 0, \pm0.05\Omega_{rf}$. The duration of the entire pulse sequence is
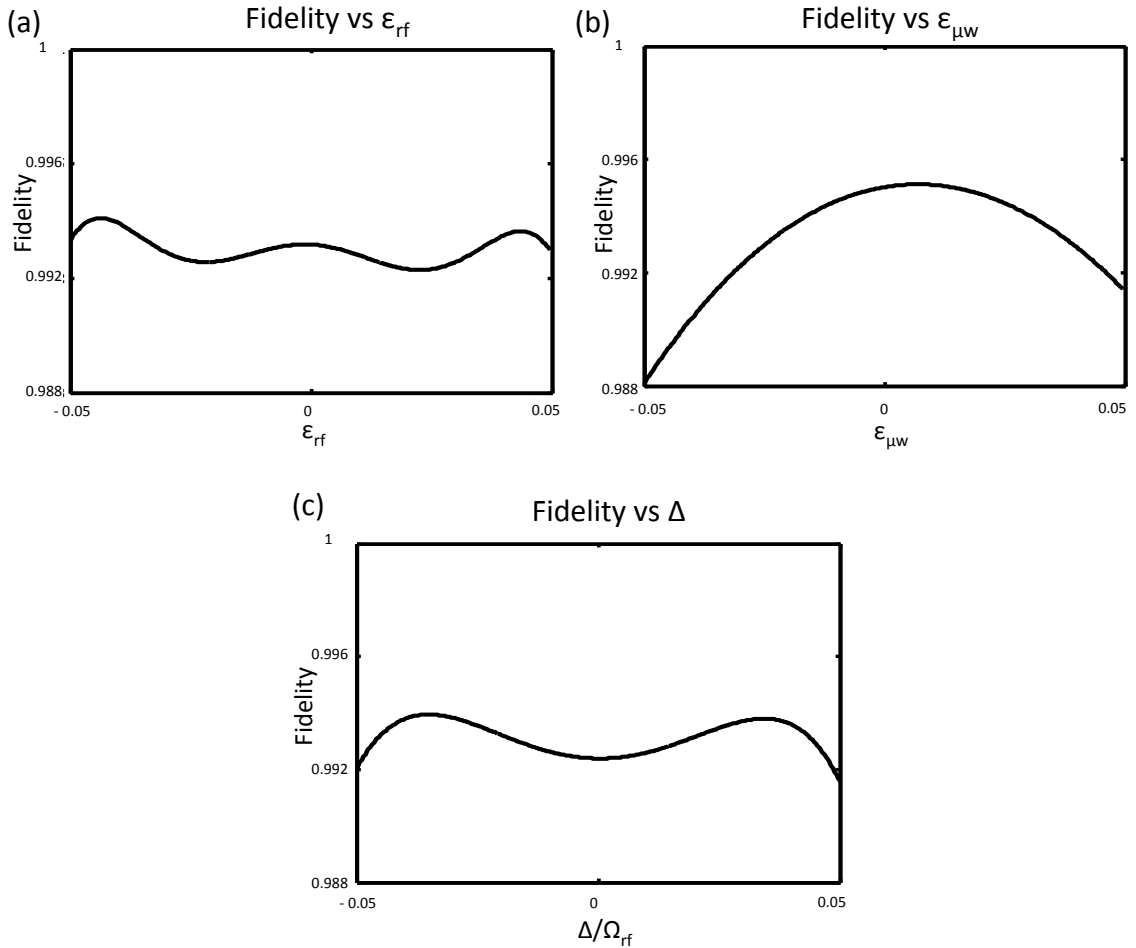
Figure 5.5: Fidelity of fully numerical state preparation vs 5% errors in ϵ_{rf}, $\epsilon_{\mu w}$, and Δ/Ω_{rf}. In (a.) the fidelity is averaged over $\epsilon_{\mu w}$ and Δ/Ω_{rf} and plotted vs. ϵ_{rf}. Similarly, in (b.) the fidelity is plotted vs. $\epsilon_{\mu w}$ and averaged over the other two variables. In (c.) the fidelity is plotted vs. Δ/Ω_{rf} and averaged over the other two variables.

5 ms. After the optimization, we calculated the fidelity on a finer grid of 15 points evenly spaced between $\pm 5\%$ for each of those errors, as shown in the figures. As can be seen from Fig. (5.5), a fidelity of over 0.988 is maintained throughout this range of parameters and we achieve an average fidelity of 0.993.
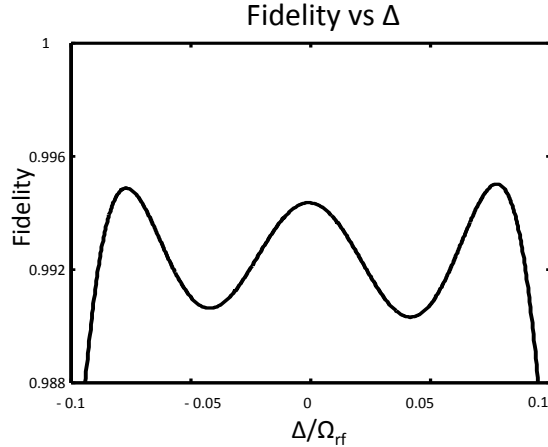
Figure 5.6: Fidelity of fully numerical state preparation vs 10% errors in Δ/Ω_{rf}.

Optimization by the fully numerical method is sufficiently powerful to compensate errors well beyond experimental uncertainty. As an example, in Fig. (5.6) we present the results of optimizing errors of $\Delta = 10\%\Omega_{rf}$. The optimization was performed on a grid of 10 evenly space points between $\pm 0.1\Omega_{rf}$. The timing is the same as the previous example. Fidelities of over 0.98 are maintained over the entire range of the detuning, while the fidelity averaged over the full range of errors is 0.9918.

Until now, we treated the deviations of the Rabi frequency and detuning from their fiducial values as experimental errors. As discussed above, these deviations can also be used as *control parameters*. For example, a spatial gradient in the detuning, imposed through an external field can be used to spatially address different regions of an ensemble. We investigate such control through the application of a spatial gradient of the detuning. In practice, this can be achieved by the fictitious magnetic field produced by the vector light shift of a circularly polarized laser beam [68]. If the intensity of the laser varies spatially, then the atoms will experience a spatially varying magnetic field and hence a spatially varying detuning. As we saw previously, an inhomogeneous detuning can be used to synthesize different
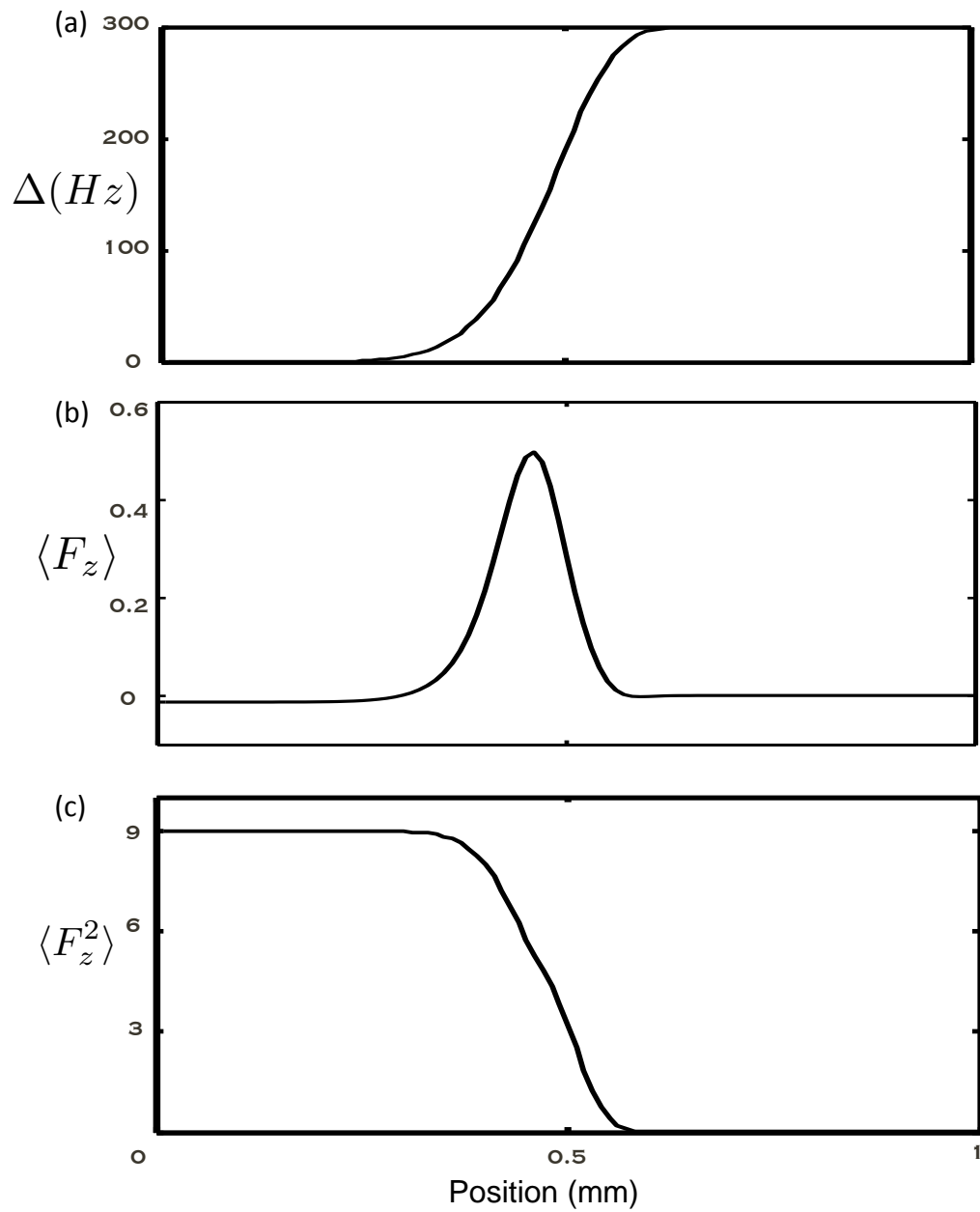
Figure 5.7: Results of spatially selective pulse. (a.) Profile of Δ vs. position. (b.) F_z vs. position. (c.) F_z^2 vs. position.

states depending on the magnetic field. In this case we have chosen to synthesize $\psi_1 = \frac{1}{\sqrt{2}}(\ |F = 3, m_F = -3\rangle + |F = 3, m_F = 3\rangle\ )$ and $\psi_2 = |F = 3, m_F = 0\rangle$.

In the ideal case, we would apply a step function in space to perfectly select two regions with two distinct detunings. However, in practice the laser which leads to the detuning cannot be focused to a perfectly sharp edge. We take this into account by modeling the spatial variation in detuning by

$$\Delta(x) = \Delta_0(1 - e^{-(x/a)^n}). \tag{5.29}$$

When n is extremely large, we recover the ideal case of two regions in space: if $x < a$, $\Delta = 0$ and if $x > a$, $\Delta = \Delta_0$. For smaller n, there is a transition between the two regions. As an example we take $a = 0.5$ mm. As depicted in Fig. (5.7), we choose $\Delta_0 = 300$ Hz, which is large enough that the two regions can be easily distinguished, but is not large compared to the rf and microwave powers. We also choose $n = 8$, which gives a transition region which is quite large compared to the wavelength of light, and so can be easily created in a laboratory.

Our goal is to synthesize ψ_1 in the region with no detuning and ψ_2 in the region with a 300 Hz detuning. To do this, we optimize on a grid defined by and $\Delta = -10, 0, 10, 290, 300$ and 310 Hz. We have included some spread in the detuning since there will still be some amount of noisy background fields. The results of the optimization can be seen in Fig. (5.7), where we have plotted both F_z and F_z^2 as a function of position. For the two target states we have $\langle\psi_1|F_z|\psi_1\rangle = \langle\psi_2|F_z|\psi_2\rangle = 0$ and $\langle\psi_1|F_z^2|\psi_1\rangle = 9$ while $\langle\psi_2|F_z^2|\psi_2\rangle = 0$. In the region between $x = 0$ and 0.3mm, where the detuning is between $\Delta = 0$ and 10 Hz, $F_z \leq 0.0125$ and $F_z^2 \geq 8.95$ as expected for ψ_1. In the region between $x = 0.6$ and 1mm, where the detuning is between $\Delta = 290$ and 300 Hz, $F_z \leq 1.5 \times 10^{-3}$ and $F_z^2 \leq 0.012$, as expected for ψ_2.

5.6   Conclusion

We have shown how a combination of rf and microwave fields can be used to synthesize arbitrary states in the hyperfine manifold of magnetic sublevels in the ground-electronic states of alkali atoms when there are inhomogeneous variations in the drive parameters. We began by assuming that all the control parameters were known precisely and showed that when the rf and microwaves are applied sequentially, the system performs a series of $SU(2)$ rotations which can be used to synthesize arbitrary states. We next extended that construction to the case of inhomogeneous controls by using ideas developed from the control of spin-1/2 systems. We also described a fully numerical approach to performing state preparation with inhomogeneous controls. The state synthesis can be performed in a manner that is robust to the expected experimental errors, or the inhomogeneous variations can be introduced intentionally, in order to gain further control of the system.

We have compared the performance of semi-analytic state synthesis to fully numerical state synthesis. For small inhomogeneities they both achieve average fidelities greater than 0.99. However, the fully numerical approach can find control sequences which require significantly less time in the lab to perform. For larger inhomogeneities, technical problems limit the approach based on a sequence of $SU(2)$ rotations, while the fully numerical approach still works well.

In the future, we intend to explore how to design entire unitary transformations in a manner that takes into account inhomogeneities in the drive fields. Such ideas would be an important step towards addressable qudit control in optical lattices. Additionally, the state preparation ideas presented here might be useful in a many body context. For instance, one could synthesize domain structures in a spinor condensate where the domains consisted of states which were highly non-classical in nature, such as ψ_1 and ψ_2 as above.

Chapter 6

Summary and Outlook

In this thesis we have described several problems related to the control of neutral atoms. In Ch. 2 we laid the ground work, and described previously known results in inhomogeneous quantum control, with a particular emphasis on $SU(2)$ rotations. We reviewed the results of [30], where Li and Khaneja showed that arbitrary transformations as a function inhomogeneities in the Rabi frequency and detuning were possible. Li and Khaneja also discussed the time required to synthesize such transformations. In the case of detuning inhomogeneities alone, the transformations may be synthesized efficiently, while the efficiency with which the transformations may be synthesized in the presence of inhomogeneity in the Rabi frequency remains an open problem. We concluded the chapter with a description of a numerical method which can often find a sequence of control pulses which will synthesize the desired transformation rapidly.

In Ch. 3 we discussed control of atomic transport in a spinor optical lattice. After describing the basics of light shifts in alkali atoms and their ability to create spin dependent potentials, we specialized to the case of 1D lattices affecting the $F = 4, m = 3$ and $F = 3, m = 3$ hyperfine states of Cs atoms. One can control

the spin and spatial degrees of freedom through a combination of rotations of the angle between the polarization of two counter-propagating lattice beams and through microwave-induced spin transitions. Because the two spin states respond differently to different laser polarizations, each experiences a different lattice potential. In particular, if the minima of the potentials are spatially offset, flipping the atom's spin causes the atom to move. Rotation of the lattice polarization provided a means to transport the atom in different directions, depending on its spin state. We described the impact of the translational invariance of the controls on the allowed state and unitary synthesis, and showed that if a state is initially localized at a particular lattice site, it can only evolve into a new state which satisfies Eq. (3.18). We next considered transformations which exactly mapped a localized wave packet to a state with an extended but finite width, and generalized this to transformations that approximately synthesize states for which the probability amplitudes went to zero for large distances. Based upon the state synthesis routine, we developed protocols for unitary synthesis when the parameters that defined the unitaries had finite Fourier transforms. No experiment is ever perfect, so we study the impact of realistic experimental errors, and various approaches to compensate for them. If the right compensation technique is used, we found that fidelities of 0.95 were possible after 25 steps.

In Ch. 4 we explored the possibility of using lin lin lattices and microwave driven spin flips to study the interaction of tightly trapped atoms. We began by reviewing the trap induced resonances originally discovered by Stock *et al.* [15, 93]. These resonances occur when the energy of a sufficiently weakly bound molecule is resonant with the energy of free trapped atoms. The interactions strongly modify the spectrum, and we found an experimental regime favorable to the detections of those modifications. In particular, if the interaction is strong enough, then even the spectra of atoms separated by $\lambda/4$ will be modified, with the energy of the molecular state well resolved from free atom resonances. As in Ch. 3, because of the spinor lattice, when the microwaves induced spin flips, they also caused the atoms to change posi-

tion. Under appropriately chosen conditions, the movement of atoms throughout the lattice is suppressed, and we can simplify our description of the system by treating the lattice wells in which the atoms move as harmonic traps. The response of the atoms to the microwaves can then be calculated by modifying the free space Rabi frequency by the Frank-Condon factors and integrating the Schrödinger equation. By driving unbound atoms into the molecular state, a spectroscopic signal of the interactions can be measured. The molecular state and free atoms states respond differently to changes in the lattice vibration frequency and we showed that measuring this difference would provide proof of the existence of trap induced resonances.

Finally, in Ch. 5 we studied the problem of inhomogeneous control of multilevel systems. After giving an introduction to rf and microwave based control of the spin of neutral atoms, we specialized to a configuration which allowed state preparation within an 8-dimensional subspace. We described a semi-analytic state preparation scheme based on an alternating series of rf and microwave rotations. Our goal was to transform $4, 4$ into an arbitrary superposition; we instead developed a routine to transform an arbitrary superposition into $4, 4$. Since our controls are reversible, we could simply reverse the scheme to find the desired transformation. At each step of the construction, we first found a sequence of rf pulses which maximized the population in $3, 3$, then used the microwaves to transfer all the population in $3, 3$ into $4, 4$. Repeating this procedure allowed us to drive an arbitrary amount of population into $4, 4$. Because the state preparation scheme was based on $SU(2)$ rotations, the results of Ch. 2 could be used to extend the scheme to the case of inhomogeneous controls. In particular, we showed that the synthesized states could vary arbitrarily with respect to the detuning and microwave power, while robust state preparation was possible with respect to variation in the rf power. We also described a fully numerical method for state synthesis based on maximizing the fidelity of state preparation, averaged over the various inhomogeneities. Microwave and rf fields were present simultaneously, and the phase of each field as a function

of time was optimized to find the desired pulse sequence. We compared the two methods and found the fully numerical method to be superior. Both methods found pulse sequences that performed robust state preparation in the presence of errors of 1%, though the fully numerical approach found a pulse sequence which worked more rapidly. Technical problems limited the utility of the semi-analytic approach for errors beyond 2%, while the fully numerical approach worked for errors as large as 10%. We also presented a simple example of a spatially selective pulse sequence, found via the fully numerical approach.

There are a variety of ways in which this work might be further extended. For the single atom transport problem, it may be possible to extend the state synthesis routine to higher bands. In a sufficiently deep lattice, each quasi-momentum mode behaves like an independent harmonic oscillator coupled to a spin-1/2 particle. We have already seen that in the single band case, each mode can be controlled independently, and it should be possible to extend that control to the multiband case. Then the original Law and Eberly scheme [77] can be used to perform state preparation, with each quasi-momentum acting as an independent mode. By keeping track of the effects of tunneling, it may even be possible to extend this construction to weaker lattices. Furthermore, we have shown that block diagonal unitary transformations in quasi-momentum space, with the blocks of $SU(2)$, may be synthesized. Yet blocks of $U(2)$ may be important in quantum simulations, since the spin independent phase represents spin independent tunneling, and it may be possible to synthesize blocks of $U(2)$ in quasi-momentum space by making use of higher bands. We have also assumed the lattice polarization is transformed sufficiently slowly that atoms remain in the lowest band. Once we have gained control over multiple bands, such adiabatic transport may no longer be necessary.

It may also be possible to relax the requirement that the controls spatially isolate two-level systems, since the methods of Sec. 3.5 should still be applicable. In

particular, the Fourier based approach can still be used to prove controllability, since the system is still block diagonal in quasi-momentum space, and the numerical approach can still be used to find a desired pulse sequence. Easing the requirement of spatial isolation would reduce the amount by which the polarization is rotated, which could substantially improve the fidelity of state preparation. The methods of Sec. 3.5 should also apply to 2- and 3-dimensional lattices, allowing state preparation in higher dimensions to be performed. Finally, we note that although linear gradients did not significantly improve the control over the system, quadratic gradients or spin dependent linear gradients may allow the translational invariance to be broken.

Although extensions to many-body systems are non-trivial, the ability to tune the interactions between atoms via Feshbach resonances may allow limited forms of control. For example, one can study nonequilibrium dynamics in the following way. Imagine beginning with the interaction strength set to zero. In this case the system is simply a collection of non-interacting particles to which we can apply the control schemes of Ch. 3. If the system is initially in its ground state, it may be driven into a state with higher energies, or a superposition of such states. The interaction strength can then be tuned to a stronger value, and the system will now generally be a strongly interacting many-body system prepared in a state far from equilibrium. Such a state may be useful for studying the dynamics of strongly interacting many-body systems. Another approach to deploying quantum control in a many-body context is to work with weakly interacting systems. If the time evolution of such systems can be calculated efficiently, then numerical optimization of state preparation should be possible.

In the case of microwave induced collisions, the current approach limited the dynamics of the two atom system to 3 lattice sites. This limitation meant that the molecular level could only be detected when it was well resolved from free atomic states. Yet the avoided crossings between the molecular and free atomic states are

one of the most important aspects of the trap-induced resonance. Because the crossings occur when the molecular state is resonant with the free atoms' states we will need to calculate the response of the two level system when the microwaves are nearly resonant with free atom states. In such a situation, the atoms will not only collide with one another, they will also move throughout the lattice. Thus, a three site approximation is inappropriate, and the movement of atoms throughout the lattice will need to be properly modeled in order to accurately calculate the spectrum. Additionally, methods for overcoming the low signal to noise ratio in the current experiment, such as evaporative cooling and subensemble selection, will need to be developed in order to make detection of the molecular state feasible in real experiments.

Understanding the interaction of pairs of atoms is only the first step in designing quantum logic gates. The next step will involve controlling those interactions in such a way that a desired unitary is synthesized. Ideas from quantum control, particular numerical optimization techniques could prove useful. The ability to bring the molecular state into and out of resonance with free atomic states via the change of lattice parameters may provide another means for controlling the strength of interactions between atoms, which is an important component in many quantum simulators.

In the case of spin control, it may be possible to extend the control of inhomogeneous spin systems to full unitary transformations. In [14], the authors describe a method for combining a series of state preparations into a full unitary transformation, and it may be possible to extend those ideas to the synthesis of inhomogeneous transformations. Alternately, a fully numerical approach to inhomogeneous unitary design may also be possible. It may even be possible to combine control over individual atoms' spin with a collective coupling among multiple spins [97] to study quantum control of many-body systems. Spatial control of an atom's spin may also have applications to spinor condensates, where one could imagine preparing the system to have different, highly non-classical spin states in different regions of space,

which may have applications to the dynamics of many-body systems. If the qudits are to be stored in an optical lattice, then individual addressing of the qudits becomes a problem. Inhomogeneous control via a spatial gradient in either a real or an effective magnetic field is one approach to single qudit addressing. We have also limited our study to the single qudit problem, though for applications in quantum information, gates between pairs of qudits will also be needed. Once again, we can expect the methods of quantum control to be useful in designing such gates.

Appendices

Appendix A

Inhomogeneous Control Code

In this appendix we present the code used to find the control sequences used to perform the inhomogeneous state preparation described in Ch. 5. There are three separate pieces of code. The first is 'uw_rf', this is the main optimization code. The second is 'make_target', which prepares a given number of random target states for the optimization. The third is 'random_state' which generates random states. The last is 'make_gen' which formats the angular momentum operators.

A.1   uw_rf

function f

%uw_rf:inhomogenous state prep code

%% top
clear

```matlab
tic
disp( 'START_uw_rf_vx')
current_file = mfilename;


warning('off', 'optim:fminunc:SwitchingMethod' );



%variables to calculate fidelity
global t_simulation ep_rf ep_uw delta n_ep_rf n_ep_uw
    n_delta ...
      n_t_simulation psi psi_target_2 s fx fy fz sig_44_x
         sig_44_y ...
      proj_44 rabi_uw_max rabi_rf_max delta_t_simulation_loop
         g_r x_last
%variables for output function
global cut_off_step


load    target_var_n_teststates=20_F=3


dtotal
n_teststates




%% form spin operators
d_3 = ddown;
s = (d_3-1)/2;
spin = make_gen(s);
```

Appendix A. Inhomogeneous Control Code

```matlab
jx = spin.jx;
jy = spin.jy;
jz = spin.jz;
jz2 = jz*jz;

id = [1 0; 0 1];
sigma_x = [0 1;1 0];
sigma_y = [0 -i;i 0];
sigma_z = [1 0; 0 -1];

fx = [0,zeros(1,d_3); zeros(d_3,1),jx];
fy = [0,zeros(1,d_3); zeros(d_3,1),jy];
fz = [0,zeros(1,d_3); zeros(d_3,1),jz];
sig_44_x = [sigma_x zeros(2, 2*s); zeros(2*s,2), zeros(2*s)
   ]; %there's no +1 because the two manifolds
    %overlap
sig_44_y = [sigma_y zeros(2, 2*s); zeros(2*s,2), zeros(2*s)
   ];
sig_44_z = [sigma_z zeros(2, 2*s); zeros(2*s,2), zeros(2*s)
   ];
proj_44 = [1 zeros(1,d_3); zeros(d_3,1), zeros(2*s+1)];




%% parameters
rabi_rf_max = 15*2*pi; %rad/s   %SINGLE COIL POWER
rabi_uw_max = 35*2*pi; %rad/s
g_r = .996819;   %g_r = abs(g_4/g_3)
```

Appendix A. Inhomogeneous Control Code

```
% multiple spreads
% delta_mult 1  = [-.15:.15:.15]*2*pi;
% ep_rf_mult 1  = [-.01 0 .01];
% ep_uw_mult 1  = [-.01 0 .01];


delta_mult 1  = 0*2*pi;
ep_rf_mult 1  = 0;
ep_uw_mult 1  = 0;


delta_mult 2  = delta_mult 1 ;
% ep_rf_mult 2  = ep_rf_mult 1 ;
ep_rf_mult 2  = [-.01 0 .01];
% ep_uw_mult 2  = [-.01 0 .01];
ep_uw_mult 2  = ep_uw_mult 1 ;


delta_mult 3  = delta_mult 2 ;
ep_rf_mult 3  = ep_rf_mult 2 ;
% ep_rf_mult 3  = [-.01 0 .01];
ep_uw_mult 3  = [-.01 0 .01];
% ep_uw_mult 3  = ep_uw_mult 2 ;


delta_mult 4  = 1*[-.15:.15:.15]*2*pi;
ep_rf_mult 4  = ep_rf_mult 2 ;
% ep_rf_mult 3  = [-.01 0 .01];
ep_uw_mult 4  = ep_uw_mult 3 ;
```

```
opt_step = length(delta_mult);
```

```
%binning loop
%this set the number of times to optimize for a given state.
    The program
%will loop until either a cut off fidelity is reached, or
    the maximum
%number of iterations, set by bin_loop_num, is reached.
%If t_end is larget enough, usually a single attempt at
    optimization is
%sufficent.  If the shortest possible t_end is desired, more
     optimization
%attempts are generally necessary.  I don't have a
    quantitative idea for
%how large bin_loop_num needs to be in this case; I usually
    set it to 10.
%some experimentation may be required
bin_loop_num = 1;
```

```
%% timing, initial and final states
% timing variables
```

```
time_total = 0;  %total time for optimization
```

Appendix A. Inhomogeneous Control Code

```
opt_counter = 1;
time_last_opt(opt_counter) = 0;




t_end = [.125];% (ms)  %total pulse time
n_t_end = length(t_end);


delta_t_simulation = [.125*10^-1];  %subpulse time
% delta_t_simulation = [10^-1];
n_delta_t_simulation = length(delta_t_simulation);


t_end_counter = 0;
for t_end_loop = t_end
t_end_counter = t_end_counter +1;


delta_t_simulation_counter = 0;
for delta_t_simulation_loop = delta_t_simulation
    delta_t_simulation_counter = delta_t_simulation_counter
        + 1;



t_simulation = 0:delta_t_simulation_loop:t_end_loop;
n_t_simulation = length(t_simulation);



%form initial state when spread is a cell
initial = [1 0 zeros(1,2*s)]';
```

Appendix A. Inhomogeneous Control Code

```
for  opt_step_loop = 1:opt_step
    n_ep_uw_mult(opt_step_loop) = length(ep_uw_mult
        opt_step_loop );
    n_ep_rf_mult(opt_step_loop) = length(ep_rf_mult
        opt_step_loop );
    n_delta_mult(opt_step_loop) = length(delta_mult
        opt_step_loop );

    psi_0 = repmat(initial ,[1 ,n_ep_uw_mult(opt_step_loop),
        n_ep_rf_mult(opt_step_loop),n_delta_mult(opt_step_loop
        )]);
    psi_mult opt_step_loop  = zeros(2*s+2,n_ep_uw_mult(
        opt_step_loop),n_ep_rf_mult(opt_step_loop),
        n_delta_mult(opt_step_loop),n_t_simulation); %2*s+1+1:
        extra +1 for 44
    psi_mult opt_step_loop (:,:,:,:,1) = psi_0 ;
end



%loop over states
for  rand_loop = 1:n_teststates




% Form Target  − multiple spreads − cell
for  opt_step_loop = 1:opt_step
    target_here = target_down_aux_rand(:,rand_loop);
```

Appendix A. Inhomogeneous Control Code

```
    abs(target_here).^2;
    psi_target_mult opt_step_loop  = repmat(target_here ,[1 ,
        n_ep_uw_mult(opt_step_loop),n_ep_rf_mult(opt_step_loop
        ),n_delta_mult(opt_step_loop)]);
end



% begin  outer  optimization  loop − loops  over  random  initial
    control
% parameters
master_cut_off = .99;  %this  is  the  fidelity  which
    terminates  the  optimization
     %if  it  is  reached  when  the  spread  in  all  three
        parameters  is  considered


cut_off_mult (1:( opt_step −1) ) = .99;  %the  cut  off  for  each
    spread  can  be  different
cut_off_mult ( opt_step ) = .99;



fid_last_main_opt =0;
bin_loop = 0;
opt_step_loop = 0;
%loop  over  the  optimization  attempts
while  bin_loop < bin_loop_num    &&...
    ( ( opt_step_loop+1)<=opt_step    fid_last_main_opt <
        master_cut_off )
```

Appendix A. Inhomogeneous Control Code

```
    bin_loop = bin_loop + 1;




%% optimization

%controls are the phases
phi_uw = 2*pi * rand(1,n_t_simulation-1);
phi_rf = 2*pi*rand(1,n_t_simulation-1);


%phi_uw = pi * ones(1,n_t_simulation-1);
%phi_rf = pi/sqrt(2)*ones(1,n_t_simulation-1);


x0 = [phi_rf; phi_uw];
x0 = x0(:);
%x0(k) k = odd are phi_rf
x_len = length(x0(:));


%set search parameters - have to be kept here because of
    x_len
MaxFunEvals_opt = 10^3; % these are fminunc
MaxIter_opt = 10^3;
%                MaxFunEvals_opt = 10^4;   %fminsearch
%                MaxIter_opt = 10^6;
TolFun_opt = 10^-7;
GradObj_opt = 'off';
options = optimset('TolFun',TolFun_opt,'MaxFunEvals',
    MaxFunEvals_opt*x_len,'MaxIter',MaxIter_opt,'GradObj',
```

```
    GradObj_opt , 'OutputFcn' , @outfun ) ;


%main optimization loop − loops over increasingly complex
%paramter space
fid_last_sub_opt = 0;
disp ( [ ' target ^2=' , num2str ( abs ( target_here ) '.^2 ) ] )
%               for opt_step_loop = 1:opt_step
opt_step_loop = 0;
exit_flag = 666;
while ( opt_step_loop+1)<=opt_step && fid_last_main_opt <
    cut_off_mult ( opt_step_loop +1)  && exit_flag ~= −2
    opt_step_loop = opt_step_loop +1; %This is here so I can
        switch between while and for loop , it 's why
    %there 's a +1 in the while statement

    disp ( [ 'bin_#=' , num2str ( bin_loop ) , ';_state#_=' , num2str (
        rand_loop ) . . .
            , ';_opt_step=' , num2str ( opt_step_loop ) , ';_time_last_
                opt_=' , num2str ( time_last_opt ( opt_counter ) ) ] )
    disp ( [ 'total_time_=' , num2str ( time_total ) ] )
    disp ( '____' )

    opt_counter = opt_counter + 1;

    delta = delta_mult opt_step_loop ;
    ep_rf = ep_rf_mult opt_step_loop ;
    ep_uw = ep_uw_mult opt_step_loop ;
    n_ep_rf = n_ep_rf_mult ( opt_step_loop );
```

```
n_ep_uw = n_ep_uw_mult(opt_step_loop) ;
n_delta = n_delta_mult(opt_step_loop);


cut_off_step= cut_off_mult(opt_step_loop);


psi = psi_mult opt_step_loop ;
psi_target_2 = psi_target_mult opt_step_loop ;



tic
%rand_loop is in a cell because each state might
%have a different # of bins
%bug_bug is a dummy variable used to deal with a bug
%in fmincon. The problem is that if outfun
%terminates the optimization, it seems to pass the
%next to last optimization point (x) to the output,
%instead of the last point. This is fixed by
%saving the x that's past to the cost function as a
%global variable, x_last. x_last at the end then
%stores the optimum set of controls
[bug_bug final_cost rand_loop(bin_loop,t_end_counter,
    delta_t_simulation_counter,opt_step_loop) exit_flag] =
     fminunc(@(x) cost_phases_44_better_uw(x), x0, options)
    ;
x0 = mod(x_last,2*pi);
x_opt_cell t_end_counter,delta_t_simulation_counter,
    rand_loop (:,bin_loop,opt_step_loop) = x0;
```

113

```
    exit_flag


    time_last_opt(opt_counter) = toc;
    time_total = time_total+time_last_opt(opt_counter);


    fid rand_loop (bin_loop,t_end_counter,
       delta_t_simulation_counter,opt_step_loop) = −
       final_cost rand_loop (bin_loop,t_end_counter,
       delta_t_simulation_counter,opt_step_loop);


    fid_last_sub_opt = −final_cost rand_loop (bin_loop,
       t_end_counter,delta_t_simulation_counter,opt_step_loop
       )


end


fid_last_main_opt = fid_last_sub_opt;


time_last_opt
time_total



end %bin_loop
end %rand_state_loop
end %t_end_loop
end %dt_loop
```

```
save addressing_try1_var %x_opt F
```

```
function cost_out_phases_44_better_uw =
    cost_phases_44_better_uw(x)

global t_simulation ep_rf ep_uw delta n_ep_rf n_ep_uw
    n_delta ...
      n_t_simulation psi psi_target_2 s fx fy fz sig_44_x
         sig_44_y ...
      proj_44 rabi_uw_max rabi_rf_max delta_t_simulation_loop
         g_r x_last

x_last = x;

psi_target = psi_target_2;

ep_uw_counter=0;
for ep_uw_loop = ep_uw
    ep_uw_counter = ep_uw_counter + 1;

ep_rf_counter=0;
for ep_rf_loop = ep_rf
    ep_rf_counter = ep_rf_counter + 1;
```

```
delta_counter = 0;
for delta_loop = delta;
    delta_counter = delta_counter + 1;

    t_counter = 1;
    for t_loop = t_simulation(2:n_t_simulation)
        t_counter = t_counter + 1;

        %x0(k) k = odd are phi_rf
        H = -(1+ep_rf_loop)*2*rabi_rf_max*cos(x(2*t_counter
            -3))*fx ...
            + (1+ep_rf_loop)*2*rabi_rf_max*sin(x(2*t_counter
                -3))*fy ...
            -delta_loop*fz ...
            +.5*(1+ep_uw_loop)*rabi_uw_max*cos(x(2*t_counter
                -2))*sig_44_x ...
            -.5*(1+ep_uw_loop)*rabi_uw_max*sin(x(2*t_counter
                -2))*sig_44_y ...
            +(g_r*delta_loop*(s+1) )*proj_44;

        psi(:,ep_uw_counter,ep_rf_counter,delta_counter,
            t_counter) = expm(-i*delta_t_simulation_loop*H)*
            psi(:,ep_uw_counter,ep_rf_counter,delta_counter,
            t_counter-1);

    end %t_loop
```

```
F_2(ep_uw_counter,ep_rf_counter,delta_counter) = abs(
    psi_target(:,ep_uw_counter,ep_rf_counter,delta_counter
    )'*psi(:,ep_uw_counter,ep_rf_counter,delta_counter,
    n_t_simulation))^2;


end %delta_loop
end %ep_rf loop
end %ep_uw loop


fid = -sum(sum(sum(F_2)))/n_delta/n_ep_rf/n_ep_uw;



cost_out_phases_44_better_uw =   fid;
```

```
function stop = outfun(x,optimValues,state)

%this is a function that will terminate the optimization
    once a cutoff
%fidelity is reached.  The idea is to set the number of
    function calls, iterations, and tolerance really
```

```
%high, then let the program run untill it hits a desired
    fidelity.

global cut_off_step


stop = false;


if (optimValues.fval<-cut_off_step) && strcmp(state,'iter')
    stop = true;
end
```

A.2 make_target

```
function f

%make random states for optimization
%
%Originally written by Seth Merkel, substantially modified
    by Brian
%Mischuck

levels = 'protected_44'; %regular_44, protected_44
ddown = 4;
dup = ddown+2;
dtotal = ddown+dup;
```

Appendix A. Inhomogeneous Control Code

```
n_teststates = 1;


% samp_coh_sph(ddown);



%can generate random states
target_down = zeros(ddown,n_teststates);
targ_name = cell(1,n_teststates);
% uw_type = cell(1,n_teststates);
target_down_aux_rand = zeros(ddown+1,n_teststates);
target_down_both_rand = zeros(dtotal,n_teststates);

for ii=1:n_teststates
    target_down(:,ii) = random_state(ddown);
    targ_name ii = strcat('rand',int2str(ii),'d',int2str(
        ddown));
%    uw_type ii  = 'subspace_44';


    target_down_aux_rand (2:(ddown+1),ii) = target_down(:,ii
        );


    target_down_both_rand ( (dup+1):dtotal ,ii) =
        target_down(:,ii);



end;
```

```
abs(target_down).^2'
```

```
save target_var
```

A.3   random_state

```
function rand_psi = random_state(d)
%generates a pure state in a d-dimensional quantum system
    drawn from the
%Harr measure.
%
%code by Seth Merkel

rand_psi = zeros(d,1);
phi = rand(1,d-1)*2*pi;
theta = asin(rand(1,d-1).^(1./(2*d - 2*(1:d-1))));

rand_psi(1,1) = cos(theta(1,1));

for ii=2:(d-1)

    rand_psi(ii,1) = prod(sin(theta(1,1:(ii-1))))*cos(theta
        (1,ii))...
            *exp(-i*phi(1,ii-1));

end;
```

```
rand_psi(d,1) = prod(sin(theta))*expm(-i*phi(end));
```

A.4 make_gen

```
unction Anggen = make_gen(s)
%generates the irrdeuciable angular momentum operators for a
    spin-s system
%
%code by Seth Merkel


d = 2*s+1;
Anggen.jx=zeros(d);
for m=1:d
    for n=1:d
        if(m+1==n)
            Anggen.jx(m,n)=(1/2)*sqrt((d-m)*m);
            Anggen.jx(n,m)=(1/2)*sqrt((d-m)*m);
        end;

    end;

end;

Anggen.jy=zeros(d);
for m=1:d
    for n=1:d
```

```
        if (m+1==n)
            Anggen.jy(m,n)=-i*(1/2)*sqrt((d-m)*m);
                Anggen.jy(n,m)=i*(1/2)*sqrt((d-m)*m);
        end;


    end;


end;


Anggen.jz=zeros(d);
for m =0:(d-1)
    Anggen.jz(m+1,m+1) = (d-1)/2 - m;
end;
clear m n d
```

References

[1] M. A. Nielsen and I. L. Chuang, *Quantum Computation and Quantum Information*, 1 edition, Cambridge University Press, 2000.

[2] S. Boixo, S. T. Flammia, C. M. Caves, and J. Geremia, *Generalized limits for Single-Parameter quantum estimation*, Physical Review Letters **98** (2007), 090401.

[3] H. Rabitz, *CHEMISTRY: shaped laser pulses as reagents*, Science **299** (2003), 525–527.

[4] R. S. Judson and H. Rabitz, *Teaching lasers to control molecules*, Physical Review Letters **68** (1992), 1500.

[5] N. Khaneja, R. Brockett, and S. J. Glaser, *Time optimal control in spin systems*, Physical Review A **63** (2001), 032308.

[6] D. D'Alessandro, *Introduction to Quantum Control and Dynamics*, 1 edition, Chapman and Hall/CRC, 2007.

[7] K. Kobzar, B. Luy, N. Khaneja, and S. J. Glaser, *Pattern pulses: design of arbitrary excitation profiles as a function of pulse amplitude and offset*, Journal of Magnetic Resonance **173** (2005), 229–235.

[8] E. Jan, G. Vidal, W. Dr, P. Zoller, and J. Cirac, *Simulation of quantum dynamics with quantum optical systems*, Quantum Information and Computation **3** (2003), 15.

[9] M. Greiner, O. Mandel, T. Esslinger, T. W. Hansch, and I. Bloch, *Quantum phase transition from a superfluid to a mott insulator in a gas of ultracold atoms*, Nature **415** (2002), 39–44.

[10] D. Jaksch, C. Bruder, J. I. Cirac, C. W. Gardiner, and P. Zoller, *Cold bosonic atoms in optical lattices*, Physical Review Letters **81** (1998), 3108.

References

[11] L. Isenhower, E. Urban, X. L. Zhang, A. T. Gill, T. Henage, T. A. Johnson, T. G. Walker, and M. Saffman, *Demonstration of a neutral atom Controlled-NOT quantum gate*, Physical Review Letters **104** (2010), 010503.

[12] I. H. Deutsch and P. S. Jessen, *Quantum-state control in optical lattices*, Physical Review A **57** (1998), 1972.

[13] S. T. Merkel, P. S. Jessen, and I. H. Deutsch, *Quantum control of the hyperfine-coupled electron and nuclear spins in alkali-metal atoms*, Physical Review A **78** (2008), 023404.

[14] S. T. Merkel, G. Brennen, P. S. Jessen, and I. H. Deutsch, *Constructing general unitary maps from state preparations*, Physical Review A **80** (2009), 023424.

[15] R. Stock, I. H. Deutsch, and E. L. Bolda, *Quantum state control via Trap-Induced shape resonance in ultracold atomic collisions*, Physical Review Letters **91** (2003), 183201.

[16] S. Flling, A. Widera, T. Mller, F. Gerbier, and I. Bloch, *Formation of spatial shell structure in the superfluid to mott insulator transition*, Physical Review Letters **97** (2006), 060403.

[17] U. Schneider, L. Hackermuller, S. Will, T. Best, I. Bloch, T. A. Costi, R. W. Helmes, D. Rasch, and A. Rosch, *Metallic and insulating phases of repulsively interacting fermions in a 3D optical lattice*, Science **322** (2008), 1520–1525.

[18] G. Roati, C. D/'Errico, L. Fallani, M. Fattori, C. Fort, M. Zaccanti, G. Modugno, M. Modugno, and M. Inguscio, *Anderson localization of a non-interacting Bose-Einstein condensate*, Nature **453** (2008), 895–898.

[19] O. Mandel, M. Greiner, A. Widera, T. Rom, T. W. Hansch, and I. Bloch, *Controlled collisions for multi-particle entanglement of optically trapped atoms*, Nature **425** (2003), 937–940.

[20] M. Anderlini, P. J. Lee, B. L. Brown, J. Sebby-Strabley, W. D. Phillips, and J. V. Porto, *Controlled exchange interaction between pairs of neutral atoms in an optical lattice*, Nature **448** (2007), 452–456.

[21] D. Jaksch, J. I. Cirac, P. Zoller, S. L. Rolston, R. Ct, and M. D. Lukin, *Fast quantum gates for neutral atoms*, Physical Review Letters **85** (2000), 2208.

[22] P. Hoyer, *Efficient quantum transforms*, quant-ph/9702028.

[23] D. P. OLeary, G. K. Brennen, and S. S. Bullock, *Parallelism for quantum computation with qudits*, Physical Review A **74** (2006), 032334.

References

[24] S. Chaudhury, S. Merkel, T. Herr, A. Silberfarb, I. H. Deutsch, and P. S. Jessen, *Quantum control of the hyperfine spin of a cs atom ensemble*, Physical Review Letters **99** (2007), 163002.

[25] S. Chaudhury, A. Smith, B. E. Anderson, S. Ghose, and P. S. Jessen, *Quantum signatures of chaos in a kicked top*, Nature **461** (2009), 768–771.

[26] L. Viola, E. Knill, and S. Lloyd, *Dynamical decoupling of open quantum systems*, Physical Review Letters **82** (1999), 2417.

[27] H. K. Cummins, G. Llewellyn, and J. A. Jones, *Tackling systematic errors in quantum logic gates with composite rotations*, Physical Review A **67** (2003), 042308.

[28] L. M. K. Vandersypen and I. L. Chuang, *NMR techniques for quantum control and computation*, Reviews of Modern Physics **76** (2005), 1037.

[29] D. Gottesman, A. Kitaev, and J. Preskill, *Encoding a qubit in an oscillator*, Physical Review A **64** (2001), 012310.

[30] J. Li and N. Khaneja, *Control of inhomogeneous quantum ensembles*, Physical Review A **73** (2006), 030302.

[31] N. Khaneja, T. Reiss, C. Kehlet, T. Schulte-Herbrggen, and S. J. Glaser, *Optimal control of coupled spin dynamics: design of NMR pulse sequences by gradient ascent algorithms*, Journal of Magnetic Resonance **172** (2005), 296–305.

[32] W. Rakreungdet, J. H. Lee, K. F. Lee, B. E. Mischuck, E. Montano, and P. S. Jessen, *Accurate microwave control and real-time diagnostics of neutral-atom qubits*, Physical Review A (Atomic, Molecular, and Optical Physics) **79** (2009), 022316–9.

[33] C. Zhang, S. L. Rolston, and S. D. Sarma, *Manipulation of single neutral atoms in optical lattices*, Physical Review A **74** (2006), 042316.

[34] B. Mischuck, I. H. Deutsch, and P. S. Jessen, *Coherent control of atomic transport in spinor optical lattices*, Physical Review A **81** (2010), 023403.

[35] G. C. Chingas, A. N. Garroway, R. D. Bertrand, and W. B. Moniz, *NMR j cross-polarization in liquids: A refocusing method*, Journal of Magnetic Resonance (1969) **35** (1979), 283–288.

[36] J. J. L. Morton, A. M. Tyryshkin, A. Ardavan, K. Porfyrakis, S. A. Lyon, and G. A. D. Briggs, *High fidelity single qubit operations using pulsed electron paramagnetic resonance*, Physical Review Letters **95** (2005), 200501.

References

[37] R. S. Said and J. Twamley, *Robust control of entanglement in a nitrogen-vacancy center coupled to a c 13 nuclear spin in diamond*, Physical Review A **80** (2009), 032303.

[38] E. Collin, G. Ithier, A. Aassime, P. Joyez, D. Vion, and D. Esteve, *NMR-like control of a quantum bit superconducting circuit*, Physical Review Letters **93** (2004), 157005.

[39] N. Timoney, V. Elman, S. Glaser, C. Weiss, M. Johanning, W. Neuhauser, and C. Wunderlich, *Error-resistant single-qubit gates with trapped ions*, Physical Review A **77** (2008), 052334.

[40] M. S. Silver, R. I. Joseph, C. Chen, V. J. Sank, and D. I. Hoult, *Selective population inversion in NMR*, Nature **310** (1984), 681–683.

[41] M. Shinnar, S. Eleff, H. Subramanian, and J. S. Leigh, *The synthesis of pulse sequences yielding arbitrary magnetization vectors*, Magnetic Resonance in Medicine **12** (1989), 74–80.

[42] N. Ohlsson, R. K. Mohan, and S. Krll, *Quantum computer hardware based on rare-earth-ion-doped inorganic crystals*, Optics Communications **201** (2002), 71–77.

[43] M. Karski, L. Frster, J. Choi, A. Steffen, N. Belmechri, W. Alt, D. Meschede, and A. Widera, *Imprinting patterns of neutral atoms in an optical lattice using magnetic resonance techniques*, 0912.2517.

[44] G. K. Brennen, C. M. Caves, P. S. Jessen, and I. H. Deutsch, *Quantum logic gates in optical lattices*, Physical Review Letters **82** (1999), 1060.

[45] D. Jaksch, H. Briegel, J. I. Cirac, C. W. Gardiner, and P. Zoller, *Entanglement of atoms via cold controlled collisions*, Physical Review Letters **82** (1999), 1975.

[46] K. D. Nelson, X. Li, and D. S. Weiss, *Imaging single atoms in a three-dimensional array*, Nat Phys **3** (2007), 556–560.

[47] D. Jaksch and P. Zoller, *The cold atom hubbard toolbox*, Annals of Physics **315** (2005), 52–79.

[48] M. Lewenstein, A. Sanpera, V. Ahufinger, B. Damski, A. Sen, and U. Sen, *Ultracold atomic gases in optical lattices: mimicking condensed matter physics and beyond - advances in physics*, Advances in Physics **56** (2007), 243–379.

[49] L. Duan, E. Demler, and M. D. Lukin, *Controlling spin exchange interactions of ultracold atoms in optical lattices*, Physical Review Letters **91** (2003), 090402.

References

[50] A. Micheli, G. K. Brennen, and P. Zoller, *A toolbox for lattice-spin models with polar molecules*, Nat Phys **2** (2006), 341–347.

[51] D. A. Steck, W. H. Oskay, and M. G. Raizen, *Observation of Chaos-Assisted tunneling between islands of stability*, Science **293** (2001), 274–278.

[52] S. Ghose, P. M. Alsing, and I. H. Deutsch, *Atomic motion in magneto-optical double-well potentials: A testing ground for quantum chaos*, Physical Review E **64** (2001), 056119.

[53] V. Y. Argonov and S. V. Prants, *Nonlinear control of chaotic walking of atoms in an optical lattice*, EPL (Europhysics Letters) **81** (2008), 24003.

[54] M. B. Dahan, E. Peik, J. Reichel, Y. Castin, and C. Salomon, *Bloch oscillations of atoms in an optical potential*, Physical Review Letters **76** (1996), 4508.

[55] S. R. Wilkinson, C. F. Bharucha, K. W. Madison, Q. Niu, and M. G. Raizen, *Observation of atomic Wannier-Stark ladders in an accelerating optical potential*, Physical Review Letters **76** (1996), 4512.

[56] A. Zenesini, H. Lignier, G. Tayebirad, J. Radogostowicz, D. Ciampini, R. Mannella, S. Wimberger, O. Morsch, and E. Arimondo, *Time-resolved measurement of Landau-Zener tunneling in periodic potentials*, 0903.3345.

[57] K. W. Madison, M. C. Fischer, R. B. Diener, Q. Niu, and M. G. Raizen, *Dynamical bloch band suppression in an optical lattice*, Phys. Rev. Lett. **81** (1998), 5093–5096.

[58] J. Sebby-Strabley, M. Anderlini, P. S. Jessen, and J. V. Porto, *Lattice of double wells for manipulating pairs of cold atoms*, Physical Review A (Atomic, Molecular, and Optical Physics) **73** (2006), 033605–9.

[59] S. Folling, S. Trotzky, P. Cheinet, M. Feld, R. Saers, A. Widera, T. Muller, and I. Bloch, *Direct observation of second-order atom tunnelling*, Nature **448** (2007), 1029–1032.

[60] O. Romero-Isart and J. J. Garcia-Ripoll, *Quantum ratchets for quantum communication with optical superlattices*, Physical Review A (Atomic, Molecular, and Optical Physics) **76** (2007), 052304–8.

[61] G. De Chiara, T. Calarco, M. Anderlini, S. Montangero, P. J. Lee, L. Brown, W. D. Phillips, and J. V. Porto, *Optimal control of atom transport for quantum gates in optical lattices*, Phys. Rev. A **77** (2008), 052333.

References

[62] I. Bloch, *Quantum coherence and entanglement with ultracold atoms in optical lattices*, Nature **453** (2008), 1016–1022.

[63] D. L. Haycock, P. M. Alsing, I. H. Deutsch, J. Grondalski, and P. S. Jessen, *Mesoscopic quantum coherence in an optical lattice*, Physical Review Letters **85** (2000), 3365.

[64] O. Mandel, M. Greiner, A. Widera, T. Rom, T. W. Hnsch, and I. Bloch, *Coherent transport of neutral atoms in Spin-Dependent optical lattice potentials*, Physical Review Letters **91** (2003), 010407.

[65] W. Dr, R. Raussendorf, V. M. Kendon, and H. Briegel, *Optical lattices*, Physical Review A **37** (2002), 052319.

[66] M. Karski, L. Forster, J. Choi, A. Steffen, W. Alt, D. Meschede, and A. Widera, *Quantum walk in position space with single optically trapped atoms*, Science **325** (2009), 174–177.

[67] A. Deb, G. Smirne, R. Godun, and C. Foot, *A method of state-selective transfer of atoms between microtraps based on the FranckCondon principle*, Journal of Physics B: Atomic, Molecular and Optical Physics **40** (2007), 4131–4142.

[68] I. H. Deutsch and P. S. Jessen, *Quantum control and measurement of atomic spins in polarization spectroscopy*, 0909.4506.

[69] P. Jessen, I. Deutsch, B. Bederson, and H. Walther, *Optical lattices*, Vol. Volume 37, Academic Press, 1996, pp. 95–138.

[70] N. Lundblad, P. J. Lee, I. B. Spielman, B. L. Brown, W. D. Phillips, and J. V. Porto, *Atoms in a Radio-Frequency-Dressed optical lattice*, Physical Review Letters **100** (2008), 150401–4.

[71] W. Yi, A. J. Daley, G. Pupillo, and P. Zoller, *State-dependent, addressable subwavelength lattices with cold atoms*, New Journal of Physics **10** (2008), 073015.

[72] M. Shotter, D. Trypogeorgos, and C. Foot, *Enhancement of on-site interactions of tunneling ultracold atoms in optical potentials using radio-frequency dressing*, Physical Review A (Atomic, Molecular, and Optical Physics) **78** (2008), 051602–4.

[73] T. Salger, G. Ritt, C. Geckeler, S. Kling, and M. Weitz, *Bloch oscillations of a Bose-Einstein condensate in a subwavelength optical lattice*, Physical Review A (Atomic, Molecular, and Optical Physics) **79** (2009), 011605–4.

References

[74] A. Zenesini, H. Lignier, D. Ciampini, O. Morsch, and E. Arimondo, *Coherent control of dressed matter waves*, 0809.0768.

[75] F. M. Cucchietti, *Loschmidt echo in the Bose-Hubbard model: turning back time in an optical lattice*, quant-ph/0609202.

[76] A. Alberti, G. Ferrari, V. V. Ivanov, M. L. Chiofalo, and G. M. Tino, *Coherent transport of atomic wave packets in amplitude-modulated vertical optical lattices*, 0903.0724.

[77] C. K. Law and J. H. Eberly, *Arbitrary control of a quantum electromagnetic field*, Physical Review Letters **76** (1996), 1055.

[78] K. Moore, M. Hsieh, and H. Rabitz, *On the relationship between quantum control landscape structure and optimization complexity*, The Journal of Chemical Physics **128** (2008), 154117–12.

[79] A. Zenesini, H. Lignier, D. Ciampini, O. Morsch, and E. Arimondo, *Coherent control of dressed matter waves*, Physical Review Letters **102** (2009), 100403–4.

[80] V. V. Ivanov, A. Alberti, M. Schioppo, G. Ferrari, M. Artoni, M. L. Chiofalo, and G. M. Tino, *Coherent delocalization of atomic wave packets in driven lattice potentials*, Physical Review Letters **100** (2008), 043602–4.

[81] A. Alberti, V. V. Ivanov, G. M. Tino, and G. Ferrari, *Engineering the quantum transport of atomic wavefunctions over macroscopic distances*, 0803.4069.

[82] A. Eckardt, M. Holthaus, H. Lignier, A. Zenesini, D. Ciampini, O. Morsch, and E. Arimondo, *Exploring dynamic localization with a Bose-Einstein condensate*, Physical Review A (Atomic, Molecular, and Optical Physics) **79** (2009), 013611–7.

[83] C. Sias, H. Lignier, Y. P. Singh, A. Zenesini, D. Ciampini, O. Morsch, and E. Arimondo, *Observation of Photon-Assisted tunneling in optical lattices*, Physical Review Letters **100** (2008), 040404–4.

[84] H. L. Haroutyunyan and G. Nienhuis, *Coherent control of atom dynamics in an optical lattice*, Physical Review A **64** (2001), 033424.

[85] B. Pryor and N. Khaneja, *Fourier synthesis methods for control of inhomogeneous quantum systems*, 0705.2566.

[86] T. Busch, B. Englert, K. Rzaewski, and M. Wilkens, *Two cold atoms in a harmonic trap*, Foundations of Physics **28** (1998), 549–559.

References

[87] T. Stferle, H. Moritz, K. Gnter, M. Khl, and T. Esslinger, *Molecules of fermionic atoms in an optical lattice*, Physical Review Letters **96** (2006), 030401.

[88] C. Ospelkaus, S. Ospelkaus, L. Humbert, P. Ernst, K. Sengstock, and K. Bongs, *Ultracold heteronuclear molecules in a 3D optical lattice*, Physical Review Letters **97** (2006), 120402.

[89] M. Khl, H. Moritz, T. Stferle, K. Gnter, and T. Esslinger, *Fermionic atoms in a three dimensional optical lattice: Observing fermi surfaces, dynamics, and interactions*, Physical Review Letters **94** (2005), 080403.

[90] L. Duan, *Effective hamiltonian for fermions in an optical lattice across a feshbach resonance*, Physical Review Letters **95** (2005), 243202.

[91] S. Will, T. Best, U. Schneider, L. Hackermller, D. Lhmann, and I. Bloch, *Multi-Orbital quantum phase diffusion*, 0911.5066.

[92] P. R. Johnson, E. Tiesinga, J. V. Porto, and C. J. Williams, *Effective three-body interactions of neutral bosons in optical lattices*, New Journal of Physics **11** (2009), 093022.

[93] R. Stock and I. H. Deutsch, *Trap-induced resonances in controlled collisions of cesium atoms*, Physical Review A **73** (2006), 032701.

[94] E. L. Bolda, E. Tiesinga, and P. S. Julienne, *Pseudopotential model of ultracold atomic collisions in quasi-one- and two-dimensional traps*, Physical Review A **68** (2003), 032702.

[95] L. Forster, M. Karski, J. Choi, A. Steffen, W. Alt, D. Meschede, A. Widera, E. Montano, J. H. Lee, W. Rakreungdet, and P. S. Jessen, *Microwave control of atomic motion in optical lattices*, Physical Review Letters **103** (2009), 233001.

[96] S. T. Merkel, G. Brennen, P. S. Jessen, and I. H. Deutsch, *Constructing general unitary maps from state preparations*, Physical Review A **80** (2009), 023424.

[97] K. Hammerer, A. S. Srensen, and E. S. Polzik, *Quantum interface between light and atomic ensembles*, Reviews of Modern Physics **82** (2010), 1041.